Reconfigurable modular battery pack for electric aircraft

MSc Thesis

Mayuresh Bhide

Technische Universiteit Delft

TU Delft

Reconfigurable modular battery pack for electric aircraft

MSc Thesis

by

Mayuresh Bhide

मयुरेश भिडे

to obtain the degree of Master of Science
at the Delft University of Technology,
to be defended publicly on Friday, September 29, 2023 at 3:00 PM.

Student number:	5622743	
Project duration:	December 20, 2022 – September 29, 2023	
Thesis committee:	Dr. ir. P. Bauer,	TU Delft, committee chair
	Dr. ir. G. R. Chandra Mouli,	TU Delft, thesis supervisor
	Dr. ir. M. R. Vogt,	TU Delft, external member
Advisor:	ir. Y. Liang,	TU Delft

This thesis is confidential and cannot be made public until September 29, 2023.

An electronic version of this thesis is available at http://repository.tudelft.nl/.
Cover image: Casey Crownhart, MIT Technology Review

TU Delft

Summary

Aviation is a growing industry responsible for over 2% of the energy-related CO_2 emissions in 2021. To achieve the 'Net Zero Emission by 2050 scenario', the aviation industry is turning towards modern propulsion technologies that reduce carbon and NO_X emissions. Research is taking place on many prospective aircraft designs, such as hybrid/turbo-electric powertrains, fuel cell/liquid hydrogen-powered aircraft and fully electric aircraft. Although fully electric aircraft offer the cleanest possible air travel, these aircraft are considered the solution for short-haul flights due to the range extension issue caused by the deficient specific energy of batteries compared to currently used aviation fuel. Many conceptual designs are made for electric aircraft, but very few are on the track of entry into service. This is because the expectations were set very high for the battery technology advancement after its boost in the Electric Vehicle (EV) industry. The challenge faced by the aircraft battery pack is mainly the weight, which restricts the payload fraction as well as the range of the aircraft. The electric aircraft concept designers rely on the potential development in battery technology while proposing their designs, and sporadic State-of-the-Art (SoA) battery designs are present concerning electric aviation.

The concept of reconfigurable battery packs involves using power switches to modify the arrangement of connected battery cells based on specific requirements. This innovative technique can potentially significantly reduce the weight of battery packs. The primary objective of this thesis was to conduct a comprehensive analysis and comparison between fixed configuration and reconfigurable battery packs in the context of electric aviation. It was imperative first to design these battery packs to facilitate this comparison. Creating a battery pack is inherently application-dependent, requiring a detailed understanding of the application's power profile. Given the limited availability of open data on electric aircraft designs, the power profile was estimated using available reference aircraft specifications and reasonable assumptions. The literature review on power systems in aircraft revealed a significant correlation between system-level voltage and the weight of power cables. This discovery led to estimating an optimal system-level voltage, a critical constraint in battery sizing. For the fixed configuration battery pack, sizing was conducted using both a high-specific energy cell and a high-specific power cell. However, it became evident that each cell type had its strengths and limitations. This realisation prompted the design of a reconfigurable battery pack, strategically leveraging both cell types. This innovative approach created a high-specific energy battery pack called the 'primary battery pack' and a high-specific power battery pack known as the 'secondary battery pack.' Together, they formed a reconfigurable battery pack capable of dynamically connecting and disconnecting the primary and secondary packs through power switches, allowing them to complement each other during high-power demand phases of flight, such as take-off and climbing.

In contrast to fixed-configuration packs, reconfigurable battery packs demonstrated the ability to meet power and energy demands with fewer cells. Software simulations were conducted to ensure the proper functioning of the reconfigurability technique. These simulations revealed that the reconfigurable battery pack experienced higher C-rates than the fixed configuration battery pack, owing to the reduced number of cells. Given that higher C-rates can impact battery health by inducing capacity loss over multiple cycles, a preliminary ageing analysis was performed to quantitatively assess the adverse effects of higher C-rates on the reconfigurable battery pack

The results quantified that around 400 kg of potential weight savings are possible by employing reconfigurable battery packs over fixed configuration battery packs at the cost of only 0.4% more capacity loss over 500 charging-discharging cycles. The weight savings can be translated into three different scenarios. Firstly, payload weight capacity can be enhanced. Secondly, flying with lesser weight will offset the power profile, saving energy. Lastly, an additional number of cells equivalent to the mass saved can realise the range extension of the electric aircraft.

Preface

Completing my master's thesis marks the conclusion of my master's degree in Sustainable Energy Technology at TU Delft. The past two years have been a constant learning curve at educational and personal levels. The rich intellectual environment of this university inspired me to learn something new every day and revived the newborn's curiosity in me. I am forever indebted to this great institution for lighting the flame of Prometheus inside me.

I would like to extend my immense gratitude to my supervisor, Dr. Gautham Ram Chandra Mouli, for his invaluable expertise and guidance throughout the thesis journey. His mentorship significantly contributed to refining my ideas and a structured action plan. I would also like to thank my committee chair, Prof. Dr. Pavol Bauer and external committee member, Dr. Malte Ruben Vogt, for dedicating their time to evaluate my thesis work. Furthermore, I am thankful to my daily supervisor, ir. Yawen Liang for her time, continuous support and feedback at each step towards completing this thesis work.

To my beloved parents, who have given me constant care and support throughout this journey, I offer my deepest gratitude. Their visits, video calls and festive courier packages kept me encouraging. I wholeheartedly thank dearest Vaishnavi, who continuously motivated me to push my horizons and achieve even more. I also thank my brothers, friends and colleagues who made the last two years in the Netherlands enjoyable and memorable. I am thankful to all those hard-working students I met in the library and EEMCS department who helped me somehow. Finally, the two things I spent the most time with, my laptop and coffee mug, thank you.

जय हिंद!

With sincere appreciation and a sense of fulfilment,
Mayuresh Bhide
Delft, September 2023

Contents

List of Figures

List of Tables

List of Acronyms

A	Wing surface area
ACARE	Advisory Council for Aeronautics Research in Europe
APU	Auxiliary Power Unit
AR	Aspect ratio
ATC	Air Traffic Control
$\mathbf{a}_{TO}$	acceleration
BESS	Battery Energy Storage System
BMS	Battery Management System
$\mathbf{C}_D$	Coefficient of Drag
$\mathbf{C}_{D_0}$	Parasitic coefficient of drag
$\mathbf{C}_L$	Coefficient of lift
CTOL	Conventional Take-Off and Landing
DEP	Distributed Electric Propulsion
DFN	Doyle Fuller Newman
DoD	Depth of Discharge
$\mathbf{d}_{TO}$	Take-off distance
ECM	Equivalent Circuit Model
EM	Electric Motor
ϵ	Dielectric permittivity
η_{cable}	Cable efficiency
$\eta_{coulombic}$	coulombic efficiency
η_{em}	Electric motor efficiency
η_{inv}	Inverter efficiency
η_{prop}	Propeller efficiency
EV	Electric Vehicle
eVTOL	e-Vertical Take-off and Landing
$\mathbf{F}_D$	Drag force
$\mathbf{F}_F$	Frictional force
$\mathbf{F}_L$	Lift force
$\mathbf{F}_T$	Thrust

IEA	International Energy Agency
L/D	Lift to Drag ratio
LCO	Lithium Cobalt Oxide
LFP	Lithium Iron Phosphate
LH_2	Liquid Hydrogen
Li_2O_2	Lithium Peroxide
LiOH	Lithium Hydroxide
Li-S	Lithium-Sulphur
LLI	Loss of Lithium Inventory
LMO	Lithium Manganese Oxide
LNMO	Lithium Nickel Manganese Oxide
LTO	Lithium Titanate Oxide
MTOW	Maximum Take-Off Weight
N	Normal reaction
NCA	Nickel Cobalt Aluminium Oxide
NiCd	Nickel-Cadmium
NiMH	Nickel Metal Hydride
NMC	Nickel Manganese Cobalt Oxide
OCV	Open Circuit Voltage
P	Power
PBM	Physics-based Model
PCM	Parallel Cell Module
PDE	Partial Differential Equations
PyBaMM	Python Battery Mathematical Modelling
Q	Total capacity
RMS	Root Mean Squared
RPK	Revenue Passenger Kilometre
s	Altitude
SAF	Sustainable Aviation Fuel
SCM	Series Cell Module
SEI	Solid Electrolyte Interface
SoA	State-of-the-Art
SOC	State of Charge
SOH	State of Health

SVD	Single Void Discharge
θ_D	Descent angle
θ	Pitch angle
UAM	Urban Air Mobility
UAV	Unmanned Aerial Vehicle
$\mathbf{v}_{TO}$	Take-off velocity
$\mathbf{v}_v$	Vertical velocity
W	Weight
XLPE	Cross-linked polyethylene

1

Introduction

1.1. Research goal statement

The primary objective of this master's thesis is to conduct a thorough analysis and comparison of fixed and reconfigurable battery pack configurations within the context of electric aircraft. The research is driven by evaluating their weight efficiency, considering various factors, including power profiles, system-level voltages, battery chemistry, and ageing characteristics. Ultimately, this study aims to determine the optimal battery pack configuration to enhance the performance and sustainability of electric aircraft.

1.2. Motivation

The aviation sector was responsible for over 2% of the energy-related CO_2 emissions in the year 2021 [7]. Towards achieving the goal of 'Net Zero Emissions by 2050 Scenario', International Energy Agency (IEA) marks the progress of this sector as 'Not on track' [6]. On the other hand, Airbus and Boeing have forecasted an increase in fleet growth of 3.5% annually from 2023-2042 [2, 8]. This highlights the urgent need for innovative aircraft concepts that can contribute to the emission reduction goal [55]. Concepts such as hybrid/turbo-electric, fuel cell-powered, hydrogen-powered, biofuel-powered and fully electric aircraft are found in the literature with potential for aviation-related CO_2 emission reduction. However, a distinguishing characteristic of aviation is that a substantial portion of the climate warming linked to aviation results from emissions other than CO_2 [23]. Although biofuels can lower overall CO_2 emissions throughout their lifecycle and hybrid/turbo-electric aircraft can reduce fuel consumption and emissions through efficiency enhancements, solely electric aircraft hold the potential for achieving zero in-flight emissions over the long run. This vision of battery-powered flight has existed for more than a century. In 1884, the airship La France, spanning 52 meters in length, achieved flight covering approximately 8 km near Paris using a 435 kg zinc-chlorine battery and became the first electric aerial vehicle. Its creator, Charles Reynard, believed such flights were a matter of time and investment [64].

A significant portion of ongoing battery research and advancement is directed toward fulfilling the requirements of land-based transportation, portable electronic devices, and grid energy storage. Aviation has distinctive demands in certain areas crucial for battery technology [64]. The current battery pack used in aircraft is a supplementary energy source responsible for powering cabin loads. In contrast, the battery packs in 'Electric Aircraft' are the sole energy source accountable for all the operations. This puts a lot of reliability and safety concerns on the electric power system for flawless on-board operation.

Moreover, the SoA battery technology can achieve cell-level specific energy of 250 Wh/kg [26], which is far less than aviation fuel specific energy (~43.1 MJ/kg). The heavy weight of the battery pack is a significant challenge for the range extension of electric aircraft. The electric aircraft concept designers are relying on the potential development in battery technology while proposing the design. No dedicated battery design efforts for aviation are publicly available or seen. Hence, the result of a tailor-made battery pack design

for electric aircraft is necessary.

A unique technique found in literature called reconfigurable battery packs might hold the potential to realise battery pack weight reduction. A reconfigurable battery pack is proposed for redundant battery pack operation in EVs. Reconfigurability involves power switches that can alter the configuration of connected battery modules/cells inside a battery pack/module as per requirement. Hence, a study that compares the novel concept of reconfigurable battery pack design with conventional fixed-configuration battery pack motivated the author to undertake this as the master's thesis.

1.3. Research questions

This section outlines the research questions that form the foundation of the thesis work. The subsequent chapters detail the progress made toward answering these research questions, and the conclusive outcomes of all these efforts are consolidated in Chapter 6.

1. How is the electric aircraft power profile for which the battery pack is designed? What aspects of the power profile dictate battery sizing?

2. What are the SoA and futuristic battery chemistries suitable for electric aircraft? What are their respective merits and demerits?

3. How is a reconfigurable battery pack beneficial? How much weight saving can it realise compared to the fixed configuration battery pack?

4. What is the significance of system-level voltage in weight minimisation?

5. What is the effect on cell ageing due to reconfigurability? Is the benefit of weight saving compromised for higher ageing of cells?

1.4. Research approach

The chronological steps followed for completing this study are presented in this section. The literature review was a continual process throughout the thesis timeline comprising upcoming aircraft concepts, electric aircraft powertrain architectures, SoA battery technologies (including their mathematical models), and reconfigurable battery packs. The review of electric aircraft was necessary for shortlisting the reference aircraft upon which the battery pack design is based. Due to the novelty of the electric aircraft technology, information regarding the detailed specifications is scarce. Hence, a power profile was calculated based on the available information and some reasonable assumptions. After generating a power profile, studies related to the power systems were referred to comprehend the system-level voltages of electric aircraft. This helped finalise the battery pack terminal voltage for minimal weight and energy losses through power cables. Subsequently, literature on SoA and futuristic battery technologies and their mathematical estimation models was done for the battery chemistry preference. After shortlisting the most suitable battery chemistry, the pre-generated power profile was analysed for battery sizing. A high specific energy cell and a high specific power cell were shortlisted as the building block of the battery pack. The battery sizing was done for two configurations, 'fixed' and 'reconfigurable', for the weight comparison of the battery packs. In terms of lesser weight, the 'reconfigurable battery pack' prevailed. However, the battery pack simulation was necessary to validate proper functioning and provide details. In a software environment, the battery is represented by mathematical equations widely known as battery models. Accordingly, Equivalent Circuit Models were developed for separate battery packs and were simulated. After analysing the operational details of both battery packs, a software-based ageing model was used to observe the difference in the ageing of these battery packs. Finally, this study was concluded after comparing these configurations regarding weight and ageing as a preferred solution for electric aircraft battery packs.

1.5. Structure overview

In this section, the report's structure is outlined. Chapter 2 provides background knowledge relevant to this thesis study. It encompasses sections summarising key insights from recent studies and reviewed literature organised by their respective domains. Chapter 3 presents the selection of the reference aircraft and its specifications, followed by the power profile and optimal system-level voltage calculations. Chapter 4 focuses on battery design and modelling. It elaborates on battery chemistry and cell selection, followed by battery sizing for both fixed configuration and reconfigurable battery packs. Additionally, it presents the methodology employed for developing ECM tailored to the respective battery packs. In Chapter 5, a software rendition of these battery packs is created to validate the proper operation and extract the operational parameters necessary for ageing analysis in both configurations. Finally, Chapter 6 presents the thesis study's conclusions, followed by a discussion of prospects and recommendations for electric aircraft battery pack design.

2

Background

This chapter offers a comprehensive background on the thesis topic, encompassing recent relevant works in specific fields. Section 2.1 provides an overview of the imminent evolution in aviation. Following this, section 2.2 presents a comprehensive overview of battery technology, encompassing the SoA and futuristic battery chemistries. Section 2.3 addresses the configuration of large-scale battery packs. Further, section 2.4 provides a concise background on cell models, with further elaboration in Chapter 4. Moreover, section 2.5 introduces the concept and necessity of reconfigurability in battery packs, alongside recent advancements in this area. Finally, in section 2.6, the research gap identified in the reviewed literature is outlined, emphasising the focal point of this study.

2.1. Future of aviation

In the coming decades, the technological enhancement in the aviation industry will aim towards reducing the emissions that cause environmental impact. Thus, the future of aviation lies in aircraft powered by carbon-neutral alternative energy sources. This opens the opportunity to redesign the whole powertrain of the aircraft as traditional fuel-powered engines will be replaced. In the literature following aircraft classes are discussed: [55, 53, 23]

- Hybrid and Turbo Electric (parallel and serial)
- Fuel cell powered aircraft
- Liquid Hydrogen (LH_2) fuelled aircraft
- More electric aircraft
- Fully electric aircraft

2.1.1. Types of aircraft

Hybrid aircraft propulsion includes various configurations of electromechanical powertrain. It consists of a battery pack, electric machines (motors/generators), and fuel-powered turbofan or turboshaft engines where fuel can be aviation fuel, Sustainable Aviation Fuel (SAF), or hydrogen. Figure 2.1 displays the unique arrangement in each configuration. Parallel hybrid comprises electrical and gas turbine systems on two different shafts. Lesser components benefit parallel hybrid in weight savings; however, mechanically coupled systems create operational complexity. In a serial hybrid, mechanical coupling is replaced by an electrical bus as the propulsive power is electrically powered either by the battery pack or by the generator powered by the gas turbine. Mechanical independence enables the gas turbine to maximise efficiency at its optimum point. Parallel/Serial hybrid is a mix of both, where a turbofan engine can also provide the thrust independently, which enables optimising engine design for particular segments [53, 55].

Turboelectric configuration is built to overcome the range issue by keeping the energy source as fuel and also has enhanced efficiency owing to its electrical drive system. It is a more realistic but intermediate

solution for emission reduction without any range compromise.

Fuel cell generates electrical energy through chemical reactions. Hydrocarbon fuel or hydrogen can both serve as the energy source for fuel cells. Hydrogen fuel cells are carbon and NO_x neutral sources of generation. However, the most explored Proton Exchange Membrane (PEM) fuel cells and Solid Oxide Fuel Cells (SOFC) require a specific operating temperature range and, importantly, lack the necessary specific power in aircraft applications. LH_2 fuelled aircraft can be beneficial due to the high energy density of hydrogen. However, LH_2 must be stored at cryogenic temperatures, requiring specialised tanks and handling procedures. Furthermore, it requires other equipment designed for low temperatures, which are unlikely to reach maturity in the coming 20-25 years [53]. In the case of hydrogen fuel cell-powered and LH2-fueled aircraft, storing liquefied or gaseous hydrogen under operational conditions raises safety concerns.

More electric aircraft use electric power for non-propulsive systems. The in-wheel motors taxi the plane to the runway, and the electric energy source replaces the fuel-burning Auxiliary Power Unit (APU). Electric systems replace all the mechanical, hydraulic and pneumatic systems. Taxing is a very inefficient part of the flight trip when propelled with a turbofan engine; hence, electric taxing increases efficiency, lowers ground-level emissions and reduces airport noise levels, which is a crucial factor in expanding air services and building new airports [55]. Modern civil aircraft such as Boeing 787 Dreamliner and Airbus A380 benefit from 'more electric' systems[39]. This can be labelled as the transition class of aircraft from conventional to fully electric.

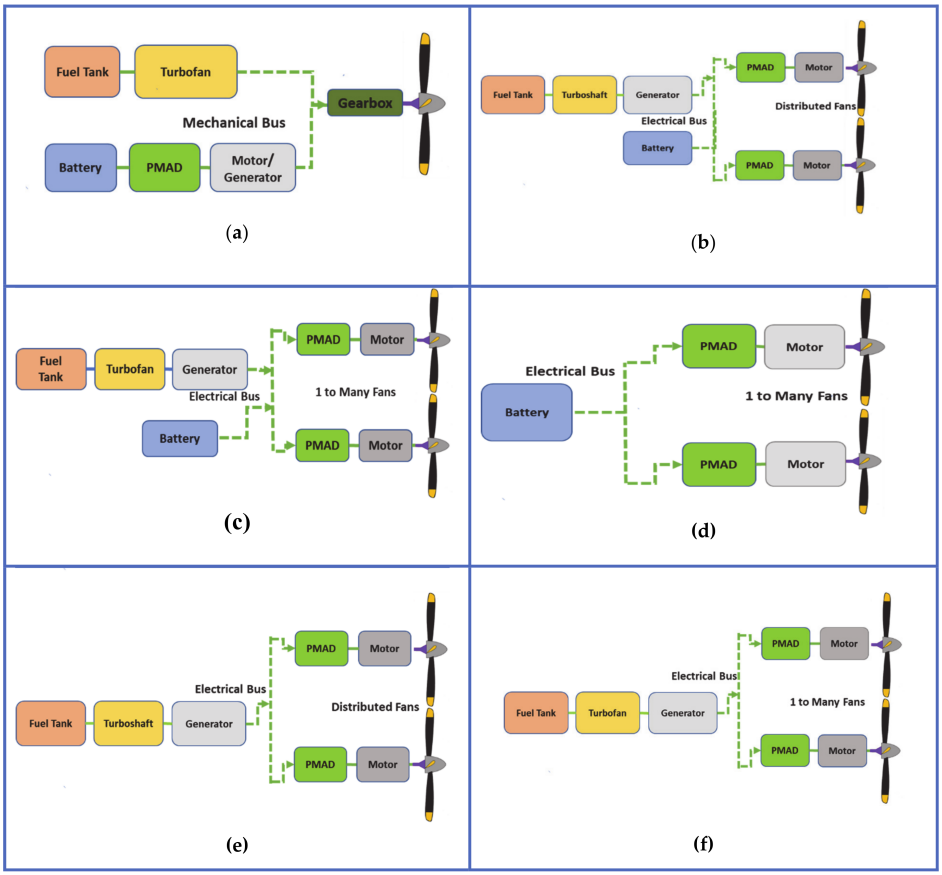

Figure 2.1: Illustration of various propulsion configurations as per Sahoo, Zhao, and Kyprianidis [53]
(a) Parallel hybrid; (b) Serial hybrid; (c)Parallel/Serial; (d) Fully electric; (e) Turboelectric; (f) Partially turboelectric

Fully electric aircraft, as the name suggests, has only an electric energy source to power all the systems. Conventional engines are replaced by innovative designs of electric motor(s). These aircraft include different types such as Unmanned Aerial Vehicle (UAV), electric powertrain retrofits of existing aircraft,

novel fixed-wing concepts and e-Vertical Take-off and Landing (eVTOL) aircraft [55]. With all-electric propulsion, the total efficiency of the aircraft is high compared to other configurations. The biggest concern regarding fully electric aircraft is the range of the flight. The specific energy the batteries provide is almost 40 times lower than that of aviation fuel, and specific power is also a limiting factor. Much higher specific energy battery packs are required for realising long-range airliners. With today's or near-term battery technological advancement, specific energy above 250 Wh/kg can realise Urban Air Mobility (UAM) vehicles such as air taxis. However, for short-haul flights, a value of 500 Wh/kg needs to be reached [57]. Studies by Gnadt et al. [23], Rendón et al. [50], Shadbolt [57] and Sahoo, Zhao, and Kyprianidis [53] provide a detailed review of the modern concept designs and demonstrators.

2.1.2. Potential of fully electric aircraft

Environmental factor	EU ACARE flightpath 2050 strategy	NASA N+3 Program (2010 to 2035)
Greenhouse gas emissions (GHG)	75% CO_2 emission reduction	25% CO_2 emission reduction within 10 years and 50% reduction within 25 years
Nitrogen oxides NO_x	90% NO_x reduction	70% reduction in NO_x emission within 10 years and 80% within 25 years
Noise	65% reduction in noise	Perceived noise reduction by a factor of 2 in 10 years and by a factor of 4 in 25 years.

Table 2.1: ACARE flightpath 2050 and NASA N+3 program goals [1]

ACARE has set forth goals to be achieved by 2050, mentioned in table 2.1. Although previously mentioned classes of aircraft conceptually demonstrate a reduction in flight emissions [53], long-term zero-in-flight emissions are only possible with fully electric aircraft [23]. Besides that, the following are the reasons why electric aviation is a plausible solution for near-future aviation:

- Not limited by the thermodynamic efficiency of a gas turbine and lesser energy loss in power conversion [23]
- Electric motor ducted-fan assemblies are better scalable in quantity than gas turbines. Hence using numerous motors allows Distributed Electric Propulsion (DEP) which is lighter, quieter and offers redundancy [23]
- Operational cost savings. For example, Ampaire projects its 15-passenger aircraft would decrease fuel costs by 90% and reduce maintenance costs by 50% [55]
- Noise reduction. Quieter taxing, take-off and landing [53]
- In the long-term, emission-free electricity sources may further reduce the environmental impacts [23]

2.2. Battery technology

2.2.1. Current status and tradeoffs

Although electrification emerges as the leading contender for sustainable air travel, its expansion in terms of range and longevity is limited by the present status of battery technology. Additionally, crucial factors such as specific energy and power-to-weight ratio are critical in the aviation industry. In recent years, the spike in the EV market has fuelled the research of different battery chemistries, yet further developments in battery chemistries are requisite to realise electric aviation. This development is multifaceted, and certain aspects may need to be traded off depending on the application. Figure 2.2 displays the battery

development tradeoffs. Different battery chemistries have different properties. The battery chemistry to be chosen depends upon the prioritisation of these tradeoffs. For example, in aviation, high specific energy and power are desirable, but a high level of safety is paramount. Hence, the correct choice of battery chemistry is the building block of battery pack design.

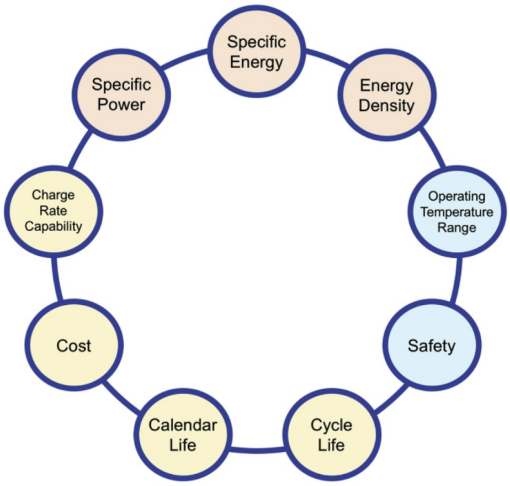

Figure 2.2: Battery trade-offs [23]

2.2.2. Lithium-based battery superiority

Li-based battery chemistries have gained significant attention due to recent advancements in the electric vehicle (EV) sector, surpassing the previously commonly used Lead-acid and Nickel Metal Hydride (NiMH) or Nickel-Cadmium (NiCd) batteries. Even though Airbus A320 family aircraft currently utilise NiCd batteries supplementing the APU, the question arises as to why Li metal-based chemistries are favoured over these conventional options. The following are the advantages of Li based batteries over others: [45]

- They have higher specific energy than the most
- Operate at higher voltages (3.7V) than NiCd (1.2V)
- Lower self-discharge rate
- Smooth intercalation mechanism prolongs the lifetime

Within the Li-ion battery domain, there exists a diverse range of chemistries, with some being considered mature and SoA, while others are still undergoing research and development (refer Figure 2.3). All these chemistries have the following things in common: [45, 25]

- They are composed of four main components, namely, cathode, anode, electrolyte and separator
- The anode is made of loosely stacked graphite layers (exception: Lithium Titanate Oxide (LTO)) where Li-ion intercalates between them while charging and opposite while discharging. Below is the chemical reaction at the anode:

$$Li_xC \longleftrightarrow C + Li^+ + xe^- \text{ [25]}$$

- The cathode is made of Li metal oxide. Li-ion leaves the cathode while charging and the opposite while discharging. Below is the chemical reaction at the cathode:

$$Li_{1-x}MO_2 + xLi^+ + xe^- \longleftrightarrow LiMO_2 \text{ [25]}$$

- The cathode structure is arranged on aluminium, whereas the anode structure is arranged on the copper current collector
- The electrolyte is composed of lithium salts and organic solvents, which enable Li-ion transport

- A micro-porous membrane serves as a separator to prevent short circuits between the electrodes, allowing the passage of Li-ion through the pores

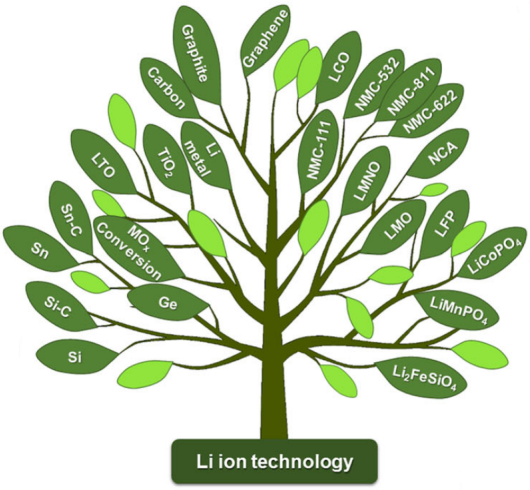

Figure 2.3: Li based battery chemistries [43]

2.2.3. Lithium-ion battery chemistries

Here is a brief description of Li-ion battery chemistries and a comparison of their properties. The anode material is mainly graphite; sometimes, it is silicon or LTO. The Li-ion batteries often differ in their cathode material. Hence, they are referred to by their cathode material elements. Figure 2.4 at the end of this subsection compares the performance parameters of these battery chemistries. A higher index value depicts better performance.

Lithium Cobalt Oxide (LCO) is often referred to as a 'layered cathode' due to its layered structure of CoO_6 octahedra [45]. It is predominantly used in portable electronic devices due to its high specific energy [25]. It fails to scale up due to the rarity, toxicity and high cost of cobalt metal. Furthermore, rapid ageing is observed if operated below half of its theoretical capacity. Ni instead of Co increases the specific energy even more, but it becomes unstable [45]. LCO is sensitive to overheating and high charge-discharge C-rates (above 1C) [25]. Hence, in large-scale battery packs, LCO is not found as the cathode material.

Lithium Manganese Oxide (LMO) has a three-dimensional spinal structure that offers a more accessible pathway to Li^+ ions than other two-dimensional structures. This allows a higher rate of charge-discharge with low resistance [25]. On the downside, it has a lower specific capacity (Ah/kg), and the cyclic dissolution of Mn into electrolyte shortens its lifespan. The combination of LMO with Nickel Manganese Cobalt Oxide (NMC) brings the best out of both chemistries, higher rate and low cost of LMO with high capacity and cycle life of NMC. This composite has recently been used in many EVs (BMW i3, Nissan Leaf and Chevy Volt). Further research is taking place in high voltage Lithium Nickel Manganese Oxide (LNMO) to achieve high specific energy (580 Wh/kg). [26, 45]

Lithium Iron Phosphate (LFP) has a olivine structure with strong bonds of PO_4 tetrahedral units. It has excellent cycle life with low toxicity [26] and a wider window of temperature tolerance (-30^{o}C to 60^{o}C). The constituent materials are cheaper than previously mentioned battery chemistries, and this cathode can withstand overcharged and undercharged conditions. It is known for its high dependability and safety [25]. On the downside, due to the heavy Fe element and low open circuit potential (nominal 3.4V), it has low specific energy (190 Wh/kg cell level), leading to higher material cost per kWh even with cheap materials [26]. One-dimensional cathode structure increases the resistance to the ion pathways, but nanoscale particle size and conductive additives overcome the drawback [45]. Due to its unmatchable benefits, LFP dominates public transport, heavy-duty market and commercial EVs.

Lithium Nickel Manganese Cobalt Oxide (NMC) is one of the extensively researched battery technology. Three different metals bring out their own merits to enhance the battery properties. Ni contributes to the high specific energy, Mn, whose spinal structure achieves lower internal resistance, and Co exhibits higher conductivity [26]. Higher Ni content can be added to increase the specific energy, but it challenges the battery's thermal stability and calendar life. The metal mix is in the proportion of 33% Ni, 33% Mn and 34% Co for lower material cost. Lesser Co contents compared to LCO reduces the material cost. Many formulations are researched to achieve different objectives, of which few are listed in Houache et al. [26], yet the battery manufacturers protect the perfect ones. This battery chemistry is in heavy demand for EV applications owing to its high specific energy and lower self-heating rate [25].

Lithium Nickel Cobalt Aluminium Oxide (NCA) is a strong contender of the NMC cathode material in EV market. Similar to NMC, Ni-rich material can realise high specific energy and lower Co content, resulting in lower cost per kWh. The differentiating Al^{3+} ions reduce the detrimental phase transition, help achieve thermal stability and increase the operational voltage (3.7V average). On the downside, this cathode material fades capacity while operating at elevated temperatures or voltages due to grain boundary breakage and strong Solid Electrolyte Interface (SEI) layer formation. This high interfacial resistance lowers the capacity and power over time. Yet, due to the high power density and specific energy, this cathode material with a lot of unique constituents formulation is found in novel EVs and the energy density and specific energy is predicted to attain 700 Wh/L and 300 Wh/kg respectively at cell level till 2025 [26].

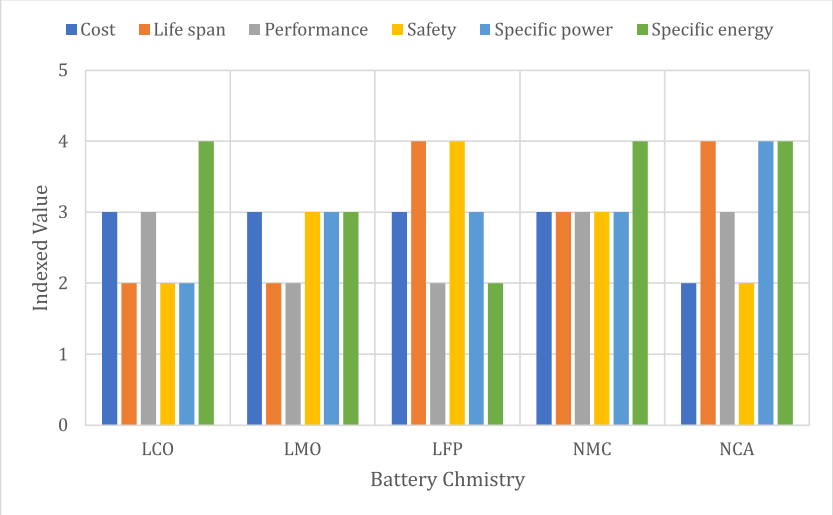

Figure 2.4: Battery Chemistry comparison

2.2.4. Futuristic Lithium-based batteries

Along with Li-ion batteries, researchers are also exploring various chemistries that can yield higher theoretical specific energy than SoA Li-ion batteries. For example, in a study by Cao, Zhang, and Li [11], numerous different batteries having anodes as Li, Na, K, Mg, Al, and Zn were thermodynamically analysed to find theoretical specific energy above 1000 Wh/kg and OCV above 1.5 V. 51 out of those satisfied the screening criteria. Such studies are guiding the researchers to analyse novel batteries further. Here is the description of often cited next-generation Li-based batteries which can realise extended-range electric aircraft.

In **Li-S** battery, the anode is Li metal, and the cathode is Sulphur, often contained in a carbon electrode structure. Following are the conversion reactions taking place at the anode and cathode:

$$\text{Anode: } Li \longleftrightarrow Li^+ + e^-$$

$$\text{Cathode: } S_8 + 2\,Li^+ + 2\,e^- \longleftrightarrow Li_2S_8$$

The formed Li_2S_8 during discharge further reduces to the lower order polysulphide, as shown below.

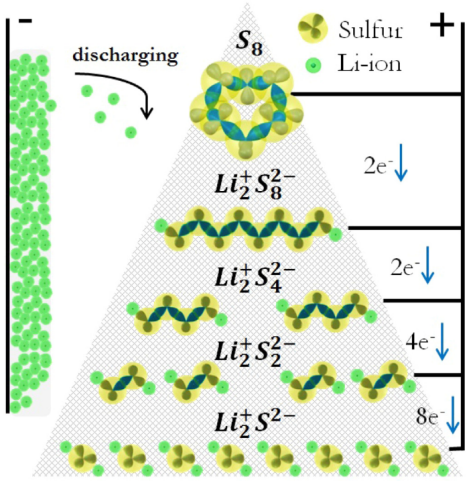

Figure 2.5: Reduction to lower chains [47]

$$Li_2S_8 \longrightarrow Li_2S_6 \longrightarrow Li_2S_4 \longrightarrow Li_2S_2 \longrightarrow Li_2S$$

Unlike higher-order polysulphides, these lower-order polysulphides are insoluble and electrically insulating. The reduction reaction chain is highly complex to analyse, and ongoing research is ongoing. Due to the presence of high-order polysulphide, a higher voltage plateau (2.35 V) is observed and later, due to the formation of lower ones, a lower voltage plateau (2.1 V) is observed. Due to the increasing concentration of insulating Li_2S and Li_2S_2, the discharging terminates, and the useful specific capacity is about 416 mAh/g. While charging lower chains oxidise to higher chains, all higher chains are not converted back to S_8. Few in contact with the anode reduce back to the lower chains. These can again get oxidised at the cathode to higher chains, and so on. This process is known as the polysulphide shuttle. This causes capacity fade and self-discharge, accounting for lower coulombic efficiency than the SoA Li-ion batteries. On the positive side, it protects against overcharge conditions [47].

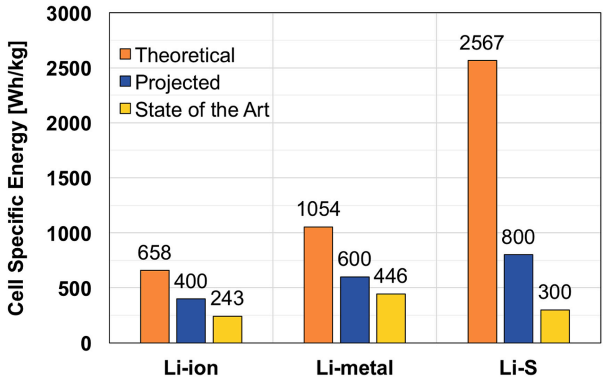

Figure 2.6: Comparison of Li-S specific energy with other Li based battery technologies [23]

A Significant amount of literature was reviewed over Li-S battery technology for its potential of yielding high specific energy. Figure 2.6 visually represents the Li-S battery superiority in specific energy. Another benefit of Li-S is its cheap constituent material cost, as high-priced metals are not present at the cathode of this battery. However, challenges are faced with Li-S batteries, such as low power capacities, limited cycle life, and capacity fade due to polysulphide shuttling [58]. The presence of higher and lower-order polysulphide leads to the formation of high- and low-voltage plateaus over a range of SOC values, and modelling this phenomenon is a complex task. Yet various researchers attempted the modelling of this battery technology. Following are the studies conducted for Li-S modelling:

- Shateri et al. [58] developed an ECM with dynamic parameter identification for ageing analysis and State of Health (SOH) estimation with an 96.7% SOH estimation accuracy

- Propp et al. [47] developed a non-linear SOC dependent ECM for Li-S batteries under discharge. The model's parameterisation was done in a laboratory at four different temperatures by subjecting the current profile. Voltage prediction was accurate with 32 mV RMS error

- Fotouhi et al. [21] reviewed the modelling techniques and concluded that 'shuttling' is a major challenge, and further work is required for modelling Li-S batteries

- Li et al. [35] presented that a porous nitrogen-doped carbon nanofiber membrane containing ultrafine and polar ZrO_2 can prevent polysulphide shuttling resulting in lesser capacity fade and long cycle life (0.039% capacity fade after 500 cycles at 0.2 C)

- Gnadt et al. [23] conducted a comprehensive technical and environmental evaluation of an electric aircraft concept resembling the Airbus A320neo. The study involved a battery technology analysis, wherein the comparative attributes of Li-S and Li-ion batteries were examined, along with their respective implications on aircraft design

Lithium-air battery theoretically has a substantial specific energy of 3000 Wh/kg [17]. It has a Li metal anode, which oxidises during discharge, and Li^+ ions are released into the electrolyte. There are two types of electrolytes: aqueous and non-aqueous. The aqueous electrolyte enters into the pores of the cathode (primarily carbon), and oxygen from the air gets reduced, forming Lithium Hydroxide (LiOH) due to the presence of water in the reaction. In the case of non-aqueous electrolytes, Lithium Peroxide (Li_2O_2) is included at the cathode [10]. This technology still faces many challenges. The supply of pure oxygen at the cathode requires specific membranes to filter other constituent gases in the air. The formed products take up the pores in the electrode, blocking the reaction path and eventually fading capacity. Furthermore, the Li metal anode is susceptible to developing dendrites after cycling. Also, this battery shows a significant power fade after 50 cycles. A few more challenges need to be solved to be used in electric aviation. For example, the design of the aircraft needs to be altered for ambient air availability at the battery cathode. It may be necessary to pressurise the air, which can add weight to the plane; there needs to be an adequate rate of oxygen supply, which can ensure continuous operation of the battery. Then, the onboard storage tank of oxygen should be included in the final weight calculations [17].

2.3. Large scale battery packs

Due to the recent advancement in sustainable mobility, the need for large-scale battery packs has risen. The distinction between small-scale battery packs used in electric appliances and devices and large-scale battery packs employed in the mobility sector or as Battery Energy Storage System (BESS) lies in their respective capacities rather than a specific predefined value.

The large-scale battery packs often have modular designs. A module comprises a certain number of cells connected in series/parallel, and a pack consists of several modules connected in series/parallel. There are no predefined values to these number distributions; it depends on the application for which the battery is being designed. The purpose of having a modular design is to simplify the cell monitoring process for the Battery Management System (BMS). A local controller monitors a single module, and a central controller monitors a group of modules. Depending upon the electrical connections of cells, there are two types of cell configurations pictorially depicted in Figure 2.7, Series Cell Module (SCM) and Parallel Cell Module (PCM). In SCM, cells are connected in series to make up a module and such modules are connected in parallel to make up a pack. In PCM, cells are connected in parallel to make up a module and such modules are connected in series to make up a pack.

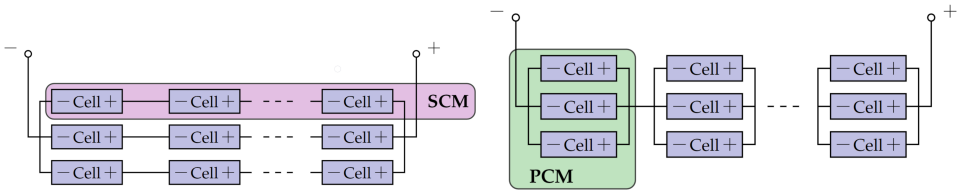

(a) SCM (b) PCM

Figure 2.7: Module configurations [44]

Several advantages and disadvantages are mentioned in the literature for both configurations.

- Advantages:

  1. PCM has distributed battery parameters, allowing for the attainment of an average value through parallel connections across the system. PCM has internal resistances of cells connected in parallel, which results in low resistance for a given [24]
  2. The average resistance value of the module mitigates the impact of an elevated cell resistance on the overall module resistance [24]
  3. PCM configuration allows cells inside the module to self-balance. The charges move from high-voltage to low-voltage cells to level out the voltages. This process continues until the equilibrium module voltage is achieved. In many EV battery packs, a dedicated circuit is used for cell balancing involving numerous passive circuit components. With PCM self-balancing of cells can be achieved [24, 75, 65]
  4. SCM has better single-point fault tolerance. When inside a module, an open circuit fault occurs, except for that module, the rest of the battery pack operates. If a short circuit fault occurs, only a cell inside the module is compromised, and the battery pack still operates [24]
  5. SCM can realise high voltage levels, and their capacity can be increased by connecting several such modules in parallel [65, 44]
  6. In SCM pack level voltage balancing can be achieved as the modules are connected in parallel [24, 65]

- Disadvantages:

  1. In PCM, when multiple modules are connected in series to form a battery pack, the internal resistance of the battery pack is nearly the same as SCM battery pack
  2. In PCM to balance the voltages of modules, a mechanism is still necessary as the voltages of modules remain imbalanced since they are connected in series [44]
  3. SCM needs a cell balancing mechanism inside each module, which is very complex to implement in large-scale battery packs [65]
  4. In PCM and SCM short circuit faults can diminish battery performance heavily since there is a huge temperature rise due to high circulating current [24, 65]

2.4. Cell models

Cell models are mathematical equations representing cell behaviour under various conditions. In the previous section, the concept of large-scale battery packs is elaborated, which underlines the usage of thousands of cells inside a battery pack. To efficiently use the electrical energy present in a battery pack, the building block of the battery pack, i.e. a cell, needs to be monitored for its optimum operation. This monitoring involves the estimation of several parameters of the cell, such as OCV, SOC, and SOH. These estimations use cell models embedded in the BMS.

2.4.1. Types of cell models

Various mathematical models describe a cell's behaviour under certain conditions and estimate the different parameters. Fundamentally, there are two types of these models, namely the 'Equivalent Circuit Model (ECM)' and 'Physics-based Model (PBM)'. As the name suggests, ECM represents the operation of a lithium-ion cell through an electrical circuit as an analogue to the cell behaviour. The parameterisation of these components is based on the lab test data such that the current/voltage values will be as close to the actual cell. These parameters are optimised after exercising charge-discharge procedures of the current profile. This model depends on empirical data. Hence, interpolation gives accurate results compared to extrapolation. ECM might produce inaccurate values if the cell operates outside of the exercised data. Although it can not describe many internal electrochemical states, it is a fast and robust simulation method. On the other hand, PBM is derived from physical laws, which describe the response of internal electrochemical reactions depending upon the input current profile. These models use Partial Differential Equations (PDE)s, which can yield accurate results but are very slow if modelled correctly. These models are useful for ageing calculations of the cell [44]. In this study, ECM is favoured over PBM; the reason is presented in chapter 4. Hence, further explanation over ECM is presented in the next section.

2.4.2. Equivalent Circuit Model

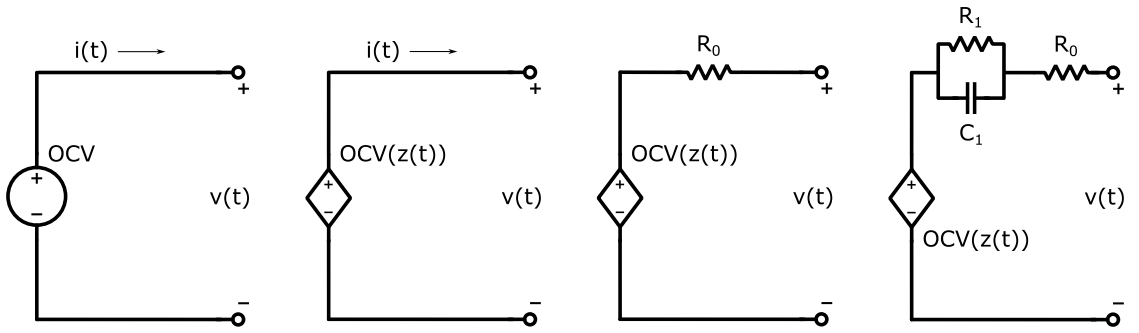

(a) Ideal voltage source with constant voltage model

(b) SOC dependent OCV model

(c) SOC dependent OCV with series equivalent resistance R_0 model

(d) SOC dependent OCV and R_0 including diffusion voltage model

Figure 2.8: Different stages of ECM

Following is the step-by-step explanation of ECM modelling displayed in Figure 2.8: [45]

- Figure 2.8a models the cell as an ideal voltage source with a constant voltage equal to 'OCV'. This is an inferior model because, although the cell provides positive terminal voltage, that voltage is never constant and depends on various factors
- Figure 2.8b includes the dependency of OCV on SOC ('z' in the figure) and SOC is a function of time. Here, the model deals only with the cell's static condition, not the dynamic one. It is observed that the cell's terminal voltage is lesser than OCV while discharging and higher than OCV while charging.
- In Figure 2.8c, the insertion of series resistance R_0, which corresponds to the cell's internal resistance, creates a voltage drop that models the dynamic phenomenon mentioned above
- When a high discharge current pulse is subjected to the Li-ion cell, a sudden voltage drop is observed, which can be modelled with existing 2.8c. But when the cell is at rest after the pulse, a slow increase in cell voltage is observed (refer Figure 2.9 where from time = 5 min to time = 20 min, the cell is discharged, and from time = 20 min to time = 40 min, the cell is at rest). To model this phenomenon, Figure 2.8d includes a pair of resistor-capacitors connected in series with R_0. This modification describes 'diffusion voltage' demonstrating the slow diffusion of Li-ions towards the anode when kept at rest after discharge

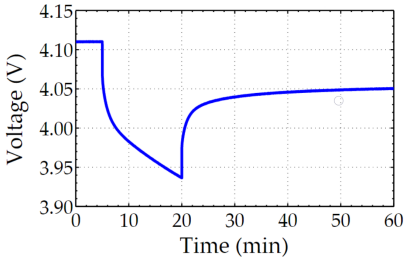

Figure 2.9: Voltage response to discharge pulse

The slow diffusion can also be demonstrated using a 'Warburg Impedence'. In literature, rarely any modelling circuits have used 'Warburg impedance', e.g. Randle's circuit. There is no exact differential equation that can model the Warburg impedance. Hence, ideally, Warburg impedance is described as infinite resistor-capacitor pairs connected in series. The reason for connecting RC pairs is that a Warburg impedance resembles a capacitor, as both have decreasing impedance with increased frequency. The difference is that the decrease in impedance with increasing frequency is greater for capacitors than Warburg impedance. Also, the phase response of the capacitor is -90^o and for Warburg impedance, it is -45^o. Hence, more RC pairs accurately model the diffusion voltages [45].

2.5. Reconfigurability in battery packs

Reconfigurability in battery packs refers to configuring connected individual cells/modules within the pack using strategically placed power switches. The fundamental behind reconfigurable battery packs is matching the cell level parameter with a specific load profile [14]. Researchers have put forth various reconfigurable topologies aimed at addressing the challenges encountered by conventional battery packs. This section provides a summarised overview of the reviewed literature, offering insights into the rationale behind incorporating reconfigurability and its implementation and practical applications.

2.5.1. Challenges faced by conventional battery packs

In conventional battery packs, the configuration is fixed according to the power and energy demand of the application. After several charge and discharge cycles, the characteristics of each cell inside a battery pack become vastly different. There are many reasons for this. First, all cells do not have the same initial parameters, such as capacity, internal resistance, SOC, etc., due to manufacturing variances. Second, over the number of cycles, all cells experience different power stresses, causing cell state imbalance due to the innate heterogeneity in the parameters, circuit design defects, employment of imperfect battery state estimators and varied thermal conditions inside a battery pack. This imbalance amplifies over multiple cycles as cells with lowered capacity get overcharged and over-discharged, causing further deterioration of the health of the cell. These cells are called weak cells, which weaken the battery pack's performance and lifespan. It also poses a threat of thermal runaway due to overcharging and discharging. To avoid this, a separate dedicated cell balancing circuit is employed to balance the states of cells connected in series for fixed-configuration battery packs. According to Ci, Lin, and Wu [14], as reconfigurable battery packs can adjust the cell configuration in real-time for specific load demands, reconfiguration according to the battery characteristics is also plausible. As a result, the battery lifespan can be extended without an additional balancing circuit.

Another challenge addressed by Kim and Shin [30] is that conventional fixed-configuration battery packs are unable to bypass the weak and faulty cells inside a battery pack, which ultimately causes the battery pack to be dysfunctional if not managed properly. These weak and faulty cells are a result of the imbalance explained earlier.

Kim, Qiao, and Qu [33] lists the challenges faced by the fixed configuration large-scale battery packs as follows:

- Low reliability and low fault tolerance under unusual operating conditions such as elevated temperature, over-charging/discharging and overcurrent

- Absence of reconfiguration according to cell states results in nonoptimal energy conversion efficiencies
- Absence of flexibility in dynamic power management resulting in nonoptimal performance
- Use of safety circuits prevents mishaps. However, it cuts off the whole battery system from the application
- To resolve imbalance, balancing circuits are employed. However, most of these circuits use dissipative resistors, leading to energy wastage. Recent works in cell balancing propose integrated circuit designs which use electronic converters to transfer the charge, which prove very costly and oversized for large-scale battery packs

Jin and Shin [28] addresses more relevant issues related to the large-scale battery packs an automotive application as follows:

- The existing reconfigurable techniques cannot fully utilise the battery pack's capacity for demanded power as the reconfiguration restricts the number of cells connected in series and parallel on conditions of equal voltage and current. Thus, even if there are enough cells to fulfil the demand, it fails to satisfy it
- To avoid the risk of switching hazards, sequential switching is usually incorporated, which makes the reconfiguration time proportional to the number of switches in the circuit. Thus, longer reconfiguration delays prolong failure recovery and power allocation
- Existing reconfiguration techniques ignore the backup number of cells required to ensure the proper functioning of the battery pack, which either compromises the operation of the battery pack due to several backup cells or surplus backup cells are required to maintain the demand of power needed

2.5.2. Proposed reconfigurability techniques

DESA

DESA stands for Dependable Efficient Scalable Architecture, which uses hierarchical management of cells. A local BMS consist of a battery cell array, local controller, sensors and CAN module. A global BMS consist of a global controller and CAN module. Through CAN communication, the global BMSs control multiple local BMS. These BMSs follow a monarchy-based centralised relationship.

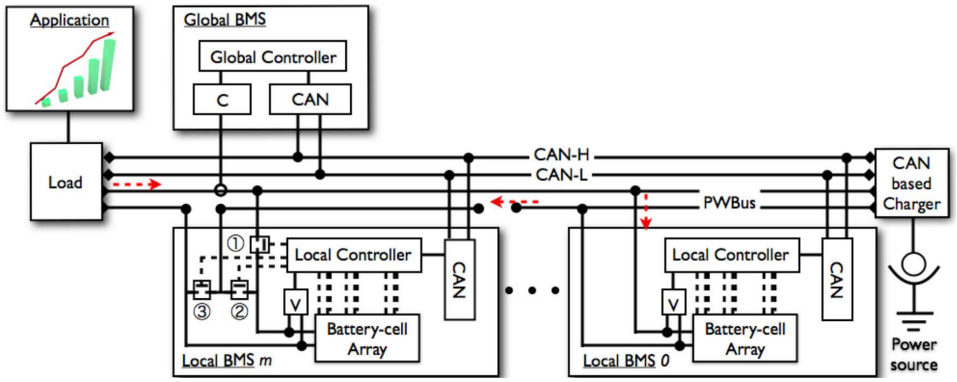

Figure 2.10: DESA schematic [30]

As shown in Figure 2.10, three switches are employed per local BMS namely switch #1 as P-switch, switch #2 as S-switch and switch #3 as B-switch. B-switch and S-switch bypass or connect the cell array in series, respectively. The p-switch makes the circuit open. A three-digit code corresponds to the respective switches for different types of connections shown in Table 2.2. These commands at array level are controlled by the global BMS and cell level (if employed) are controlled by the local BMS

Type	NULL	INIT	BYPASS	PARALLEL	SERIES
Code	000	100	001	101	010

Table 2.2: Connection type and code [30]

Dynamic reconfigurable framework by Kim and Shin [31]

This framework aimed to address two primary concerns: firstly, enhancing fault tolerance by bypassing identified faulty cells or modules, and secondly, providing different output voltages tailored to different applications, as diverse loads are connected to large-scale battery packs.

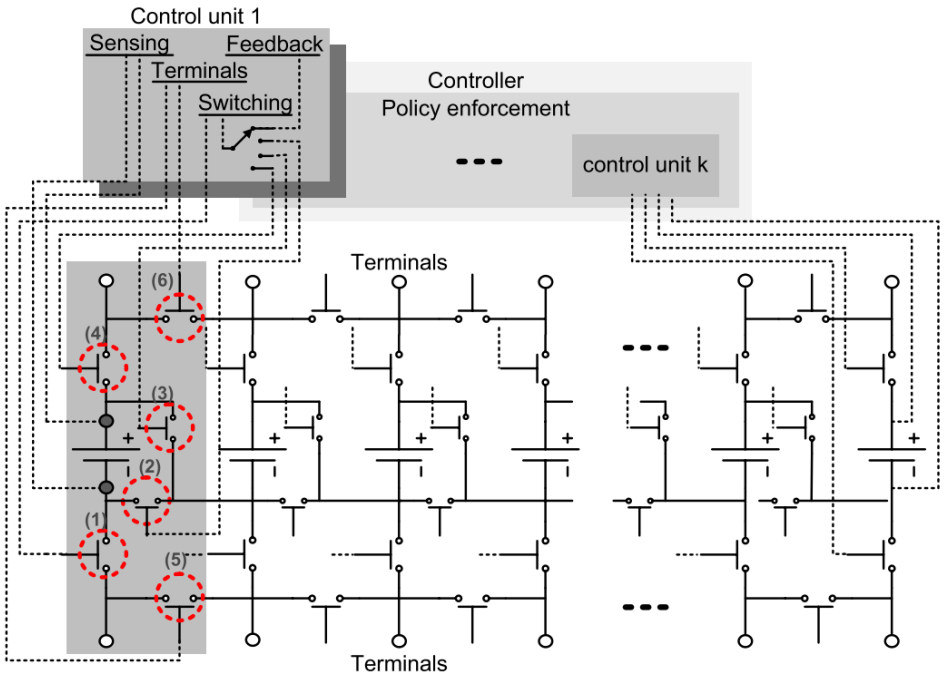

Figure 2.11: Schematic of dynamic reconfiguration framework [31]

A syntactic and semantic bypassing mechanism is used where the syntactic mechanism provides a set of rules for the reconfiguration, and the semantic mechanism reconfigures the cell structure by keeping the supply voltage constant for a certain application or dynamic voltage for multiple applications online. Six switches are placed around each cell to gain a high level of flexibility (refer Figure 2.11). These switches are used for a similar function as mentioned in DESA. Control units monitor cell SOC by Coulomb counting method and estimate voltage using Kalman filter.

Further development on this technique is done by Jin and Shin [28], where power trees are used to model the cell connection, enabling full utilisation of the battery pack's capacity and providing required power. A power tree contains several ways a specific series X parallel combination can be arranged. It can be visualised as an inverted tree with the entire battery pack configuration size as the root and indivisible subpack sizes as the leaves. The pack of cells is divided into sub-packs through series and parallel connections, dividing a pack with dimensions (Ns × Np) into a set of n sub-packs (Nsi × Npi), where i = 1, 2...n. This division continues until it cannot be further divided, known as the atomic node. However, the extent of division is determined by the maximum and minimum number of power levels. This approach incorporates features like Fast Failure Recovery (FFR) and Fast Power Reallocation (FPR). Through this power tree-based implementation, the number of extra cells has also been optimised and reduced to an optimal amount. The battery connections are set up so that fewer switches are required for fault tolerance, unlike 2.11.

Self-X by Kim, Qiao, and Qu [33]

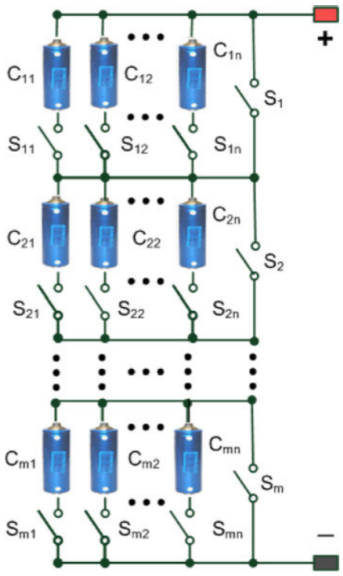

Figure 2.12: Schematic of Self-X topology

This work is an extended version of the previous work [32]. Self-X stands for self-reconfiguration, self-optimisation, self-balancing and self-healing. Each string containing N cells in parallel has an option to connect or isolate them using a dedicated switch. When M of these strings are linked in series, they can be bypassed using one switch per string. Consequently, a total of M X (N+1) switches are necessary to operate this topology. The main advantage of this design is the reduced number of switches per cell (refer to Figure 2.12). However, this causes much less flexibility in connections and can not connect two cells of different strings in parallel or two cells of the exact string in series. Monitoring is done by developing a hybrid cell model based on ECM and kinetic battery model, which captures nonlinear variations in capacity.

Work by Viswanathan, Palaniswamy, and Leelavinodhan [65]

The authors reviewed the existing reconfigurability techniques in this study and provided brief information about each. Also, Table 2.3 presented a comparison in properties of existing reconfiguration techniques. The authors propose a novel approach that bears a resemblance to DESA. However, they highlight a distinction: a monarchy-level relationship is employed in DESA. This places significant reliability pressure on the central controller, as a failure in it would lead to the entire system failing. The study also implemented the optimised number of cells and connections to cater to load demand.

Sr. No.	Topology type	Switches per cell	Increase in operating time	Increase in reliability	Configurability	Scalability	Hardware complexity	Computational complexity
1	DESA	NA (3 per battery array)	High	High	Medium	High	Medium	Medium
2	Dynamic reconfigurable framework	6	High	High	High	Medium	High	High
3	Power tree	3	High	High	High	High	High	High
4	Self-X	2	Medium	Medium	Medium	Low	Medium	Low

Table 2.3: Comparison of different reconfiguration techniques

2.6. Research gap

Upon extensive literature review spanning diverse disciplines, including electric aircraft, battery technologies, large-scale battery packs, and the concept of reconfigurability. In studies regarding electric

aviation, the recurring obstacle of heavy-weight battery packs is addressed, posing a significant challenge to achieving extended range in fully electric aircraft. Due to the innovative and relatively nascent nature of aircraft battery pack design, many research findings in this area remain confidential within aviation companies. Consequently, the details regarding the advanced battery technologies utilised in electric aircraft that have successfully undergone test flights remain undisclosed.

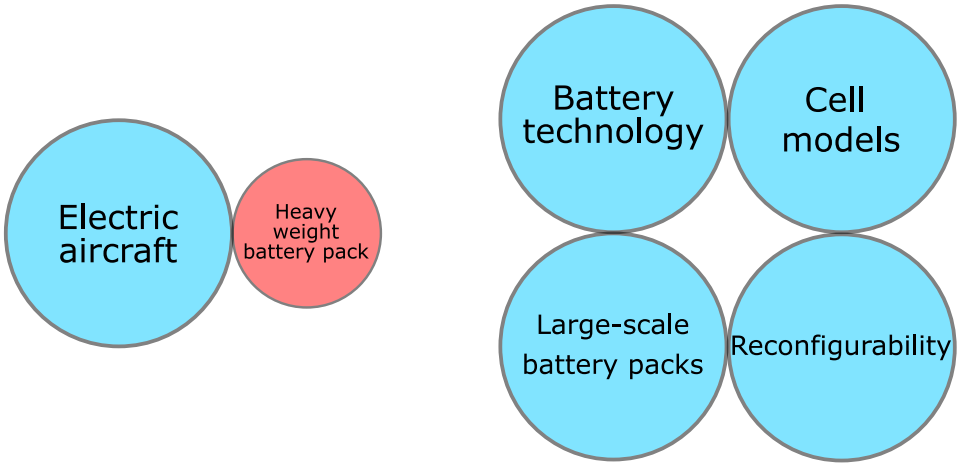

Figure 2.13: Pictorial representation of the literature clusters

It is evident that a research intersection exists between battery technologies and cell models, as well as between cell models and large-scale battery packs with reconfigurability. However, what is notably absent is an intersection encompassing all these elements, which could potentially provide a solution to the issue of heavy-weight batteries in fully electric aircraft. The concept of reconfigurability is frequently discussed as a fault tolerance technique. Nevertheless, as outlined in section 2.5, studies also emphasise its potential in enabling the optimal number of cells to make full use of battery pack capacity. While this feature has been explored conceptually in literature, its practical application remains unaddressed. Figure 2.13 pictorially describes the detached link. Therefore, this study centres on the potential for weight reduction by integrating reconfigurability in battery packs designed for electric aircraft. Given the limited availability of data on power profiles and battery pack specifications for electric aircraft, there is a pressing need to develop a battery pack uniquely tailored for these aircraft, with a primary emphasis on reducing weight and enhancing energy efficiency.

3

Aircraft and Power Profile

The design of a battery pack is tailored to the specific application and its corresponding power profile. In this chapter, the rationale behind the reference aircraft selection and the calculations about the power profile are presented in section 3.1 and section 3.2 respectively. Moreover, the calculation of system-level voltage for minimal power cable weight and energy losses are elaborated in section 3.3. These calculations are a function of the aircraft's peak power and hence are presented after the power profile calculations.

3.1. Reference aircraft selection

Electric aviation is a modern aviation industry, and unlike conventional aircraft, technological maturity is at a very primitive stage. As discussed in section 2.1, many conceptual designs with varied technologies are presented in the literature, and the possibility of these design rolling out of an aircraft hanger are quite uncertain due to many reasons such as technological readiness, level of complexity, cost and its purpose in the near future. Literature studies conducted by Schwab et al. [55], Sahoo, Zhao, and Kyprianidis [53], Rendón et al. [50] present assessments of upcoming aircraft in detail. Also, the technological assessment is carried out for different subsystems in literature studies by Dever et al. [17] and Gnadt et al. [23]. Reviewing this literature resulted in narrowing the choice of reference aircraft. It also indicated the unavailability of data due to aircraft manufacturing companies' secrecy of aircraft specifications. Following were the selection criteria for finalising the reference aircraft:

Filters	Criteria
Type	Narrow body
Status	Under development
Powertrain	Fully electric

Table 3.1: Reference aircraft selection criteria

The reasons behind the selection criteria mentioned in Table 3.1 are as follows:

- Narrow-body aircraft are utilised more than wide-body or any other type of aircraft for commercial flights [71, 72]
- Many conceptual designs make use of futuristic technologies and estimated figures. The companies in the manufacturing phase must employ the SoA technologies or at least recent realistic improvements that have yet to be disclosed. Considering such aircraft as a reference will give a more realistic approach to the battery design
- For short-haul flights, the fuel consumption corresponding to CO_2 emissions per Revenue Passenger Kilometre (RPK) is more than long-haul flights. Hence, the short-haul flight segment's electrification can realise more emissions reductions [56]. Therefore, although fuel cell-powered or hybrid

powertrain aircraft can realise long-range flights, fully electric powertrain aircraft are ideal candidates for short-haul flights

Eviation Alice, Wright One and Ampaire Tailwind-E satisfied all the criteria from the list of aircraft mentioned in a study by Gnadt et al. [23]. Eviation Alice has released some specifications which can help estimate the aircraft's power profile. Wright Electric's website shows they are now focused on the electric propulsion system of the existing BAe 146 and Lockheed C-130 [69, 70]. Ampaire Tailwind-E is still a concept as the company has not provided information regarding the aircraft on their website [4]. Hence, Eviation Alice is finalised as the reference aircraft. Moreover, Eviation conducted the maiden flight of Alice in September 2022, which is considered a major milestone in the electric aviation sector. Table 3.2 and Figure 3.1 presents the specifications found on the website of Eviation Alice as of August 2023 and the further detailed specifications found in the analysis report by Russo [51]:

Specifications on website	
Max operating speed	260 ktas = 481.52 km/h
Day VFR range	250 nm = 463 km
Maximum Take-Off Weight (MTOW)	18,400 lbs = 8346.1 kg
Landing distance (MTOW, ISA, sea level, dry)	2,040 ft = 621.8 m
Take-off distance (MTOW, ISA, sea level, dry)	2,750 ft = 838.2 m
Useful payload (commuter)	2,500 lbs = 1134 kg
Propulsion motor	2 x magni650
Power output	700 kW each
Specifications from analysis report	
Wing surface area (A)	28.9 m2
Aspect ratio (AR)	12.7
Parasitic coefficient of drag (C_{D_0})	0.029
Maximum Lift to Drag ratio (L/D)	18.5
Velocity to achieve maximum range	152 knots = 281.5 km/h
Propeller efficiency (η_{prop})	0.85
Electric motor efficiency (η_{em})	0.93
Inverter efficiency (η_{inv})	0.98
Cable efficiency (η_{cable})	0.98

Table 3.2: Eviation Alice specifications [3, 51]

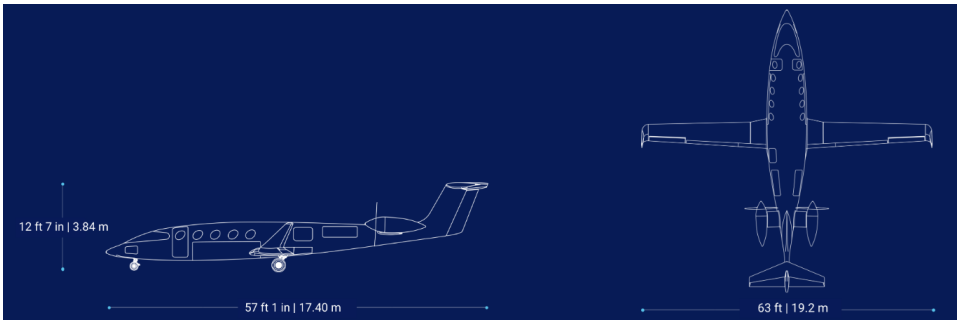

Figure 3.1: Model design of Eviation Alice [3]

Based on the above specification and some assumptions, the power profile for each phase of the flight trip is calculated and presented in the next section.

3.2. Power profile calculation

A power profile is obtained to design the battery pack specifically for that application. A power profile is the amount of power the application demands to complete the operation successfully. In the case of Conventional Take-Off and Landing (CTOL) aircraft, the power profile is divided mainly into eleven different phases shown in Figure 3.2 [15, 29]. The power demanded for these phases is vastly different. Hence, the calculation for each phase is shown separately, followed by the energy requirement per phase ($Energy = Power * Time$)

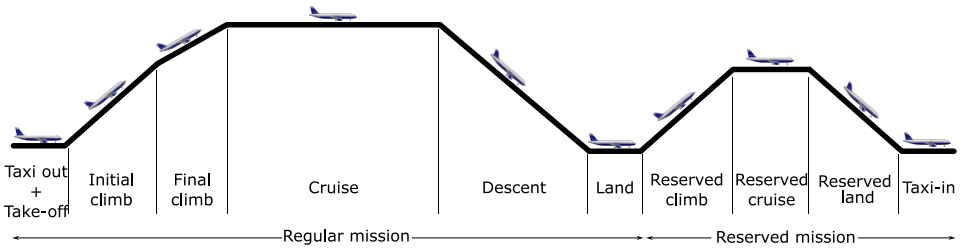

Figure 3.2: Flight trip phases

3.2.1. Taxiing

Taxiing is a self-powered ground movement of an aircraft from the parking position to the runway trip or vice versa. Depending upon the airport size and traffic, the time required for taxiing usually changes, hence the energy requirement. For reference, the mean of the taxi time data collected by Eurocontrol for the summer of 2021 for 567 airports around the globe is used for calculations [62]. The mean taxi time data is rounded to 6 minutes one way.

The power profile calculation of this phase involves the following assumptions:

- Non-stop taxiing with a constant velocity. The taxiing speed changes as per different airports, safety norms and Air Traffic Control (ATC) instructions. Generally, the speed is between 20 to 30 km/h. Hence, for calculations speed is 25.2 km/h = 7 m/s [74]
- Coefficient of Drag (C_D) at taxiing is equal to C_D at cruise equal to 0.029 i.e. C_{D_0}, as induced drag is insignificant [51]
- Due to the low velocity, the contribution of the lift force is negligible. As a result, the normal reaction is equal to the weight. Further explanation can be found below
- The forces exerted on the aircraft include friction and drag forces, with no additional forces resulting from factors such as gradient

Equation 3.1, Equation 3.2, Equation 3.3 and Equation 3.4 are the expressions for Frictional force (F_F), Drag force (F_D), Normal reaction (N) and Lift force (F_L) respectively.

$$F_F = \mu \, N \tag{3.1}$$

$$F_D = \frac{1}{2} \rho \, C_D \, A \, v_{taxi}^2 \tag{3.2}$$

$$\begin{aligned} N &= MTOW \, g - F_L \\ &= MTOW \, g \qquad (\because MTOW \, g >> F_L) \end{aligned} \tag{3.3}$$

$$F_L = \frac{1}{2} \rho \, C_L \, A \, v_{taxi}^2 \tag{3.4}$$

where,

μ : Coefficient of rolling friction = 0.03 [22]
ρ : Air density
v_{taxi} : Taxi velocity
C_L : Coefficient of lift

In Equation 3.4, although the Coefficient of lift (C_L) is unknown, after plugging in the other values mentioned previously, the lift force is relatively insignificant compared to the weight of the aircraft (Weight (W) = MTOW * 9.81) and hence neglected as mentioned in third assumption. Equation 3.5 gives Power (P) required for taxiing providing Thrust (F_T) at a certain velocity v_{taxi}. Refer to Equation 3.1, Equation 3.2, Equation 3.3, Equation 3.4 and Figure 3.3.

$$\begin{aligned} P &= \frac{F_T \, v_{taxi}}{\eta_{prop} \, \eta_{em} \, \eta_{inv} \, \eta_{cable}} \\ &= \frac{(F_D + F_F) \, v_{taxi}}{\eta_{prop} \, \eta_{em} \, \eta_{inv} \, \eta_{cable}} \\ &= \frac{(\frac{1}{2} \rho \, C_D \, A \, v_{taxi}^2 + \mu \, W) \, v_{taxi}}{\eta_{prop} \, \eta_{em} \, \eta_{inv} \, \eta_{cable}} \end{aligned} \tag{3.5}$$

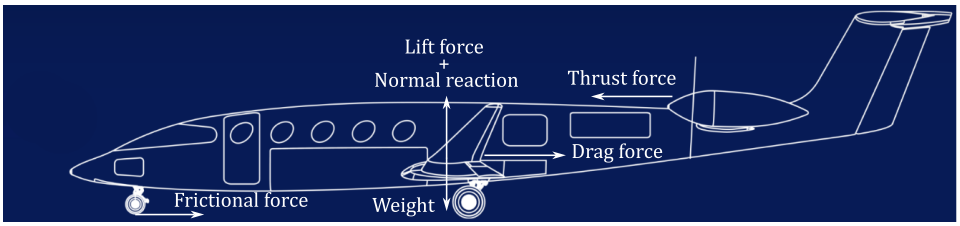

Figure 3.3: Forces acting on the aircraft

3.2.2. Take-off

The take-off phase achieves a certain velocity to lift the aircraft off the ground. The distance covered while gaining this velocity is called the take-off distance. In this phase, the aircraft is in contact with the ground. Hence, the forces acting on the aircraft are similar to Figure 3.3. In this phase, flaps are also extended to generate more lift. Hence, the lift force is significant in this phase given by Equation 3.4. The value for C_L depends on aircraft geometry and aerodynamic data, which is not revealed by the aircraft company of the reference aircraft. Eviation Alice aircraft geometry highly correlates with Cessna Citation III, and considering the C_L at take-off between 1.5-2 is a reasonable assumption for these aircraft types. Thus, C_L value of 1.7 is considered for the calculation.
Take-off is successful when the normal reaction on the aircraft is equal to zero. That implies, at some instantaneous moment, the lift force (Equation 3.4) should be in equilibrium with the weight of the aircraft. The Take-off velocity (v_{TO}) required to achieve that is given by Equation 3.6:

$$v_{TO} = \sqrt{\frac{MTOW \, g}{\frac{1}{2} \rho \, C_L \, A}} \tag{3.6}$$

The initial velocity of the aircraft on the runway is zero, and to attain the velocity of v_{TO} in a certain Take-off distance (d_{TO}) (mentioned in Table 3.2), the acceleration (a_{TO}) during this phase is given by:

$$a_{TO} = \frac{F_T - F_F - F_D}{MTOW} \tag{3.7}$$

The thrust F_T varies inversely with the velocity of the aircraft given by:

$$F_T = \frac{P_{max} \, \eta_{propTO} \, \eta_{em}}{v_{TO}} \tag{3.8}$$

Here, the η_{prop} value is entered, obtained by the following expression, where thrust is static thrust for the first time step. Further, the η_{prop} is calculated for the previous thrust value and henceforth.

$$\begin{aligned} \eta_{propTO} &= \frac{2}{1 + \sqrt{1 + T_c}} \\ T_c &= \frac{2 \, F_{T(t-1)}}{n \, \rho \, {v_{TO}}^2 \, \pi \, R^2} \end{aligned} \tag{3.9}$$

where,
n : Number of propellers
and at v_{TO} = 0 m/s, static thrust is given by: [41]

$$F_{T static} = 1.283 * 10^{-12}\ RPM^2\ (2\ R)^4\ \rho\ K_t\ g \tag{3.10}$$

where,
RPM : Rotations per minute of propeller
R : Radius of the propeller (in inches)
ρ : Air density
K_t : Static thrust coefficient = 0.73 [41]

The F_F is given by:

$$F_F = \mu\ (MTOW\ g - \frac{1}{2}\ \rho\ C_L\ A\ {v_{TO}}^2) \tag{3.11}$$

The F_D is given by:

$$F_D = \frac{1}{2}\ \rho\ A\ {v_{TO}}^2\ ({C_{D_0}} + \frac{{C_L}^2}{\pi\ AR\ e}) \tag{3.12}$$

where,
e : Oswald factor = 0.83 [51]

Operating the Electric Motor (EM)s at the manufacturer-specified maximum operating point for this phase is a more practical approach, so the P_{max} for the aircraft is known. However, the above procedure is followed to determine the takeoff time and ensure the take-off is achieved in the given distance. The takeoff time determined is rounded up to ~30 seconds.

3.2.3. Initial and final climb

The initial climb phase is when the aircraft has become airborne after takeoff. The aircraft pitches upward, forming an angle with the ground known as the pitch angle. This angle is a highly crucial factor in determining the forces acting on the aircraft(shown in Figure 3.4 as Pitch angle (θ)).

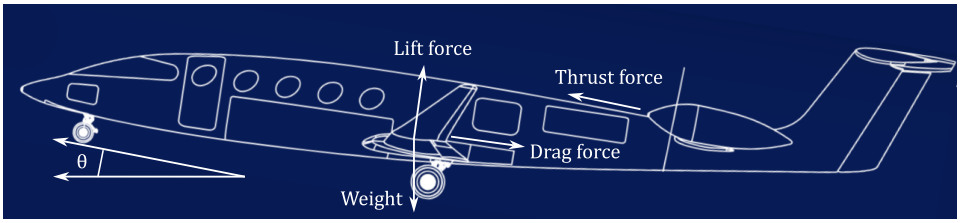

Figure 3.4: Forces acting on the aircraft in climb phase

Again, it is a practical approach to continue operating the EMs at a maximum operating point similar to take-off for the initial climb phase. This phase's initial velocity will be the take-off phase's final velocity. The lift and drag forces are calculated as per Equation 3.4 and Equation 3.2. In the climbing phase, the propeller efficiency is given by:

$$\eta_{propcl} = \frac{2}{1 + \sqrt{1 + T_c}} \tag{3.13}$$

where,

$$T_c = \frac{2\ F_T}{n\ \rho\ v_{cl}^2\ \pi\ R^2} \tag{3.14}$$

where,

n : Number of propellers

ρ : Air density (inversely proportional to the altitude)

v_{cl} : Velocity of climb

R : Radius of propeller

At a given power and velocity, re-arranging the first expression in Equation 3.5 gives a relationship between F_T and η_{prop}. Substituting T_c from Equation 3.14 in Equation 3.13 gives another relationship between F_T and η_{prop}. Solving Equation 3.5 and Equation 3.13 simultaneously gives the values for thrust and propeller efficiency at a given velocity.

Due to the pitching of the aircraft, acceleration is in the vertical direction as well as the horizontal direction. The two accelerations are given by:

$$a_h = \frac{F_T\, cos\theta - F_D\, cos\theta - F_L\, sin\theta}{MTOW} \tag{3.15}$$

$$a_v = \frac{F_L\, cos\theta + F_T\, sin\theta - W - F_D\, sin\theta}{MTOW} \tag{3.16}$$

The angle between the resultant of these two accelerations and the longitudinal axis of the aircraft is given by:

$$a = \sqrt{a_h^2 + a_v^2} \tag{3.17}$$

$$\beta = tan^{-1}(\frac{a_v}{a_h}) - \theta \tag{3.18}$$

if a_h is negative:

$$\beta = tan^{-1}(\frac{a_v}{a_h}) + 180^o - \theta \tag{3.19}$$

Therefore, the increase in velocity of the aircraft in the direction of pitch is given by:

$$\delta\, v_{cl} = a\, cos\beta\, \delta t \tag{3.20}$$

The Vertical velocity (v_v) and Altitude (s) gained is given by:

$$v_v = v_{cl}\, sin\theta \tag{3.21}$$

$$\delta s = v_v\, \delta t \tag{3.22}$$

Since the pitch angle θ is not known, a range of θ from 2^o to 15^o was chosen for each of which v_v and δs are calculated. The initial climb aims to gain a certain altitude and accelerate the aircraft to its cruising velocity. After gaining that velocity, the aircraft reaches the cruising altitude in the final climb phase. The demarcations between these two phases are subtle and can be influenced by weather conditions, flying techniques, and instructions provided by ATC. The thrust setting in the final climb phase is usually 75-80% of the maximum thrust setting, meaning the EMs are operating at 75-80% of the maximum operating point [51]. Therefore, after putting the power value for the initial climb phase, the cruise velocity was roughly achieved at 30 seconds. The final climb phase achieved the cruising altitude of 10,000 ft in 6 minutes when the pitching angle was 8^o. These values closely match those mentioned in the analysis report by Russo [51]. Additionally, the rate of climb of Eviation Alice mentioned in a study by Shadbolt [57] is 2000 ft/min, which also roughly matches the calculated rate of climb of 1538.46 ft/min.

3.2.4. Cruise

The cruising phase refers to a phase of flight during which an aircraft maintains a steady level of altitude and speed over a longer distance, typically after it has climbed to its intended cruising altitude. This phase is a significant part of a flight. For calculations, the cruising altitude is 10,000 ft, and the cruising speed is

152 knots = 281.5 km/h [51]. During this phase, the forces acting on the aircraft are balanced in vertical and horizontal directions. The value of thrust required is given by:

$$F_T = \frac{1}{2}\rho_{alt}\left(C_{D_0} + \frac{MTOW}{\frac{1}{2}\rho_{alt} A v_{cr}^2}\right) A v_{cr}^2 \tag{3.23}$$

where,

ρ_{alt} : Air density at cruising altitude

v_{cr} : Cruising velocity

After determining F_T, using Equation 3.5, 3.14 and 3.13. The power required for this phase can be determined.

3.2.5. Descent and Land

This phase occurs after cruising, where the aircraft starts to drop altitude. Although gliding is a viable option in e-aviation to save energy, in this study, the propulsion system is in operation as a safety measure in this phase. The angle by which the descent (Descent angle (θ_D)) takes place decides the power required to maintain the velocity. The deceleration is in the direction of descent, meaning there is a horizontal and vertical component of deceleration that should be considered. The thrust required is given by:

$$F_T = \frac{F_D\, cos\theta_D + MTOW\, a_{hd} - F_L\, sin\theta_D}{cos\theta_D} \tag{3.24}$$

and

$$F_T = \frac{F_D\, sin\theta_D + MTOW\, a_{vd} + F_L\, cos\theta_D - W}{sin\theta_D} \tag{3.25}$$

There are two equations, but more than two unknowns, F_L and F_D, are quite challenging to calculate as the air brakes are deployed in both phases, changing the C_D and C_L values. Also, the change in altitude vastly depends on the instructions provided by ATC. Hence, due to a lack of aerodynamic information to calculate power requirements, values mentioned in the analysis report of Russo [51] are used.

3.2.6. Missied approach

This phase is crucial as unprecedented circumstances cause difficulty in landing the aircraft safely, and the aircraft is commanded to regain a certain altitude and retry the approach to land. In such cases, similar to the initial climb phase, high power is demanded to gain a certain altitude again. This height varies from region to region, and the regulations in the EU say that the altitude needs to be 500 ft clear of the tallest building in a certain amount of range [16]. Hence, it is reasonable to assume that the altitude needs to be equal to the altitude after the initial climb, which is ~ 1000 ft. Thus, the time and power required are the same as the initial climb phase. This phase is named the reserved climb phase.

Furthermore, according to the Eviation Alice website, the aircraft is designed for a day VFR range, meaning the aircraft must contain reserved energy for flying 30 minutes extra at cruising speed. Thus, the time for this reserved cruise phase is predefined, and power is equal to cruising power. Finally, the re-approach is named the reserved landing phase, where the time and power are identical to the ordinary landing phase.

3.2.7. Results

Phase	Duration (seconds)	Cabin Power (kW)	EM Power (kW)	Total Power (kW)	Cabin Energy (kWh)	EM Energy (kWh)	Total Energy (kWh)
Taxi	360	60	47.82	107.82	6	4.78	10.78
Takeoff	30	60	1553.2	1613.2	0.5	12.94	13.44
Initial climb	30	60	1553.2	1613.2	0.5	12.94	13.44
Final climb	360	60	1164.9	1224.9	6	116.49	122.49
Cruise	1980	60	462.63	522.63	33	254.45	287.45
Descent	360	60	130	190	6	13.00	19
Landing	120	60	200	260	2	6.67	8.67
Reserve Initial climb	30	60	1553.2	1613.2	0.5	12.94	13.44
Reserve cruise	1650	60	462.63	522.63	27.5	212.04	239.54
Reserve landing	120	60	200	260	2	6.67	8.67
Taxi	360	60	47.82	107.82	6	4.78	10.78
Total	**5760**	-	-	-	**96**	**657.70**	**753.70**

Table 3.3: Power and energy values

Table 3.3 shows the values of power and energy demanded in total and per phase. The cabin power values take into account the auxiliary power demands. In this study, cabin energy is considered solely to contribute to the overall energy calculation of the battery pack's total energy [20]. The time duration of each phase, excluding the cruise phase, is either calculated or derived from the literature [51]. The battery pack's total energy for the Eviation Alice aircraft is documented as 820 kWh [57]. To be well within the limits, a 750 kWh mark was set. After the calculation, the energy value 753.7 kWh was determined. By subtracting the energy consumption of other phases from the total energy of 753.70 kWh, the duration of the cruise phase is estimated. This duration, equal to 1980 seconds (33 minutes), corresponds to a cruising range of approximately 155 km, considering the cruise speed of 281.5 km/h. Although the range mentioned on the website of Eviation Alice claims a 250 nm day VFR range, which translates to 463 km [3], the cruising speed, in this case, is different compared to the one used for the range calculation on the website. Note that the range mentioned on the website is still very optimistic as expected advancements in battery technology have not been realised, making the entry into service delay from 2024 to 2027 [18]. Additionally, the calculation of distance covered during other phases is omitted, given its variability from flight to flight. If incorporated, accounting for the distances covered in other phases would increase the estimated total range.

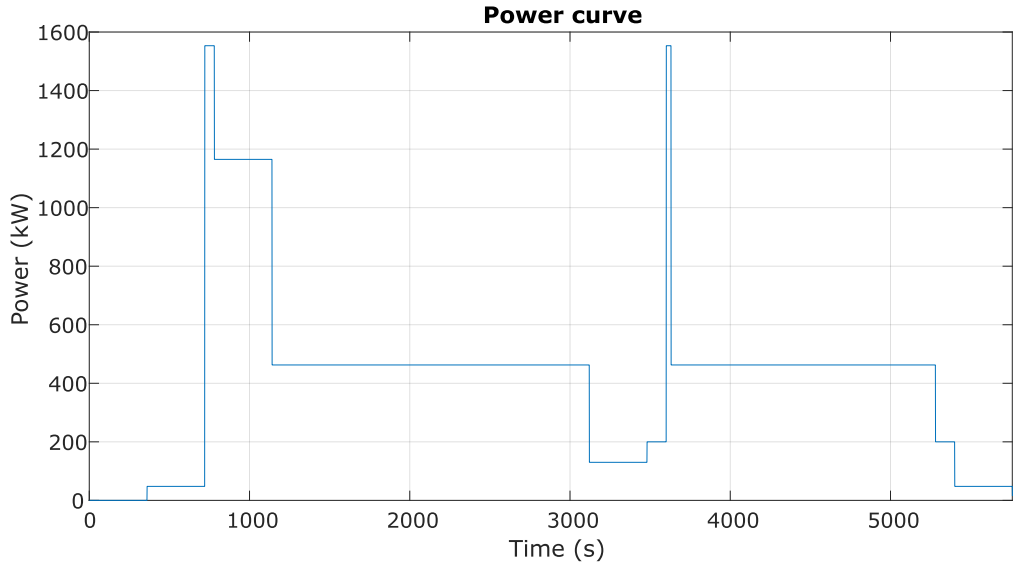

Figure 3.5: Power profile

In Figure 3.5, the power profile of the full flight trip as calculated in 3.2 is displayed. The first 360 seconds (6 min) is the boarding period. Hence, no power from the battery is demanded. Refer to Figure 3.2 to follow the order of phases in the power profile. Note that this power profile considers all the efficiency and power losses occurring in the powertrain. Hence, this power profile is directly the battery power demanded at a specific point in time.

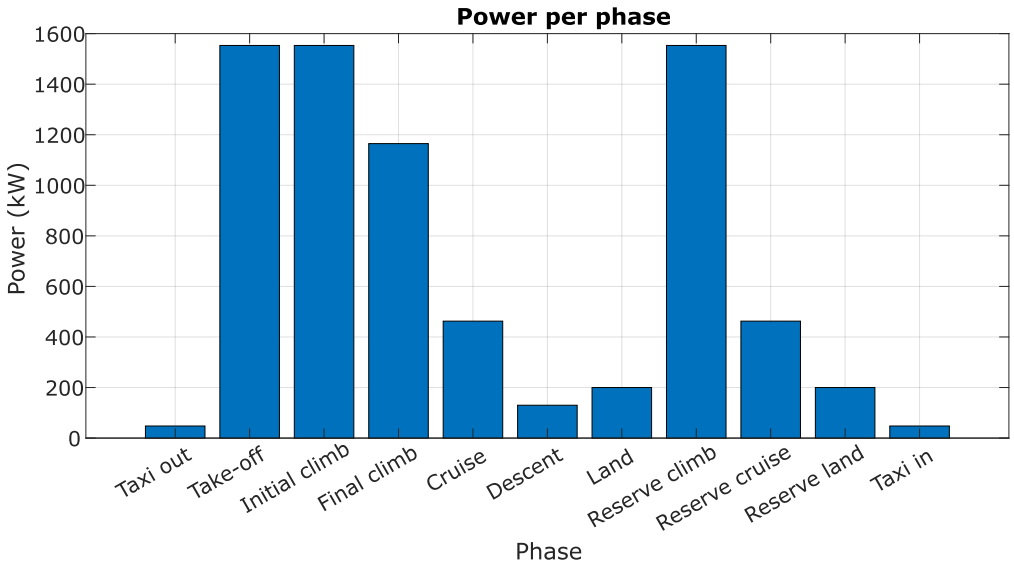

Figure 3.6: Power per phase

Figure 3.6 compares the power demanded from the battery in each phase, and Figure 3.7 compares the energy required from the battery per phase. It is observed that, for take-off, the initial and final climb, the power requirement is very high and due to the smaller time duration, the energy requirement is quite low. This factor significantly influences the sizing of the battery pack and will be further elaborated upon in the subsequent chapter.

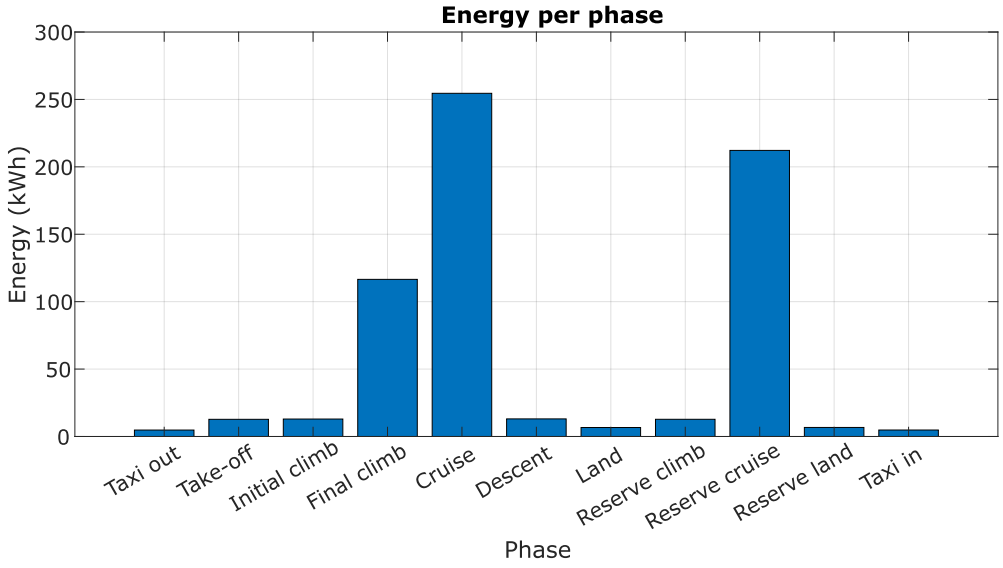

Figure 3.7: Energy per phase

3.3. System voltage calculation

A battery pack can be configured to deliver voltage matching the system-level voltage, allowing it to directly connect to power cables without requiring a DC-DC converter. While a DC-DC converter is essential for safety, its efficiency can be maximised due to the potentially insignificant difference between the battery's terminal voltage and the system-level voltage [67].

Electrification of the propulsion system involves the connection of the battery to the EMs through power cables. Although it is said that the efficiency of electric powertrains is higher than conventional powertrains, high power requirements through power cables might cut down these advantages in terms of copper losses. To avoid these losses, boosting system-level voltage is necessary. The N3-X design study by NASA recommended incorporating a minimum voltage threshold of 6 kV to take advantage of the weight reduction benefits at the system level [53]. Increased system-level voltage requires a thicker insulation layer, increasing the power cables' weight. Hence, finding the optimal system-level voltage value for this aircraft to have lightweight power cables is necessary.

A power cable consists of multiple layers, and to achieve a cable with reduced weight, it's essential to ascertain the thickness of these individual layers. Figure 3.8 shows the layers of a power cable. This study approximates the inner and outer semiconducting layer as one, and the jacket layer's weight is neglected. The semiconducting and conducting shield layers typically have standard thickness values irrespective of the other design parameters. For calculations, the thickness of the semiconducting layer (t_{sc}) is considered to be 1.2 mm [42]. Although the study referred to is for underground cables, the voltage class is similar, and the purpose of the semiconducting layer is to smooth out the voltage over the conductor's surface. The thickness of the conducting shield (t_s) in industrial applications is usually between 1 mm to 2 mm [5]. Thus, it is assumed to be 2 mm. As a result, the variables to be minimised come down to the conductor's thickness and the insulation's thickness. A range of voltages from 700 V to 9000 V is chosen for which the thicknesses are calculated, and the voltage value with minimum power cable weight is finalised as the system voltage. Given that the battery is located in the belly of the aircraft and the EMs are aft-mounted, considering the geometry of the Eviation Alice, the cable length is estimated to be 20 meters long [18, 3]. For the weight calculation, the weight of a single cable is estimated as the quantity is linearly scalable for the optimal system voltage.

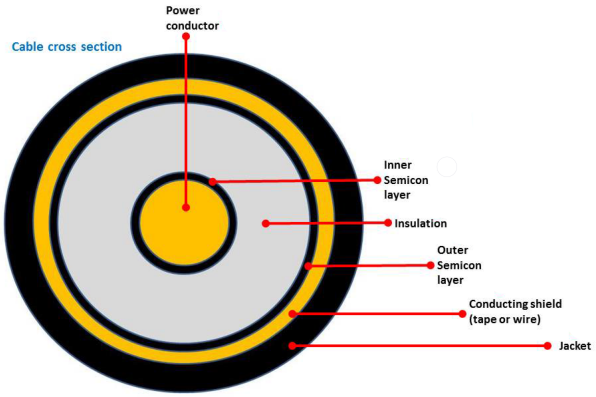

Figure 3.8: Layers inside a power cable [59]

3.3.1. Conductor sizing

The two conductor materials widely used in power cables are copper and aluminium. While selecting the appropriate material, there are two criteria where these two materials differ:

- The density of aluminium (2700 kg/m^3) is much less compared to the density of copper (8900 kg/m^3)
- The conductivity of copper (58.7 × 10^6 S/m) is comparatively higher than aluminium (36.9 × 10^6 S/m)

$$\frac{R}{l} = \frac{1}{\sigma\, A} \tag{3.26}$$

$$\frac{m}{l} = \rho_c\, A \tag{3.27}$$

where,

R : Resistance of the conductor
l : length of the conductor
σ : conductivity of the conductor
A : cross-sectional area of the conductor
m : mass of the conductor
ρ_c : density of the conductor

The Equation 3.26 and 3.27 are written per unit length as the cable length remains unchanged for both materials. For the same resistance value per unit length of the conductor, the aluminium conductor has a cross-sectional area of 1.59 times that of a copper conductor. Even with the increased cross-sectional area, the mass of the aluminium conductor would be less as the density of copper is almost 3.3 times more than that of aluminium. Since the application is weight-sensitive, aluminium is preferred over copper as a conductor.

It is known from power profile calculation that the take-off phase requires peak power from the battery. A reasonable voltage drop of 2% over the power cable is considered for the calculation. Hence, with the above information, the permissible value of conductor resistance is calculated by:

$$I = \frac{\mathrm{P}}{V_{max}\ 0.98} \tag{3.28}$$

$$V_{loss} = 0.02\ V_{max} \tag{3.29}$$

$$R = V_{loss}/I \tag{3.30}$$

It is important to consider that the power lost gets converted into heat, which further increases the resistance of the conductor. Therefore, the value of R in Equation 3.30 needs to include the increased resistance due to temperature. Then, the permissible conductor resistance is given by:

$$P_{loss} = I^2\, R \tag{3.31}$$

$$\Delta T = \frac{P_{loss}}{\pi\, l\, k} \tag{3.32}$$

$$R_{ref} = \frac{R}{1 + \alpha_r\, \Delta T} \tag{3.33}$$

where R_{ref} is the temperature independent resistance of conductor, k is the thermal conductivity (W/(m^{o}C)) of aluminium and α_r is the temperature coefficient of resistance ($/^oC$) of aluminium. The radius of the cylindrical conductor is given by:

$$r = \sqrt{\frac{l}{\sigma\, R_{ref}\, \pi}} \tag{3.34}$$

The conductor mass is calculated by multiplying the conductor density with the volume of the conductor:

$$M_c = \rho_c\, \pi\, r^2\, l \tag{3.35}$$

3.3.2. Insulator sizing

Single Void Discharge (SVD) method used by Cheng [13] is employed for calculating the thickness of the insulation layer. Insulator material used widely in aviation power cables is Cross-linked polyethylene (XLPE) [40]. The Dielectric permittivity (ϵ) of XLPE is 2.3, and the density is 930 kg/m^3. The Equation 3.36 gives the thickness of the insulation for a specific voltage value (V_{max}) and void limit (d_v).

$$t_i = r\left(exp\left(\frac{K\,V_{max}\;d_v}{\alpha\,r}\right) - 1\right) + C \tag{3.36}$$

$$K = \frac{3\,\epsilon}{1 + 2\,\epsilon} \tag{3.37}$$

Where t_i represents the thickness of the insulator, r is the conductor radius, and K stands for the void's shape factor, which is assumed to be spherical. V_{max} corresponds to the highest voltage the line experiences during the mission. d_v signifies the thickness of the void or inclusion 50 μm, a manufacturing standard. α denotes the minimum breakdown voltage of air within the cavity at low air pressures, which is approximately 400V according to Paschen's law (Pashchen's curve in Figure A.1). The constant C takes a value of 0cm for cables with voltages equal to or exceeding 20kV and 0.1cm for cables with lower voltages [5]. The mass of the insulator is determined by:

$$M_i = \rho_i\, l\, \pi\, ((r + t_{sc} + t)^2 - (r + t_{sc})^2) \tag{3.38}$$

where M_i is the mass and ρ_i is density of the insulation layer, t_{sc} is the thickness of semiconducting layer. The total mass of the cable is calculated by multiplying the corresponding material densities with material volumes:

$$M_{total} = M_c + M_i + \rho_{sc}\, l\, \pi\, ((r + t_{sc})^2 - r^2) + \rho_s\, l\, \pi\, ((r + t_{sc} + t_i + t_s)^2 - (r + t_{sc} + t_i)^2) \tag{3.39}$$

3.3.3. Results

As presented in 3.3, lower voltage values increase the circulation current, leading to power losses. At the same time, higher voltage values increase the weight of cables due to a thicker insulation layer. The weight of the cable was calculated over a range of voltages to determine the voltage at which the weight of the cable is minimum. In Figure 3.9, the minima of the curve in the given range of voltages is at 3610 V. The weight of the cable below 3610 V is increasing due to an increase in the radius of the conductor to reduce the resistance according to the increase in current. In contrast, the weight of the cable above 3610 V is increasing due to the thickness of the insulation layer. Note that the weight of the cable indicated on the Y-axis is not an absolute value, as it considers only the cable layers affected by the system voltage.

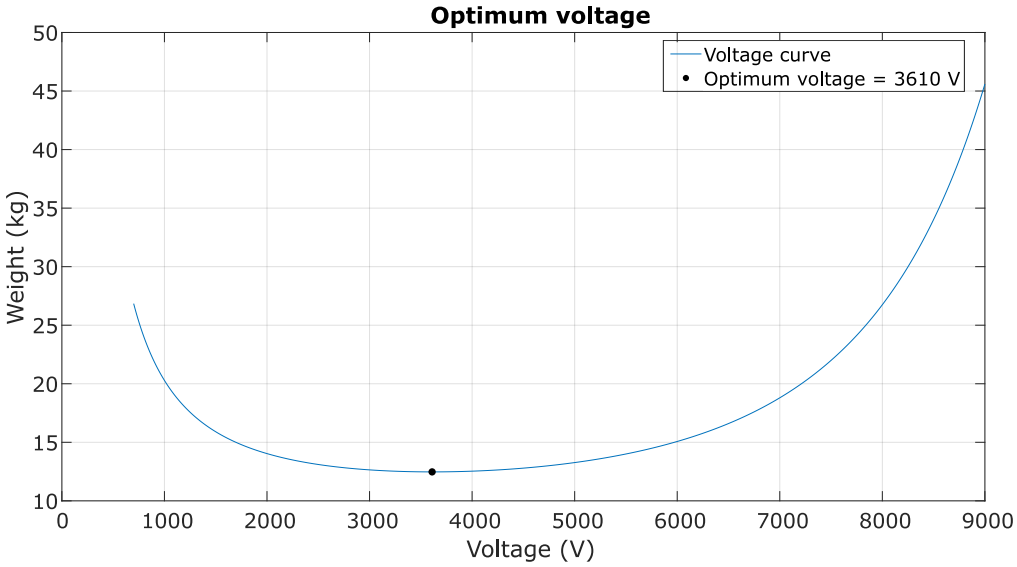

Figure 3.9: Cable weight over a range of system voltages

The voltage value of 3610 V falls within the range of voltages projected by researchers for the anticipated system-level voltages of upcoming fully and hybrid electric aircraft [27, 53, 9].

4

Battery Design and Modelling

Designing a battery pack involves various technical disciplines due to its intricate nature, from electrical design to thermal management and mechanical design. It also involves configurations, packaging technology, safety measures, regulatory compliance, performance testing and lifetime estimation. In this study, the design of the battery pack is limited to the following aspects:

- Battery chemistry
- Battery pack sizing (two configurations)
- Battery mathematical model

Section 4.1 delves into the battery chemistry and preferred cell types. Section 4.2 presents the battery pack sizing process for two competing configurations. Finally, in section 4.3, mathematical models tailored for simulating these battery configurations in a software environment are presented.

4.1. Battery chemistry

4.1.1. Li-ion over Li-S

Presently, the SoA lithium-ion battery technology has gained full control of the battery industry, and the choice of battery technology is very clear. But as mentioned in Chapter 2, there are multiple different battery chemistries under the umbrella of lithium-ion batteries with their benefits and challenges. Although the electric vehicle market is booming with the SoA lithium-ion batteries, the electric aviation industry still seeks improvements in battery technology, especially in terms of specific energy. The researchers predict that within the next 10-15 years, a specific energy of approximately 400 Wh/kg can be achieved. Furthermore, Li-S and lithium-air batteries can realise the potential of high specific energy of 500-600 Wh/kg[17]. Presently, the Li-S batteries are far less since the technology is developing. In the literature of Li-S batteries, consistent citation across the studies concerning the testing data was Oxis Energy Ltd. Unfortunately, the company reportedly encountered bankruptcy, resulting in the unavailability of the cell data [68]. This absence of cell data posed a challenge for the parameterisation of ECM. As a result, due to lack of data, the utilisation of SoA Li-ion battery technologies offers a more pragmatic approach to the design of the battery pack in this study.

Figure 2.4 offers a categorical comparison of Li-ion batteries. When choosing the optimal battery chemistry for a specific application, giving weight to these categories becomes crucial. The ones mentioned in Figure 2.4 hold varying degrees of significance, and prioritisation is relative. Hence, averaged indexed value for each battery chemistry is compared. NMC and NCA have highest averaged indexed value [25]. For aviation applications, safety is paramount, and because NMC is more widely used in the electric mobility sector presently, the ideal candidate for the battery chemistry of electric aircraft is Li-NMC [15].

The geometry of the cell is another important design aspect while selecting the cell. Li-ion battery cells are generally made in cylindrical, prismatic and pouch geometries. Cylindrical cells are commonly manufactured in two standard dimensions, 18650 (18 mm X 65 mm) and 21700 (21 mm X 70 mm). Prismatic cells are cuboidal cells preferred in applications where packing volume is crucial. Pouch cells are known for their flexibility and shape adaptability. All these geometries are seen in different EV battery packs. In this study, cylindrical geometry is preferred because, compared to other geometries, the energy or capacity per cell of cylindrical geometry is lower, making the battery pack less dependent on the condition of a single cell. In contrast, the failure of a larger prismatic cell from the battery pack could largely diminish the energy available in the battery pack, rendering it highly unreliable [66].

Figure 4.1 shows different Li-ion cells plotted on the gravimetric energy density vs gravimetric power density graph. In the case of aircraft, power and energy are both equally crucial parameters for battery sizing. Hence, battery pack sizing is executed for a cell with high specific energy and gravimetric power density. In Figure 4.1, the placement of the chosen high specific energy LG-INR21700-M50 cell on the gravimetric specific energy scale is indicated by the horizontal red line for a comparison with the other cells. Similarly, the vertical red line designates the chosen high gravimetric power density SAMSUNG-INR21700-40T cell on the gravimetric power density scale, providing a reference point among the other cells. Although these cells do not have the highest values in their respective categories, the following are the merits of selecting these cells:

- Resides within the upper segment of their respective categories
- Trusted cell manufacturer guarantees cell data availability
- Widely used in research papers for cell testing

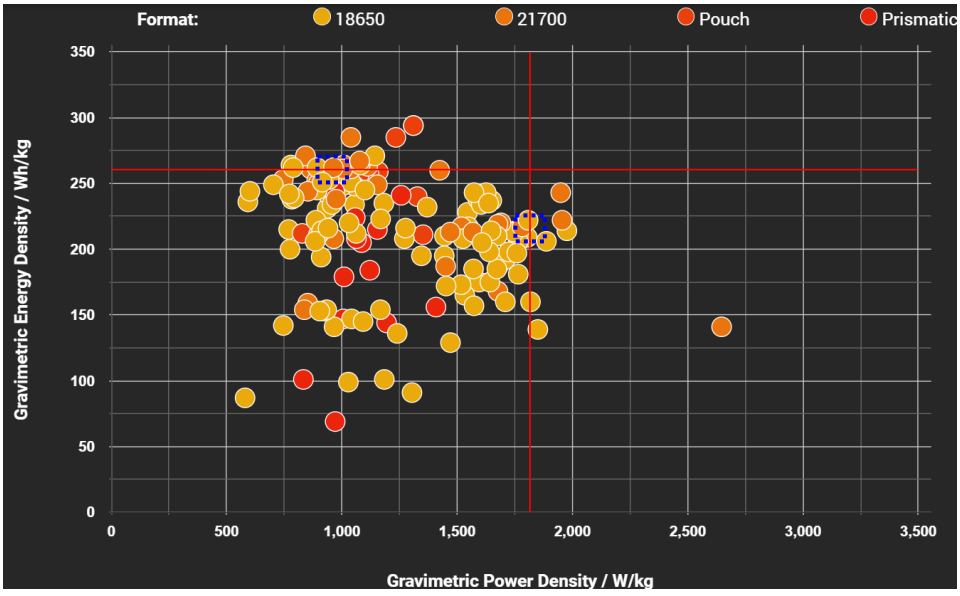

Figure 4.1: Cells plotted on gravimetric energy density vs gravimetric power density [19]

	LG-INR21700-M50	SAMSUNG-INR21700-40T
Energy (Nominal) **(Minimum)**	18.20 Wh 17.60 Wh	14.4 Wh 12.636 Wh
Nominal voltage	3.63 V	3.6 V
Standard charge (Constant current) **(Constant voltage)** **(End current)**	0.3 C (1.455 A) 4.2 V 0.05 A	0.5 C (2 A) 4.2 V 0.2 A
Max. charge current	0 ~25 ^{o}C: 0.3 C (1.455 A) 25 ~50 ^{o}C: 0.7 C (3.395 A)	Standard: 0.5 C (2 A) Rated: 1.5 C (6 A)
Standard discharge (Constant current) **(End voltage)**	0.2 C (0.970 A) 2.50 V	0.2C (0.8 A) 2.50 V
Max. pulse discharge (10 sec), 25 ^{o}C ± 2 ^{o}C	≤ 80 W (SOC 80%)	-
Max. discharge current	-30 ~-20 ^{o}C: 0.2 C(0.970 A) -20 ~5 ^{o}C: 0.3 C(1.455 A) 5 ~45 ^{o}C: 1.5 C(7.275 A) 45 ~60 ^{o}C: 1.5 C(7.275 A)	Without temp. cut: 8.9 C (35 A) temp. cut at 80%: 11.54 C (45 A)
Weight	68.0 ± 1.0 g	70.0 g

Table 4.1: Datasheet of both the cells [34, 54]

Table 4.1 displays the important specifications of the LG-INR21700-M50 and SAMSUNG-INR21700-40T cells. LG-INR21700-M50 has high specific energy (~ 263 Wh/kg). On the other hand, SAMSUNG-INR21700-40T has a high gravimetric power density (1800 W/kg). It is observed that the test current of SAMSUNG-INR21700-40T is confined to 20 A despite the rated current being 35 A. This limitation is due to the undesirable increase in temperature while operating the cells beyond this limit [38].

4.2. Battery Sizing

The number of cells required to fulfil the energy and power requirements are calculated in battery sizing. Additionally, the module sizing and configuration of these cells are determined. Here, the sizing of two different battery pack configurations is presented. The first battery pack is called the 'Fixed configuration' battery pack, and another is a novel battery pack design called the 'Reconfigurable' battery pack. A fixed configuration battery pack comprises a single cell type with a predefined configuration of cells connected in series and parallel. The reconfigurable battery pack involves two internal battery packs of primary and secondary cells. The configuration of this battery pack changes as these two internal battery packs can be connected or disconnected through power switches. The fixed and reconfigurable battery packs are designed to exclusively fulfil the energy and power needs of the propulsion system. Given the consistent power demand of cabin loads, it is assumed that a separate, dedicated battery pack is used to meet the cabin loads' requirements and that the pack's battery sizing is not included. In this section, a weight comparison of the two mentioned battery packs is done based on the number of cells used in the battery pack. Further operational comparison is made in the subsequent chapter.

4.2.1. Fixed configuration battery pack

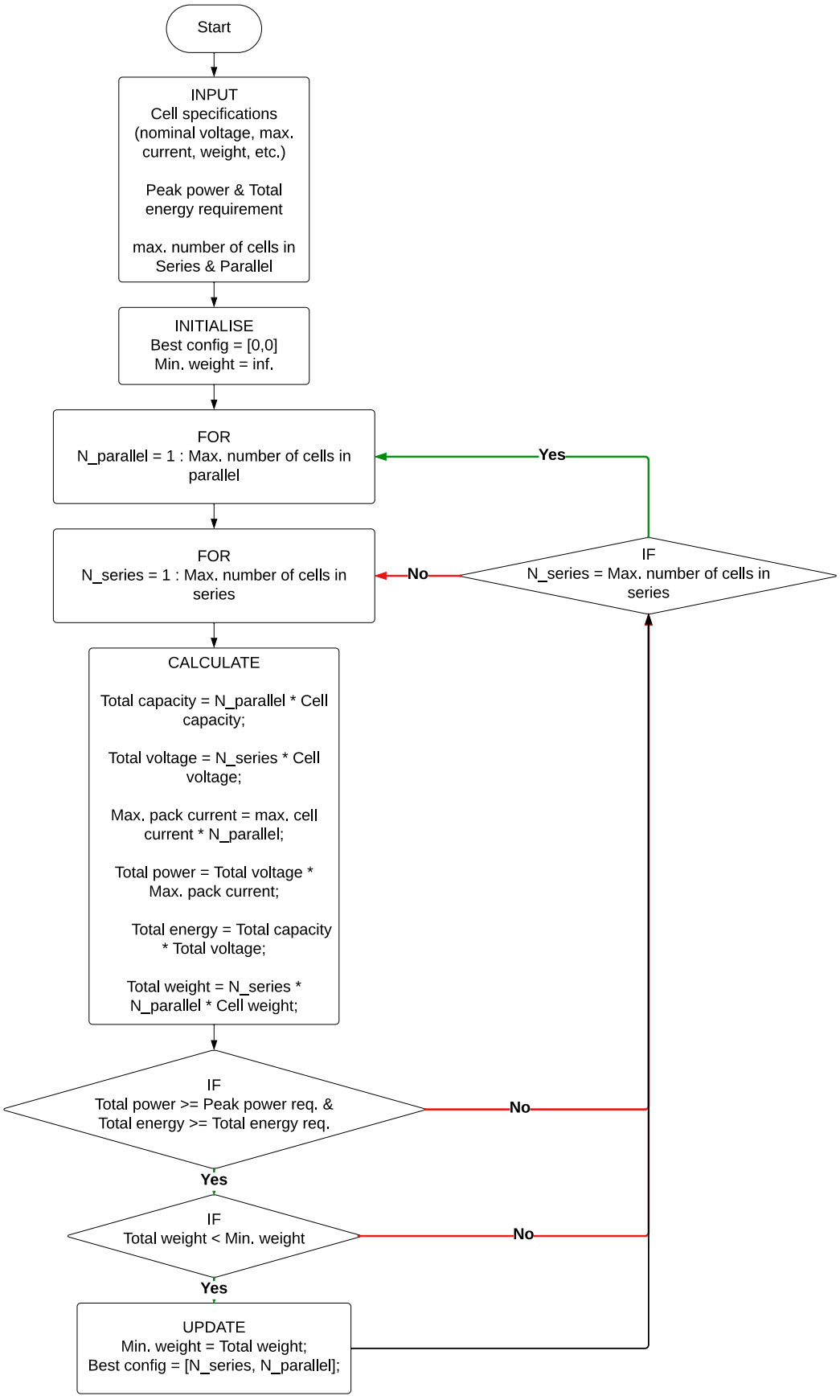

Figure 4.2: Flowchart for fixed configuration battery pack cell calculation

In subsection 3.2.7, it is stated that a huge difference in power demand per phase in the power profile significantly influences the battery sizing. The peak power requirement is the power demanded in take-off and initial climb phase P_{peak} = 1553.2 kW. The total energy requirement from the EM is E_{EM} = 657.36 kWh (refer Table 3.3).

Criteria	LG-INR21700-M50	SAMSUNG-INR21700-40T
Energy requirement	$\frac{657.36\ kWh}{(3.63*4.9*0.9)\ Wh}$ = 41064	$\frac{657.36\ kWh}{(3.6*3.9*0.9)\ Wh}$ = 52023
Power requirement	$\frac{1553.2\ kW}{7.275\ A*3.63\ V}$ = 58815	$\frac{1553.2\ kW}{20\ A*3.6\ V}$ = 21573

Table 4.2: Number of cells required for both cell types

As presented in subsection 4.1, two cells possessing different characteristics are selected for battery sizing. Since a fixed configuration battery pack comprises a single type of cell, two fixed configurations battery packs of LG and SAMSUNG are sized to demonstrate the difference in the quantity of high specific energy cells and high specific power cells to satisfy the energy and power demand. The number of cells required to fulfil the total energy demand is given by dividing the energy requirement by nominal per cell. Similarly, the quantity of cells required to satisfy power demand is calculated. The larger of the two calculated numbers dictates the number of cells essential to satisfy energy and power demands. Table 4.2 shows the number of cells required for energy fulfilment and power fulfilment in both types of fixed-configuration battery packs. The cell energy value taken is a nominal value for estimating the total number of cells. The factor of 0.9 is introduced because subjecting a cell to a 100% Depth of Discharge (DoD) can adversely impact its long-term health. As a result, a permissible limit of 90% DoD is imposed to ensure better cell durability and longevity. The approach employed to determine the configuration with a minimum number of cells to satisfy the energy and power demand is given in Figure 4.2. The LG-M50 battery pack requires 919 cells in series and 64 in parallel, resulting in a 4058.3 kg weight of cells. Whereas SAMSUNG-40T requires 1041 cells in series and 50 in parallel, resulting in a 3643.5 kg weight of cells. Considering the best possible cell-to-system level packing efficiency of 82% [36], the weights of the LG-M50 battery pack and SAMSUNG-40T battery pack are 4950 kg and 4440 kg, respectively. These weights are over 50% of the MTOW. Hence, it will reduce the total payload weight capacity significantly as the projected battery weight of Eviation Elice is less than these two quantities. Figure 4.2 provides a more precise method for calculating the required number of cells compared to Table 4.2.

From the required number of cells, it is evident that in the case of a high specific energy cell, a large number of cells (~ 1.43 times) are still necessary to satisfy the power requirement. Similarly, in the case of a high-specific power cell, more than double the number of cells are required to satisfy the energy requirement compared to power. This indicates that each battery pack contains more cells due to their limitations. Another notable comparison is battery pack terminal voltage. In the case of the LG-M50 battery pack, the nominal terminal voltage is 3.63 V/cell*919 cells = 3336 V, and the SAMSUNG-40T battery pack's nominal terminal voltage is 3.6 V/cell* 1041 cells = 3747.6 V, which is close to optimal system level voltage of 3610 V calculated in the previous chapter. In both cases, maintaining a constant voltage of 3610 V is unfeasible due to voltage variations corresponding to SOC. Determining the optimal system voltage is to establish a reference point where energy losses and weight are minimised. Therefore, the preferred approach is to aim for a system voltage close to the optimal level. The following are possible solutions and corresponding trade-offs for this issue:

- Introduce a DC-DC buck-boost converter to step up/down the voltage. The downside is energy loss due to the converter's efficiency and the converter's additional weight. Also $\eta_{converter} \propto \frac{1}{\Delta V}$
- Let the system voltage equal to the battery pack terminal voltage. The downside is the additional weight of the insulation layer or the bigger conductor diameter
- Let the system voltage equal to the battery pack terminal voltage and the optimum conductor diameter of the power cable with a safe insulation layer. The downside is higher I^2R losses as $R \propto \frac{1}{cable\ diameter}$

A quantitative comparison of these solutions is presented in the next chapter, where the battery packs are modelled and run in a software environment to get the actual voltage, SOC and current values for further comparison. As the fixed configuration battery pack, the LG-M50 battery pack is chosen over the SAMSUNG-40T battery pack because, considering cabin energy requirements, the total weight of the SAMSUNG-40T battery pack exceeds the weight of the LG-M50 battery pack. This is due to the superior specific energy of the LG-M50 battery pack.

4.2.2. Reconfigurable battery pack

In literature, reconfigurability is employed mainly for fault tolerance, dynamic cell balancing and optimised performance. The idea of using reconfigurable battery packs for high-power phases in electric aircraft is not in the literature on battery packs. Apart from the merits of the reconfigurable battery pack mentioned in previous studies, the concept of reconfigurability can be used to enable the simultaneous operation of a hybrid battery pack composed of distinct cell types. This approach leverages the advantages of each cell type per the specific phases of aircraft operation. The previous section presented the battery sizing of two battery packs made of two different cells. In this section, battery sizing of a reconfigurable battery pack made of two different cells is presented.

In many applications, battery sizing is predominantly determined by the energy requirement, as the primary purpose of a battery pack is to meet the energy demand. The same applies to electric aircraft except for the high power demand phases. LG-M50 cell maximum discharge current is limited to 7.275 A (1.5 C). Hence, for the phases with power to energy ratio greater than 1.5, the battery pack made up of LG-M50 cells require additional cells to meet the power demand. Table 4.3 shows the power-to-energy ratio for different phases of the flight trip:

Phases	Power to energy ratio
Taxi	0.1339
Takeoff	4.3486
Initial climb	4.3486
Final climb	3.2614
Cruise	0.6664
Descent	0.3640
Land	0.5600
Reserved climb	4.3486
Reserved cruise	0.6664
Reserved Land	0.5600
Taxi	0.1339

Table 4.3: Power to energy ratio per phase

In the case of the LG-M50 cell, it is observed that additional cells are required to meet the power demand of the Takeoff, Initial climb, Final climb and Reserved climb phases. Cumulatively, these phases last for 7.5 minutes in the calculated power profile, which is just 8% of the total duration of the flight trip, including the VFR reserved phase duration. To satisfy the power demand of 8% of the flight trip, an additional battery weight of around 1225 kg must be carried (refer Table 4.2). On the other hand, in the case of the SAMSUNG-40T cell, high power demand can be managed with fewer cells. However, an additional weight of 2131.5 kg must be lifted to fulfil the energy demand. Therefore, the proposed approach is to supplement the LG-M50 battery pack with a high-specific power SAMSUNG-40T battery pack in high-power demand phases. In this design, the LG-M50 high specific energy battery pack is called the 'Primary battery pack', and the SAMSUNG-40T high specific power battery pack is called the 'Secondary battery pack'. The objective of the primary battery pack is to fulfil a substantial share of the energy demand. In contrast, the secondary pack is intended to meet a significant proportion of the power demand. Further in this section, the sizing of this reconfigurable battery pack is presented.

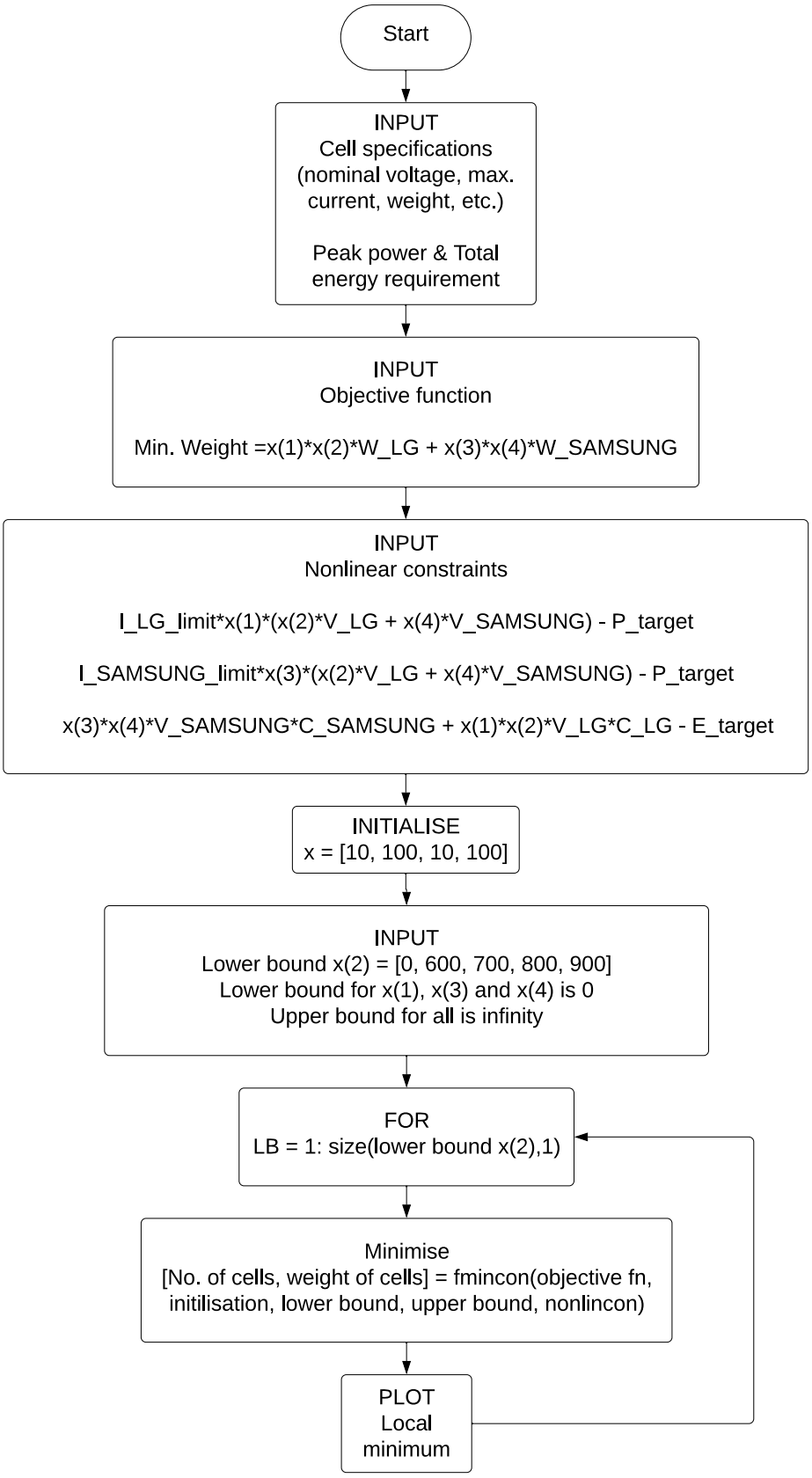

Figure 4.3: Flowchart of the optimal number of cells in reconfigurable battery pack

Figure 4.3 presents a flowchart of the optimisation code written for finding the number of cells in the reconfigurable battery pack. Variables x(1): No. of cells in parallel of primary, x(2): No. of cells in series of primary, x(3): No.of cells in parallel of secondary and x(4): No. of cells in a series of secondary. Three nonlinear constraints are the energy and power requirement expressions. The power requirement expression shows that these two battery packs are connected in series as the voltages are added. The reason behind connecting the battery packs in series is the reduced battery pack current resulting from the combined battery pack voltage. Consequently, the primary battery pack requires fewer cells in parallel. Additionally, the secondary battery pack's capability to handle higher currents necessitates an even smaller number of parallel cells than the primary pack (refer 5.1b). However, if these packs were connected in parallel, the overall battery pack current would be evenly distributed across the parallel branches of both battery packs. This arrangement would negate the intention behind incorporating a secondary battery pack with a higher specific power. Further, the lower bounds are assigned to the number of cells in series in the primary battery pack. This is done to identify a local minimum that ensures the battery pack voltage is as close to the system-level voltage. If not, the weight saved in terms of cells will be added back to undesirable heavy power cables.

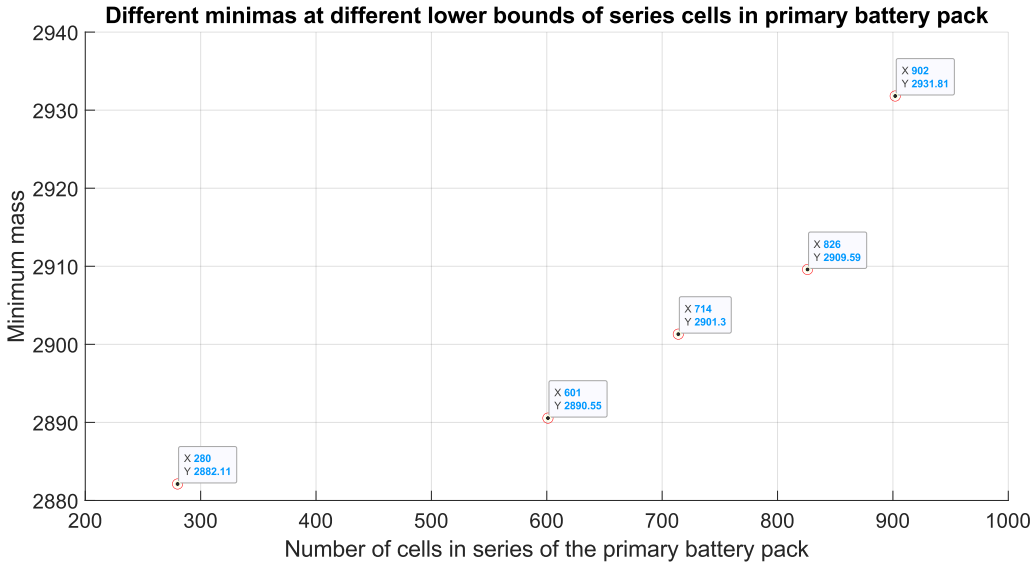

Figure 4.4: Local minimums for each lower bound of series cells in primary battery pack

Configuration	Np_primary	Ns_primary	Np_secondary	Ns_secondary	Total Cells	Weight (kg)
1	111	280	41	257	41617	2882.11
2	52	601	19	552	41740	2890.55
3	44	714	16	655	41896	2901.30
4	38	826	14	759	42014	2909.6
5	35	902	13	828	42334	2931.81

Table 4.4: Number of cells and weight of all five minimums

Five local minimums are plotted in Figure 4.4 and the corresponding number of cells for each minimum is given in Table 4.4. The configuration with the lowest weight is the first configuration. However, this configuration comprises only 280 cells in series within the primary battery pack and 257 cells in series within the secondary battery pack, yielding a nominal voltage of 1016.4 V (when the primary pack is operational individually) and 1941.6 V (when both battery packs are connected in series). These values deviate significantly from the system-level voltage (3610 V). They may necessitate one of the solutions outlined in the latter part of subsection 4.2.1, similar to the approach used with fixed configuration battery

packs. Configuration #2, #3 and #4 are almost evenly distributed by increasing weight of approximately 10 kg, configuration #2 being the lightest. Finally, configuration #5 is the heaviest among the plotted configuration. Configuration #2 has 601 cells in series within the primary battery pack and 552 cells in series within the secondary battery pack, resulting in 2181.63V (when the primary pack is operational individually) and 4168.83 V (when both battery packs are connected in series). These voltages are comparatively closer to the optimum system level voltage value than the first configuration. Similar voltage calculations done for the remaining configurations are shown in 4.5. Given the differences in weights of these configurations and the smaller deviation of voltages from the optimum system level voltage, configuration #2 is considered the optimum cell configuration modelled for further software validation. The weight of this battery pack considering 82% packing efficiency is $\frac{2890.55\ kg}{0.82}$ = 3525 kg.

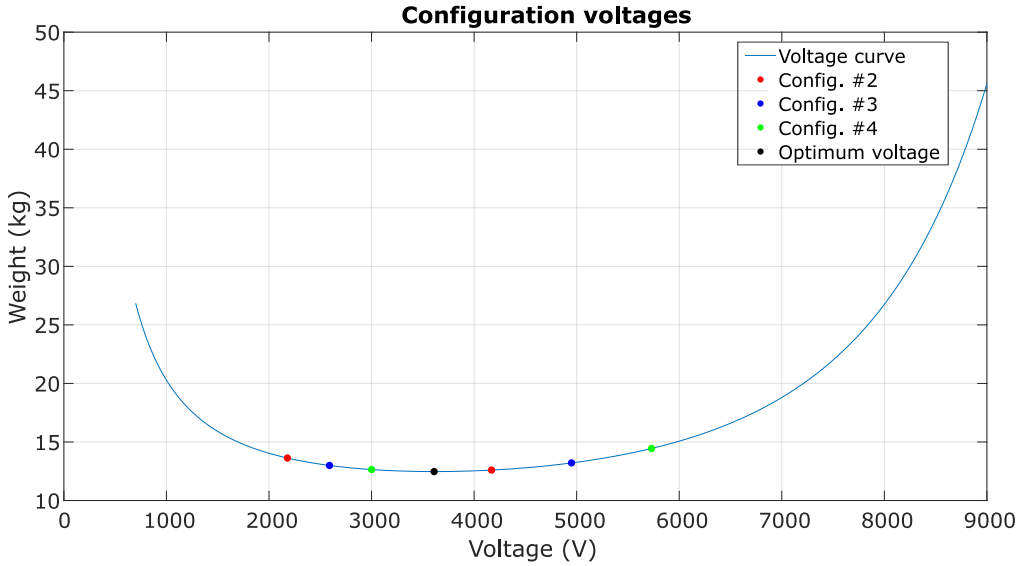

Figure 4.5: Battery pack voltages on the system-level voltage curve

4.3. Equivalent Circuit Model

Before modelling the battery pack in a software environment, a cell model must be created to make the digital battery pack as close as possible to reality. Because, after all, the depiction of a battery in a software environment is a bunch of complex mathematical equations that depict various battery characteristics. The developed cell model predicts the OCV of the cell according to the given power profile. The preference for ECM over PBM is attributed to its simplicity and robustness. In numerous applications, if not all, ECMs are chosen for their ability to provide rapid and precise internal cell state estimation [45]. In the case of large-scale battery packs, where a considerable number of cells require efficient monitoring by the BMS with an acceptable level of accuracy [15], ECMs prove to be particularly advantageous. Additionally, to conduct simulations, ECMs offer a straightforward and expeditious solution. Hence, here ECM is built for the primary battery pack (LG-M50 battery pack) since this battery pack is in continuous operation throughout the flight trip, subject to the dynamic states. The secondary battery pack is operated only during high-power operations, subjected to a constant current output.

Building an ECM involves parameterising the circuit components so that the estimated results closely align with the real cell states. The parameterisation of these components is based on cell test data collected in laboratory tests. OCV exhibits a static relationship with SOC, and temperature and all other factors vary dynamically in a cell model. Hence, two different cell tests are required to generate the parameters of ECM. The procedure for conducting these tests and subsequent data processing is referred from the work of Plett [45], as elaborated in detail in this section.

4.3.1. Static model parameter

OCV test script #1(at test temperature)

1. Soak the fully charged cell at the test temperature for at least 2 hours to ensure a uniform temperature throughout the cell
2. Discharge the cell at a constant-current rate of C/30 until cell terminal voltage equals manufacturer-specified v_{min}

OCV test script #2(at 25^oC)

1. Soak the cell at 25^oC for at least 2 hours to ensure a uniform temperature throughout the cell
2. If the cell voltage is below v_{min}, then charge the cell at a C/30 rate until the voltage is equal to v_{min}. If the cell voltage is above v_{min}, then discharge the cell at a C/30 rate until the voltage is equal to v_{min}

OCV test script #3(at test temperature)

1. Soak the cell at the test temperature for at least 2 hours to ensure a uniform temperature throughout the cell
2. Charge the cell at a constant current rate of C/30 until the cell terminal voltage equals v_{max}

OCV test script #4(at 25^oC)

1. Soak the cell at 25^oC for at least 2 hours to ensure a uniform temperature throughout the cell
2. If the cell voltage is below v_{max}, then charge the cell at a C/30 rate until the voltage is equal to v_{max}. If the cell voltage is above v_{max}, discharge the cell at a C/30 rate until the voltage equals v_{max}.

Since conducting the lab tests was not possible, PyBaMM tool was used to conduct these lab tests. PyBaMM is an open-source battery simulation package written in Python. PyBaMM consists of: [48]

- A framework for writing and solving systems of differential equations
- A library of battery models and parameters and
- Specialised tools for simulating battery-specific experiments and visualising the results

PyBaMM has developed the parameter sets for a few cells using various physical-based models for which Python script experiments can be conducted. These parameter sets are built using the cell test data collected from various research papers. The parameter set of the LG-M50 cell is based on the studies by [12, 49, 73, 46, 52, 61] and generate very high fidelity results using Doyle Fuller Newman (DFN) model. The above-mentioned laboratory test scripts are written in PyBaMM, and the data sets of voltage, discharge and charge capacity, current, and time are collected for test temperatures 15^oC, 25^oC and 35^oC for every script. The assumption is made that the thermal management system effectively sustains the temperature of the battery pack within this specified range, as the optimal performance of the battery pack is achieved within these temperature boundaries [29].

When the test temperature is 25^oC, all the scripts are run under the same temperature. First, the coulombic efficiency ($\eta_{coulombic}$) of the cell is calculated at 25^oC by: (coulombic efficiency is adjusted such that charging is multiplied by the efficiency and discharging is at 100% efficiency)

$$\eta_{coulombic}\ (25^oC) = \frac{Total\ discharge\ capacity\ @\ 25^oC}{Total\ charge\ capacity\ @\ 25^oC} \tag{4.1}$$

Followed by Total capacity (Q) calculation at 25^oC, where j is a time step going from 0 to the second last time step of the 2nd script, and i is the discharging current:

$$Q\ (25^oC) = \sum_{j=0}^{k-1} \eta_{coulombic}(25^oC)[j]\ i[j] \tag{4.2}$$

Similarly, coulombic efficiency and capacity calculation is done for the other two test temperatures:

$$\eta_{coulombic}\ (T) = \frac{Total\ discharge\ capacity - (\eta_{coulombic})\ (Total\ charge\ capacity\ @\ 25^{o}C)}{Total\ charge\ capacity\ @\ T} \tag{4.3}$$

$$Q\ (T) = \sum_{j=0}^{k-1} \eta_{coulombic}(T)[j]\ i[j] \tag{4.4}$$

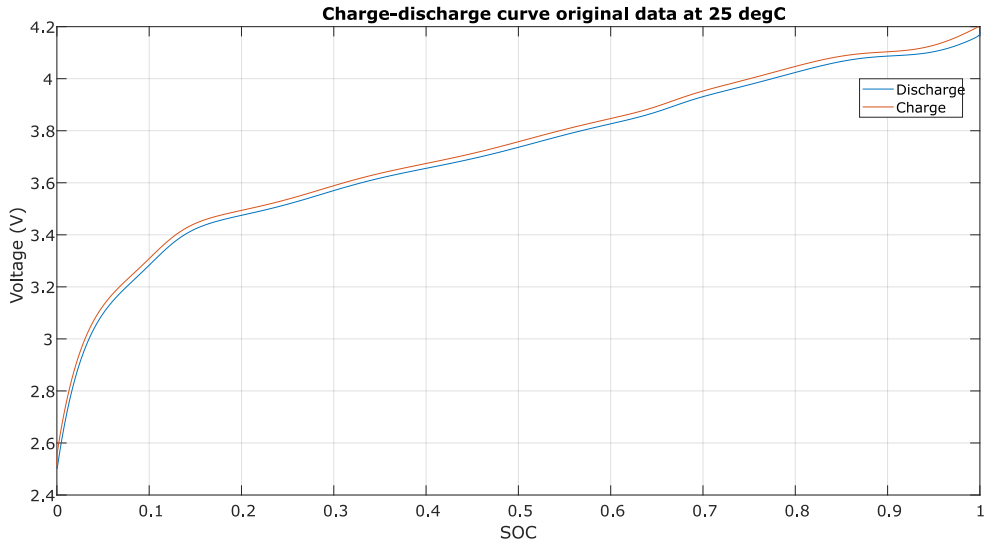

Figure 4.6: Charge and Discharge voltage curve at 25^{o}C

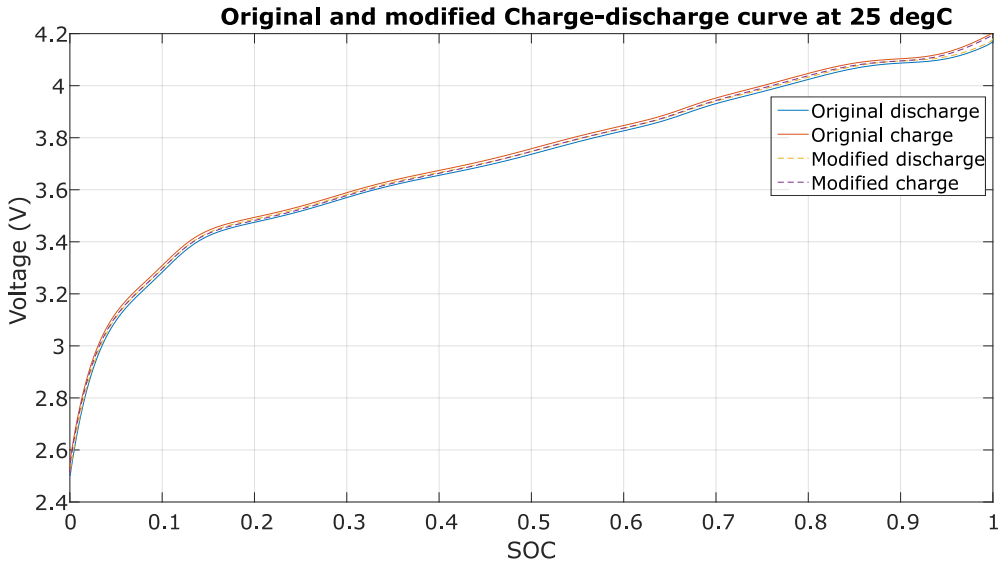

(a) Original and modified charge-discharge curves at 25^{o}C

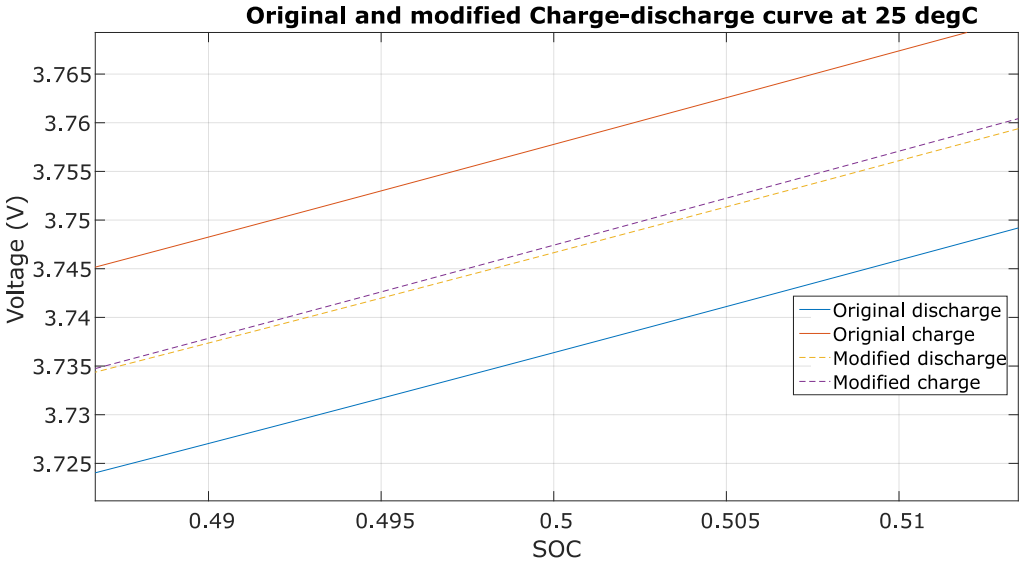

(b) Zoom in figure at 50% SOC

The experimental data set of discharge and charge voltages at 25^oC are plotted against SOC in Figure 4.6. To develop a relationship between OCV and SOC, a single OCV value should correspond to the SOC value. Hence, a single charge-discharge curve for each temperature should be obtained. For that, first, the iR_0 factor is eliminated from the original curves. At 100% SOC, when the discharge script (script #1) starts via instant voltage change, the 100% SOC discharge resistance can be determined (as the discharge current is known). Similarly, 0% SOC discharge resistance, 0% SOC charge resistance and 100% SOC charge resistance can be calculated via instant voltage change at the end of the discharge script #2, start of the charge script #3 and end of the charge script #4 respectively. After getting the resistance values, the resistance value is assumed to change linearly from 0% to 100% SOC. Then, the voltage curves are adjusted by removing iR_0. Figure 4.7a shows the modified curves with removed iR_0 from the original data. Since the resistance is linearly varied, the maximum resistance occurs at 50% SOC for both curves, resulting in a very small difference between them. The second modification is blending linearly the modified charge and discharge curve such that the blend is half at 50% SOC. In practice, it is observed that while discharging, the voltage is missing for lower SOC values because the cut-off voltage of 2.5V reaches before the cell reaches 0% SOC. Similarly, while charging, the higher SOC voltage data is missing [45]. Consequently, as the State of Charge (SOC) approaches 0%, the voltage curve smoothly transitions towards the charging curve, and when nearing 100% SOC, the voltage curve gradually merges with the discharging curve, as shown in figure 4.8. A similar process is followed for both of the remaining temperatures. From Figure 4.9, it can be seen that for positive temperature values, the variation of OCV concerning temperature at a given SOC is nearly linear. Hence, it is reasonable to develop a relationship between OCV values and temperature for different SOC values given by:

$$\mathrm{OCV}(\mathrm{SOC}, T) = \mathrm{OCV}(\mathrm{SOC}, 0^oC) + K\,T \tag{4.5}$$

where K is the slope of the linearity between voltage and temperature. In Equation 4.5, OCV(SOC,T) and K are unknown. The equation can be rearranged:

$$\begin{bmatrix} \mathrm{OCV}(\mathrm{SOC}, T_1) \\ \mathrm{OCV}(\mathrm{SOC}, T_2) \\ \mathrm{OCV}(\mathrm{SOC}, T_3) \\ \vdots \\ \mathrm{OCV}(\mathrm{SOC}, T_n) \end{bmatrix} = \begin{bmatrix} 1 & T_1 \\ 1 & T_2 \\ 1 & T_3 \\ \vdots & \vdots \\ 1 & T_n \end{bmatrix} \begin{bmatrix} \mathrm{OCV}(\mathrm{SOC}, 0^oC) \\ K \end{bmatrix} \tag{4.6}$$

Therefore, a 1-D lookup table can determine the OCV value if SOC and temperature are known.

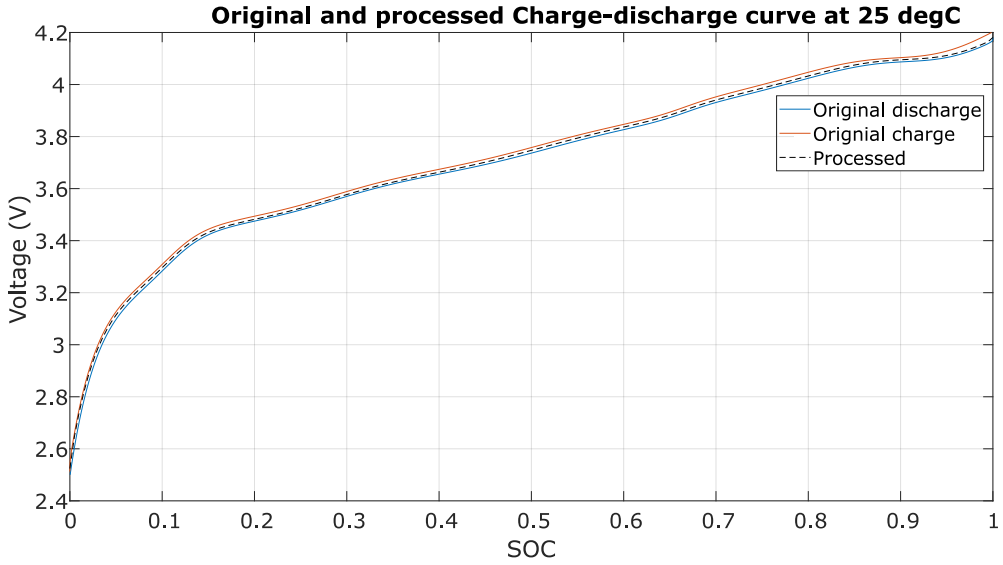

Figure 4.8: Processed OCV curve at 25^{o}C

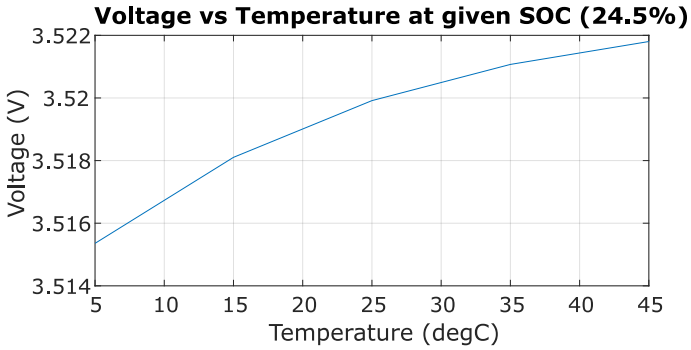

Figure 4.9: Variation of OCV with respect to temperature at given SOC

4.3.2. Dynamic model parameters

Dynamic model parameters depend on the cell's charge or discharge rate. During the static model parameter test, the cell's C-rate was intentionally set very low (C/30). This was aimed to maintain the cell in a quasi-equilibrium state and minimise the impact of dynamic factors on the test results. Here, the cell is subjected to the actual current profile of the end application so that it can be exercised to align with the current profile closely.

Dynamic test script #1 (at test temperature)

1. Soak fully charged cell at test temperature for at least two hours to ensure uniform temperature throughout
2. Discharge cell at constant-current at a C/1 rate for 6 min (avoid over-voltage later)
3. Execute dynamic profiles over SOC range (aircraft power profile)

Dynamic test script #2 (at 25^{o}C)

1. Soak cell at 25 C for at least two hours to ensure uniform temperature throughout
2. Bring cell terminal voltage to min by dis/charging at C/30 rate

Dynamic test script #3 (at 25^{o}C)

1. Charge cell using a constant-current C/1 rate (or as specified by the manufacturer) until voltage equals max; then, maintain voltage constant at max until current drops below C/30

The application of dithering, a technique used by Plett [45] to eliminate hysteresis voltages, is intentionally omitted in both the testing and processing phases. This decision is attributed to the complexity of the processing, which occasionally fails to converge to a solution. Even in the absence of hysteresis voltages, the model retains a satisfactory level of accuracy. Further, the current profile is obtained by dividing the power profile by the nominal voltage of the battery pack. It's important to note that the dynamic model parameters of the ECM are established separately for the fixed configuration battery pack and the reconfigurable battery pack since the nominal voltage of both battery packs differs, resulting in different C-rates at given power. Hence, the above-mentioned scripts are followed separately for both battery packs. Similar to static model parameter's test scripts, the data sets of voltage, discharge, and charge capacity, current, and time are collected for temperatures 15^oC, 25^oC and 35^oC for every script. The dynamic data is used to identify all ECM model parameter values (except OCV vs. SOC relationship). The following steps are followed:

1. Computed $\eta_{coulombic}$ and Q as previously done for static model parameter (OCV)
2. Computed SOC at each time step using Equation 4.7 and corresponding OCV using Equation 4.5

$$\text{SOC} = 1 - \sum_{j=0}^{k-1} \frac{\eta_{coulombic}[j]\; i[j]}{\text{Q} * 3600} \tag{4.7}$$

3. Subtracted OCV from the voltage values to get the unknown part of the cell voltage

$$v_{unknown} = v - \text{OCV}(\text{SOC}, T) \tag{4.8}$$

4. Subspace system identification technique was used to find the R-C time constants. This technique is more effective than non-linear optimisation for minimising RMS voltage error [45]. Higher RC pairs yield accurate voltage prediction. Hence 3 RC pair ECM was considered (the modelled ECM is shown in 4.10)
5. Computed i_R for each step given by:

$$i_R[k] = A_{RC}\; i_R[k-1] + B_{RC}\; i[k-1] \tag{4.9}$$

$$A_{RC} = \begin{bmatrix} exp\left(\frac{-\Delta t}{R_1\, C_1}\right) & 0 & \dots \\ 0 & exp\left(\frac{-\Delta t}{R_2\, C_2}\right) & \\ \vdots & & \ddots \end{bmatrix} \tag{4.10}$$

$$B_{RC} = \begin{bmatrix} \left(1 - exp\left(\frac{-\Delta t}{R_2\, C_2}\right)\right) \\ \left(1 - exp\left(\frac{-\Delta t}{R_2\, C_2}\right)\right) \\ \vdots \end{bmatrix} \tag{4.11}$$

A_{RC} and B_{RC} are obtained in step 4

6. In case of discharging, the terminal voltage is always less than the OCV, hence $v_{unknown}$ in Equation 4.8 is a negative value given by:

$$v_{unknown} = -\sum_{j=1}^{3} R_j\; i_{R_j} - R_0\; i \tag{4.12}$$

(4.13)

where j is the index value of the RC pair, i_{R_j} is the current flowing from the resistance branch of jth RC pair, and i is cell output current (positive value for discharge). The above equation is written for each time step, and those equations are solved for R_j and R_0 as follows:

$$\begin{bmatrix} v_{unknown[1]} \\ v_{unknown[2]} \\ \vdots \end{bmatrix} = \begin{bmatrix} -i_{R_j}[1] & -i[1] \\ -i_{R_j}[2] & -i[2] \\ \vdots & \vdots \end{bmatrix} \begin{bmatrix} R_j \\ R_0 \end{bmatrix} \tag{4.14}$$

7. Computed RMS voltage error for the model given by:

$$v_{predicted} = \text{OCV(SOC)} - \sum_{j=1}^{3} R_j \, i_{R_j} - R_0 \, i \tag{4.15}$$

$$v_{error} = v - v_{predicted} \tag{4.16}$$

$$v_{rms} = \sqrt{\frac{1}{N} \sum_{j=1}^{N} v_{error}^2} \tag{4.17}$$

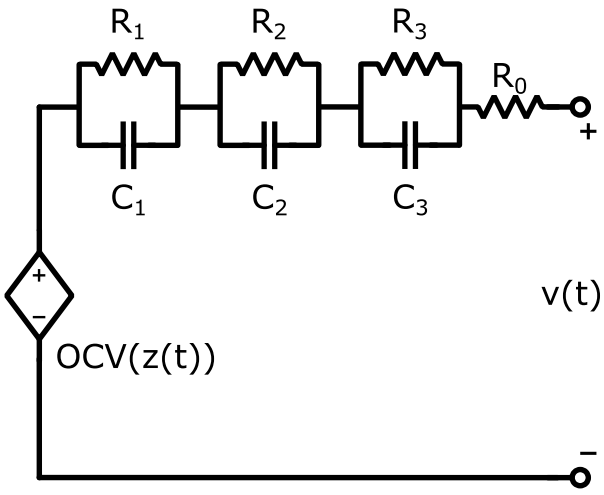

Figure 4.10: Modelled ECM

Figure 4.10 shows the modelled 3RC ECM whose values are given in Table A.1 and A.2. Figure 4.11, 4.12 and 4.13 present the graphs of predicted voltage in comparison with the originally measured voltage after performing these steps for three different temperatures and two different battery packs.

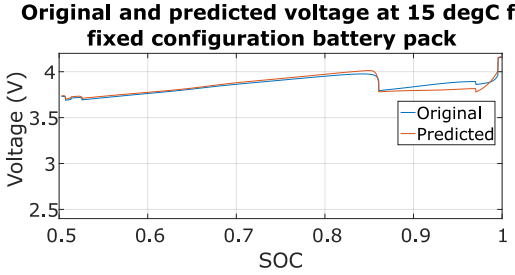

(a) Original and predicted voltage at 15^{o}C for fixed configuration battery pack

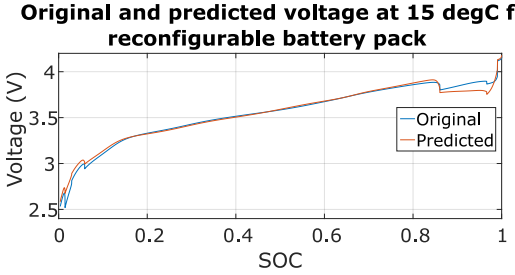

(b) Original and predicted voltage at 15^{o}C for reconfigurable battery pack

Figure 4.11: Voltage predictions at 15^{o}C for both battery packs

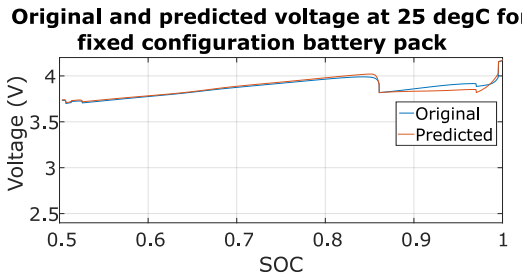

(a) Original and predicted voltage at 25^{o}C for fixed configuration battery pack

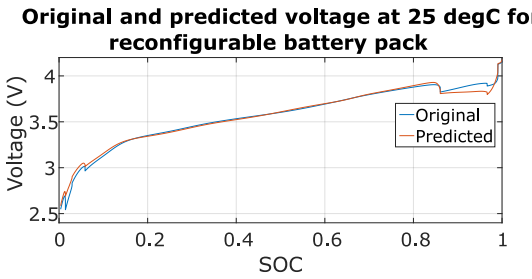

(b) Original and predicted voltage at 25^{o}C for reconfigurable battery pack

Figure 4.12: Voltage predictions at 25^{o}C for both battery packs

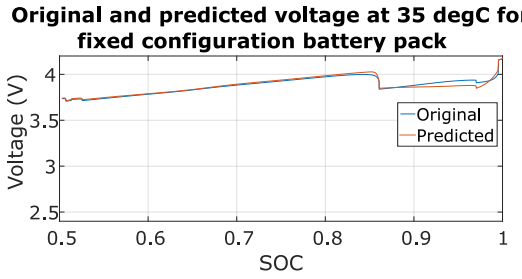

(a) Original and predicted voltage at 35^{o}C for fixed configuration battery pack

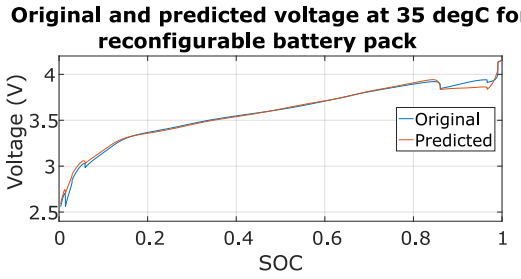

(b) Original and predicted voltage at 35^{o}C for reconfigurable battery pack

Figure 4.13: Voltage predictions at35^{o}C for both battery packs

Configuration	15	25	35
Fixed Configuration battery pack	22.2 mV	16.8 mV	14.3 mV
Reconfigurable battery pack	29.7 mV	24.2 mV	20.8 mV

Table 4.5: RMS voltage error values for each case

Table 4.5 shows the RMS voltage error values between predicted and measured voltage for each case. RMS error of around 15 mV is considered fairly accurate in voltage prediction. Hence, the values obtained are reasonable since the hysteresis voltages are neglected, and the number of RC pairs is restricted to three. Furthermore, in the case of a fixed configuration battery pack, the entire range of SOC is not fully utilised. Additionally, more cells flatten the voltage decay curve, resulting in lesser RMS error. This reduction in error arises from the absence of dynamic changes, a characteristic that distinguishes it from reconfigurable battery packs. The effect of different dynamics indeed affects the ageing of the cells in two different configurations, which is further discussed in the subsequent chapter.

5

Software validation and Battery ageing

This chapter is focused on the software modelling of the battery packs and simulation. The proposed battery design is modelled and simulated to validate the proper working. Additionally, the results of the simulations are used for comparative ageing analysis of both configurations. Section 5.1 elaborates on the battery modelling done using MATLAB Simscape Battery tool. Section 5.2 explains the Simulink system model in which the simulation of the battery pack is carried out. Consequently, the results of the simulations are discussed in Section 5.3. Finally, comparative ageing results are discussed in Section 5.4.

5.1. Simscape battery modelling

This section provides information regarding the modelling of the Simscape battery. In an earlier chapter, the battery sizing results in the number of cells used. Before modelling a battery into a software environment, it is necessary to finalise the module configuration of the battery pack.

5.1.1. Module configuration

In section 2.3, the background of SCM and PCM, along with their advantages and disadvantages, is presented. Studies by Zhu et al. [75] and Gunlu [24] underline a standard reference which carried out a comparative study of battery performance for both configurations and concluded that PCM structure can realise capacity maximisation compared to SCM. Also, Viswanathan, Palaniswamy, and Leelavinodhan [65] stated that PCM structure is more suitable for high capacity utilisation and high power application. Moreover, PCM offers a self-balancing feature at the cell level, which is crucial in large-scale battery packs since a dedicated balancing circuit inside each module is a complex procedure. The challenge of balancing the series of connected modules is trivial in the case of electric aircraft as after each flight; the systematic charging procedure can be followed, which resets the SOC of all the modules, unlike other applications. Hence, PCM structure is incorporated for fixed and reconfigurable battery packs.

5.1.2. Building a Simscape battery pack in Simulink

Simscape is a physical modelling platform developed by Mathworks to reproduce a physical system simulation environment. Simscape Battery provides design tools and parameterised models for designing battery systems. It supports creating digital twins, BMS designs, battery system behaviour under normal and fault conditions, a combination of electrical and thermal effects on battery systems, parameterised models of battery packs, cell balancing and SOC estimation [60].

Simspcape battery builder allows building customised battery packs from scratch to be further connected to the load side to run simulations. The modelling starts by creating a cell, followed by the parallel assembly. The number of parallel assemblies connected in series or parallel makes up a module. Since here, the module structure employed is PCM, a single cell is present in each parallel branch. The following are the properties fed to model a module object:

Properties	Primary battery pack	Secondary battery pack
Geometry	Cylindrical	Cylindrical
Height	0.07015 m	0.0703 m
Radius	0.01055 m	0.01061 m
Dynamic parameters	3 RC pairs	-
Temperature dependence	Yes	Yes
Mass	0.069 kg	0.07 kg
Number of parallel assemblies	64 or 52	19
Number of parallel assemblies in series	1	1
Ambient thermal path	Cell-based thermal resistance	Cell-based thermal resistance

Table 5.1: Model properties for the primary battery pack and secondary battery pack

In Table 5.1, the number of parallel assemblies are 64 and 52 for fixed configuration battery pack and reconfigurable primary battery pack, respectively. Similarly, the secondary battery pack module in the reconfigurable battery pack is modelled as per battery sizing. Figure 5.1 visually represents the difference between the fixed configuration and reconfigurable battery pack for better understanding, and Figure 5.2 shows a module created using Simspcape, containing 52 LG cells connected in parallel.

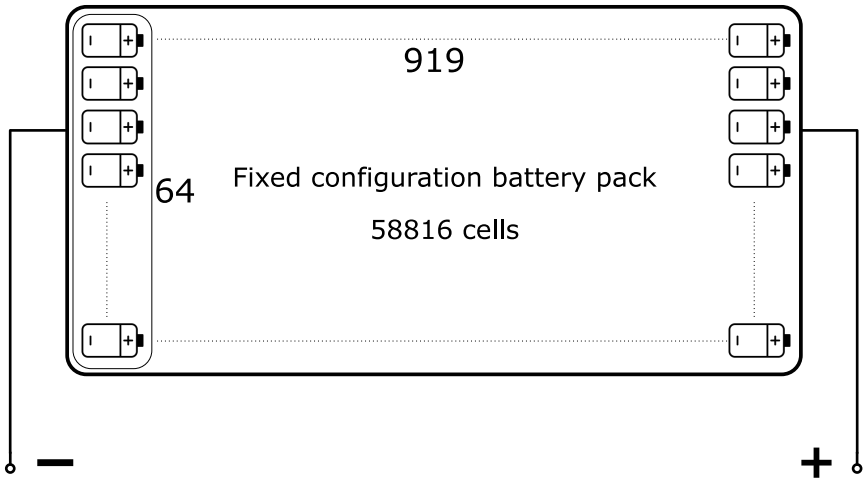

(a) Fixed configuration battery pack

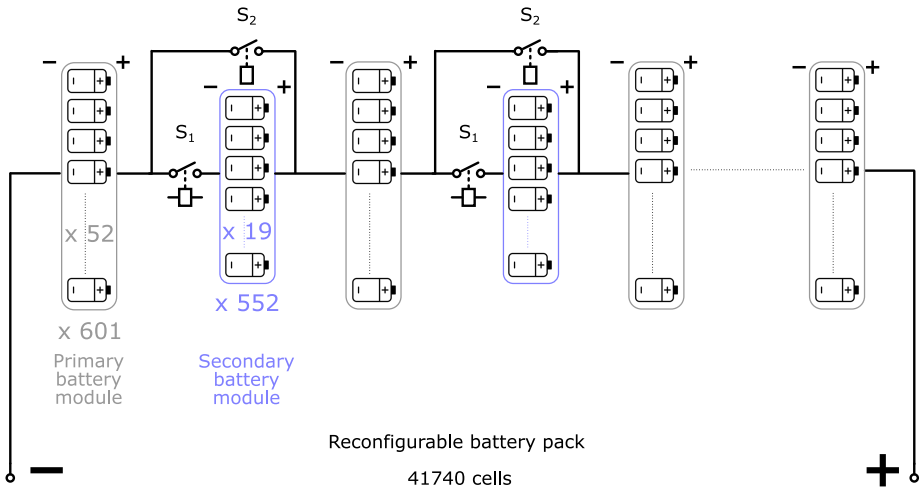

(b) Reconfgirable battery pack

Figure 5.1: Scematic of both battery packs

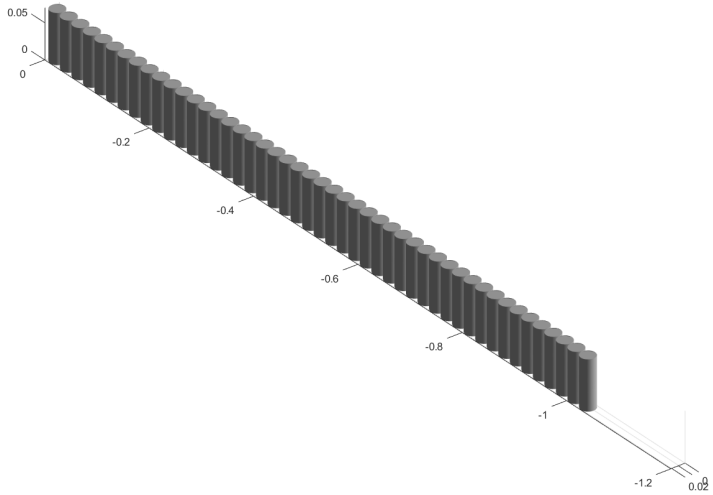

Figure 5.2: A Simscape battery module

5.1.3. Parameter library

Following the model creation, a parameter library is established to facilitate access and modification of module parameters. This library's default Simscape battery-cell parameters are available, which are fairly rudimentary and generalised. Therefore, to closely depict the actual behaviour of the battery in the software environment, these parameters are replaced by values extracted from the cell datasheet and those generated through ECM at three distinct temperatures. The parameters include the SOC array, voltage array, temperature array, values for three RC pairs, cell capacity, and temperature-related cell parameters.

5.2. Simulink model

Once a module is created, a battery pack can be assembled by connecting these modules in series. However, in this scenario, where several thousand cells are being modelled, the computational demands of processing the mathematical set of equations for the RC3 cell model are extensive. This necessitates prolonged computation time and significant computing power, especially for a flight trip of 5400 seconds (90 minutes) (including reserved phases). This level of computational intensity exceeds the capabilities of a standard computer, making it impractical to handle such simulations.

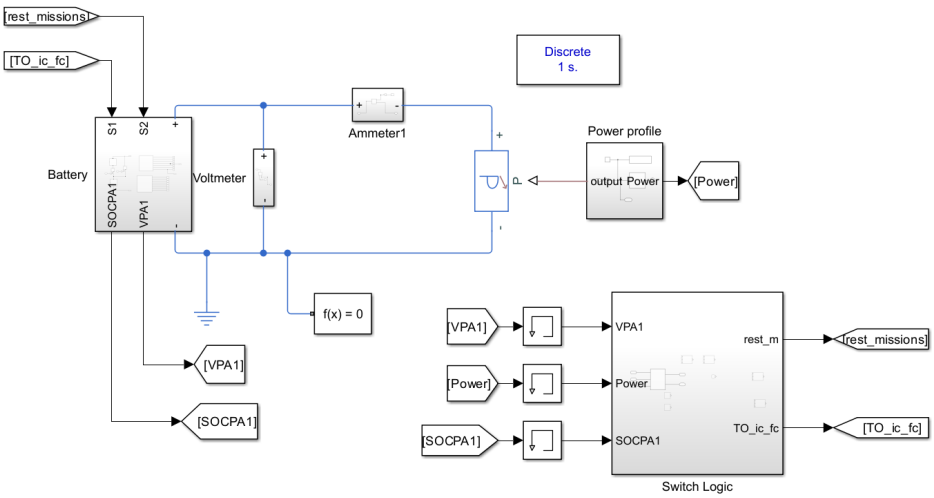

Figure 5.3: Simulink model

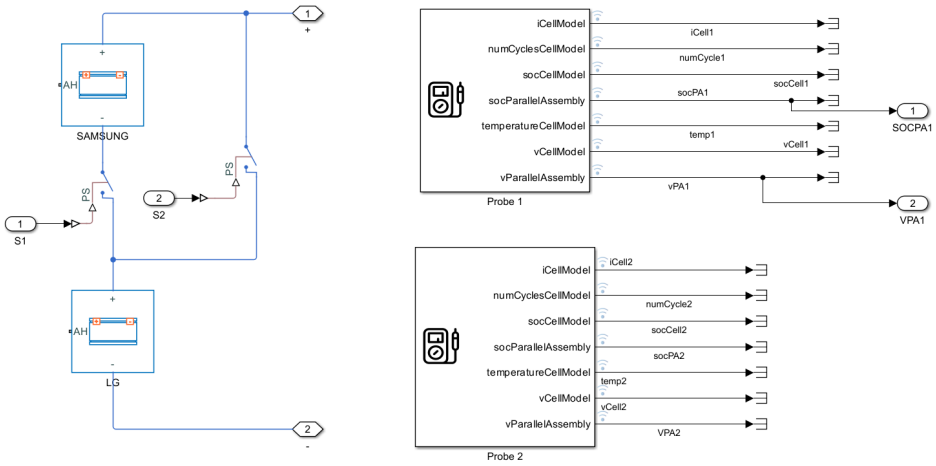

(a) Battery circuitry

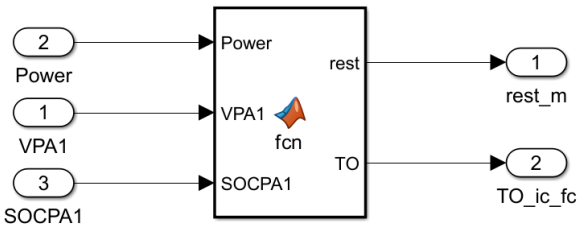

(b) Control logic

Figure 5.4: Battery and control logic subsystems

To overcome this challenge, only one module is used to represent the battery pack and the load-side power profile is normalised for a single module using the nominal voltage of the cells connected in series. The Simulink model of the whole system is shown in Figure 5.3. On the right-hand side of Figure 5.3, is the battery subsystem. The blocks inside that subsystem are shown in Figure 5.4a where the LG (primary) module and the SAMSUNG (secondary) module are connected in series through a power switch S1 and the SAMSUNG module is bypassed using the power switch S2. The switches used are assumed to have a very low closed resistance of 1 mΩ, whereas, in reality, it depends on the type of power switch. This reconfigurability technique is similar to the Self-X reconfiguration design, where only two switches are used to bypass the cell. Here, the importance is given to the design with lesser weight rather than the flexibility of the reconfiguration. Further, the probes are shown in the 5.4a, which measure the battery parameters and are plotted in the data inspector. On the left-hand side of the 5.3, is the dynamic power block to which the power profile data is given. The power profile subsystem involves a 1-D look-up table for normalised power values, taking time as input. At the bottom of the 5.3, is the control logic which performs the reconfigurability. The control logic is displayed in Figure 5.4b where the instantaneous power demand of the propulsion system and instantaneous value of the voltage of the primary battery pack are given as input to the function. Inside the MATLAB function, the instantaneous power that can be provided by the primary battery pack is calculated, and it is compared with the instantaneous power demanded by the propulsion system. If the power demand exceeds the power provided by the primary battery pack, the signal 'series' is given the command '1' or 'true', and the signal 'bypass' is given the command '0' or 'false', and vice versa. As it can be seen from Figure 5.3, these are the input commands of switch 'S1' and switch 'S2', respectively. Thus, whenever the primary battery pack is insufficient to satisfy the power demand, the secondary battery pack is connected in series. Otherwise, it is bypassed, and the primary battery pack is directly connected to the load. The power demand is high in phases such as Take-off, Initial climb, Final climb, and Reserve climb. Hence, this technique is employed. During the reconfigurable battery pack sizing process, the energy constraint was met by summing up the nominal energy values of both the primary and secondary battery packs. However, since the primary battery pack operates for most of the trip duration, there is a potential scenario where, during the reserved mission

phase, the primary battery may deplete to zero SOC, leaving all the remaining energy in the secondary battery pack. To mitigate this, the SOC value of the primary battery pack (SOCPA1) is inputted into the control logic function. If the SOCPA1 value falls below 0.2, the secondary battery pack will be connected in series, thus averting the complete depletion of the primary battery pack. A similar model is built for a fixed configuration battery pack where only one single battery module is on the energy source side, and no control logic is present (refer Figures A.2 and A.3).

5.3. Results of simulation

This section presents the simulation results for both configurations using a normalised power profile. As previously outlined, the fixed configuration battery pack comprises a single cell type, while the reconfigurable one comprises a primary and a secondary battery pack.

Figure 5.5a illustrates that the fixed configuration battery pack retains more than half of the battery capacity, while the reconfigurable battery pack utilises 92% of the battery capacity. The remaining energy in the fixed configuration battery pack underscores that the sizing of the fixed configuration battery pack is primarily influenced by the high power demand during take-off and climbing phases. It's worth noting that the remaining energy in a fixed-configuration battery pack can be utilised by cabin loads throughout the mission. As indicated in Table 3.3, the total cabin energy requirement is 96 kWh, and the unused energy in the fixed configuration battery pack is approximately 418 kWh. Therefore, even after providing energy to cabin loads throughout the journey, a substantial 322 kWh of unused energy would still be available in a fixed-configuration battery pack. In this scenario, when estimating the weight benefit of the reconfigurable battery pack, it is essential to factor in the weight of the cabin load battery pack. On a preliminary basis, the independent battery pack for cabin loads would weigh $\frac{96\ kWh}{(3.63\ V * 4.9\ Ah * 0.9)} * 0.069\ kg$ = 420 kg. Considering an 82% packing efficiency, as previously mentioned, the weight of the cabin load battery pack would be 512 kg, resulting in a total weight of (reconfigurable battery pack + cabin load battery pack) = (3525 + 512) = 4037 kg. Even though the weight of power switches per module is neglected, the weight difference between the reconfigurable battery pack and fixed configuration battery is nearly 400 kg.

Figures 5.5b and 5.6a compare the cell voltage and battery pack current for both configurations. As explained in Section 5.2, at nearly 65 minutes, the condition of primary battery pack SOC below 0.2 is provoked in the Reserved cruise phase. The reflection of this event can be explicitly seen in Figures 5.6a where at 65 min the current of the primary battery pack is instantaneously lowered and 5.7 where steady SOC of secondary battery pack starts to reduce as it gets connected n series. Figure 5.6b serves as the input to the ageing experiments conducted in PyBaMM, which are explained in the subsequent section.

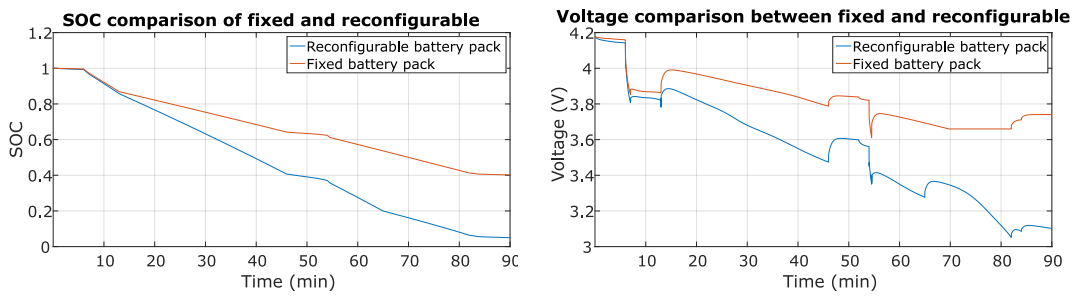

(a) SOC of both configurations vs. time

(b) Voltage of both configurations vs. time

Figure 5.5: SOC and voltage comparison between two configurations

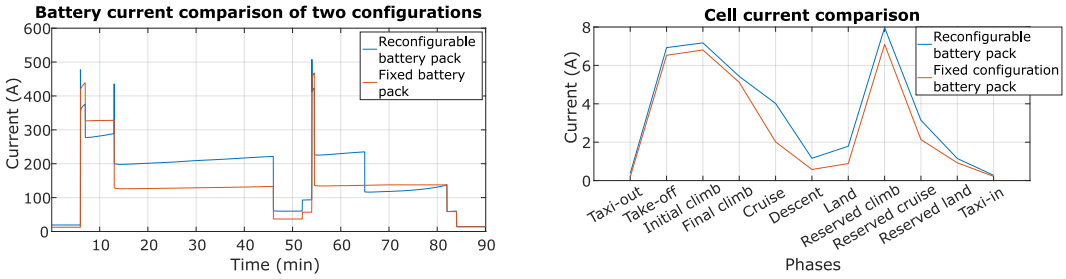

(a) Battery current of both configurations vs. time

(b) Primary battery cell current pack of both configurations vs. time

Figure 5.6: Battery and cell current comparison between two configurations

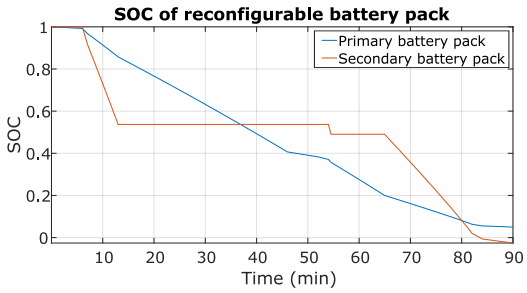

Figure 5.7: SOC of primary and secondary battery pack in reconfigurable battery pack

5.4. Ageing results

In this section, the ageing of the fixed configuration battery pack is compared with the reconfigurable battery pack. Since there are more cells in the fixed configuration battery pack, intuitively, the ageing of the battery pack should be less than the reconfigurable battery pack. Thus, to quantify this characteristic, both battery packs are ageing in PyBaMM. Note that the ageing cycles are simulated for the LG cells in both the battery packs since the parameter set for the ageing of only LG-M50 cells is available in PyBaMM. It is important to note that the intention to perform ageing simulations is to address the effects of higher cell currents in the reconfigurable battery pack.

The cell current profile from the Simulink battery model is given as input to the PyBaMM experiment script. While scripting the ageing algorithm in PyBaMM, it is assumed that there exists a sophisticated thermal management system which keeps the battery pack temperature at 25^{o}C. Hence, the temperature is kept constant at 25^{o}C. Five hundred cycles with a discharging current profile from the Simulink battery model and charging profile recommended in the cell datasheet are executed. Ageing results are focused on all factors causing LLI, and other ageing phenomenons are neglected since the difference in C-rate is usually reflected in LLI.

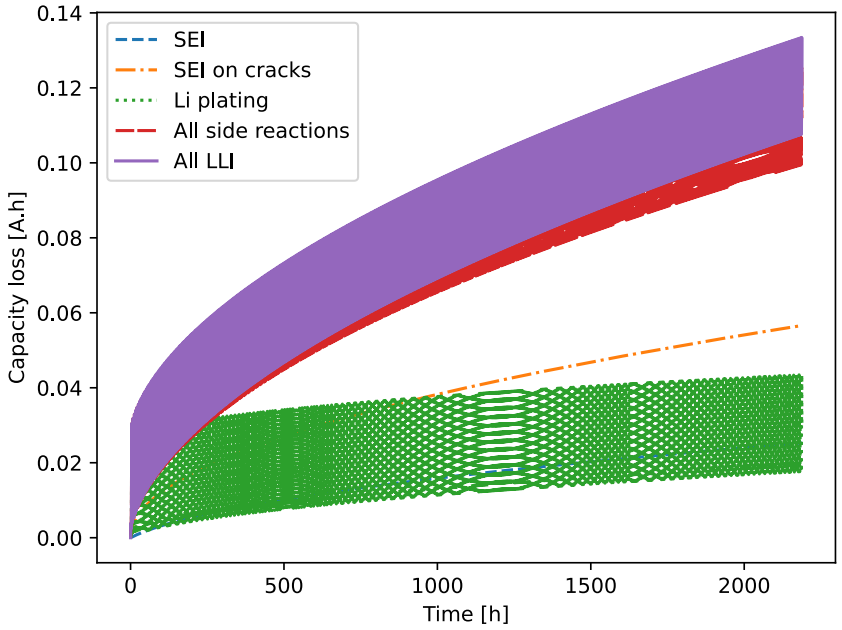

Figure 5.8: Ageing results generated by PyBaMM for fixed configuration battery pack

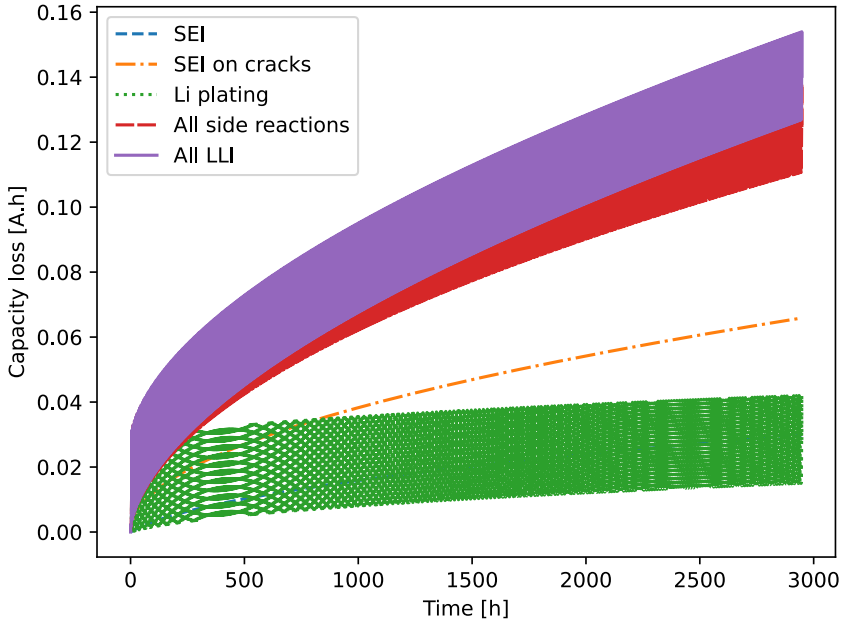

Figure 5.9: Ageing results generated by PyBaMM for reconfigurable battery pack

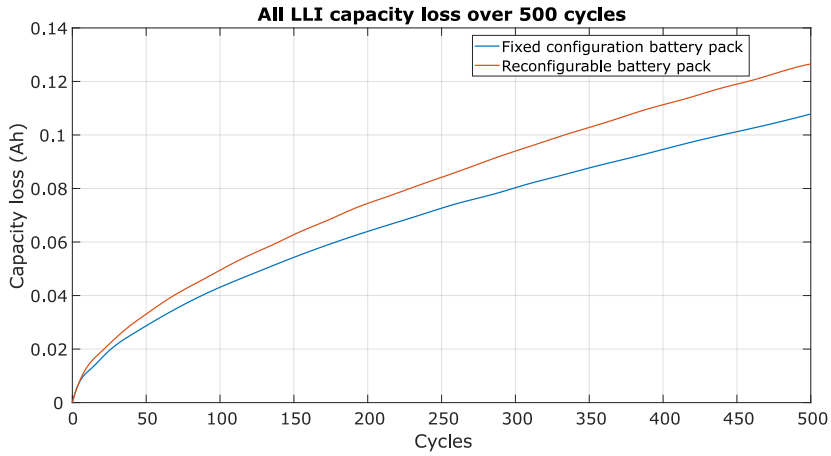

Figure 5.10: Comparison of all LLI capacity loss for both configurations

Figures 5.8 and 5.9 show the different aspects in which capacity loss is faced by a cell over 500 cycles. All LLI, side reactions, and Li plating are visible as a band in the figure, whereas those are closely plotted waves, as these three factors oscillate in each charging-discharging cycle. To provide a clearer comparison, Figure 5.10 displays the lower amplitude of LLI capacity loss for both configurations.

It can be seen from 5.10 that the capacity loss is greater in reconfigurable battery packs compared to fixed-configuration battery packs due to comparative high C-rate discharge. However, the difference in the capacity loss of these configurations is almost 0.02 Ah after 500 cycles, meaning the LG-M50 cell in the reconfigurable battery pack holds only 0.4% less capacity than the LG-M50 cell in the fixed configuration battery pack.

6

Conclusion and Future scope

This chapter is intended to conclude the thesis set out with the research question formulated in Chapter 1. The concluding remarks are drawn from the results presented in each chapter and discussed in section 6.1. Furthermore, the author highlights recommendations in section 6.2 to underline areas for development in future work.

6.1. Conclusion

The purpose of this study was to conduct a thorough analysis and comparison of fixed and reconfigurable battery pack configurations for electric aircraft. The crucial challenge in current electric aircraft battery technology concerns the specific energy of the battery pack. Hence, a battery pack design with energy maximisation and weight minimisation is desired. This led to conducting the preliminary level analysis of factors such as the power profile of the electric aircraft, system-level voltage, battery chemistry, and ageing characteristics with the ultimate goal of enhancing the weight efficiency of the battery pack in electric aircraft. The research took place by attempting to answer the following research questions.

1. *"How is the electric aircraft power profile for which the battery pack is designed? What aspects of the power profile dictate battery sizing?"*

   The reference electric aircraft for determining the power profile, as detailed in Section 3.1, is the Eviation Alice. This profile is segmented into distinct mission phases, with power and energy values for each phase determined based on the available aircraft specifications. These mission profiles are further categorised into regular and reserved profiles. Figures depicting the power profile, power per phase, and energy per phase (see Figures 3.5, 3.6, and 3.7) provide a visual representation of the electric aircraft's characteristics. Ground operations, specifically Taxi-in and Taxi-out, demand the least power. In contrast, Take-off, Initial Climb, and Reserved Climb constitute high-power, short-duration phases, while Final Climb is characterised by high-power, long-duration requirements. The Cruise and Reserved Cruise phases, being the longest, demand the maximum energy. Finally, the Descent, Land, and Reserved Landing phases are the least power-intensive aerial stages.

   The sizing of the battery pack is primarily contingent on the nominal energy and maximum discharging power of the chosen cell, which serves as the fundamental building block. Table 4.2 outlines the quantity of a single cell type needed to fulfil the energy and power requisites, considering both LG-M50 and SAMSUNG-40T cells. In the case of LG-M50 cells, battery sizing is influenced by power requirements, particularly due to the high demand during Takeoff and climbing phases. Conversely, with SAMSUNG-40T cells, energy requirements play a more pivotal role in determining the battery size.

2. *"What are the SoA and futuristic battery chemistries suitable for electric aircraft? What are their respective merits and demerits?"*

   In the aviation industry, weight efficiency holds paramount importance, given the industry's acute sensitivity to aircraft performance concerning weight. When designing any subsystem for an aircraft, including the battery pack of an electric aircraft, along with weight efficiency, factors such as safety, performance, life span and cost are also crucial. Among SoA battery technologies, Li-NMC emerges as the preferred battery chemistry for small electric aircraft, exhibiting superior attributes, as illustrated in Figure 2.4. While the prospect of futuristic battery technologies like Li-S and Lithium-air batteries holds promise for even greater advancements compared to current SoA options, the present landscape of research in advanced battery technologies remains nascent. This poses significant challenges in their immediate applicability. Consequently, in this study, Li-NMC is the preferred choice over futuristic battery technologies for near-term small electric aircraft development, offering a more pragmatic approach to battery design.

3. *"How is a reconfigurable battery pack beneficial? How much weight saving can it realise compared to the fixed configuration battery pack?"*

   The reconfigurable battery employs power switches to alter the arrangement of cells within a battery pack. In the case of an electric aircraft, the battery pack comprises a substantial number of cylindrical cells, ranging from 40,000 to 60,000, depending on the type of cells utilised. These cells are organised into modules that collectively constitute the battery pack. Given the many cells involved, implementing reconfiguration at the individual cell level proves impractical. Consequently, modular-level reconfiguration is employed. Tables 4.4 and 4.2 present a comparison between the number of cells required in reconfigurable battery packs and fixed configuration counterparts. The reconfigurable battery pack capitalises on the strengths of each cell type per specific phases of aircraft operation, resulting in a reduced overall cell count.

   A high-specific energy cell may lack the capacity to meet power demands during high-power phases when the battery pack is sized based on energy requirements. Conversely, sizing the pack according to power requirements might necessitate a higher cell count. Similarly, a high-specific power cell may struggle to meet energy demands when sized for power, and vice versa. The reconfigurable battery pack combines both cell types in a complementary manner, ultimately leading to a diminished cell count. The reconfigurable battery pack involves a control logic to command the power switches according to the power demand. Whenever the propulsion power demand is greater than the nominal power supply of the primary battery pack at that particular instance, the secondary pack gets connected in series, which decreases the overall pack current. Another case is when the primary battery pack SOC goes below 20%, the secondary battery pack get connected in series to prevent the full discharge of the primary battery pack. Thus, the reconfigurable battery pack control logic operates on the available power, SOC of the primary battery pack and propulsion power demands. Hence, although theoretically, take-off, initial climb, final climb, and reserved climb are known high-power demand phases, this technique can prove useful in emergency cases where high power might be demanded by the propulsion system to avoid mishaps. The transition from the primary battery pack to the (primary + secondary) battery pack, or vice versa, should be modular in predefined high-power phase transitions, e.g. Taxi to Take-off or final climb to cruise, meaning the switches must be programmed so that voltage builds gradually and power electronics are not compromised. However, this is unfavourable in emergency situations where a quick response from the throttle to the motor is expected. In such cases, the power electronics must withstand a sudden change in high voltage, or the battery cells must undergo overcurrent conditions, whichever is efficient, for a few seconds until all the modules are connected.

   Considering the supplementary battery pack weight required to power cabin loads in the case of the reconfigurable battery pack, a reduction of 400 kg in battery weight can be achieved compared to fixed-configuration battery packs (refer Section 5.3). It's important to note that the weight of

power switches per module has been omitted from this calculation. Even if accounted for, the weight savings remain notably substantial.

This weight saving can lead to three scenarios of realising the benefit:

- Eviation also showcases Alice's cargo version with the same specifications. With a reconfigurable battery pack, the saved weight can load 400 kg of cargo if volume permits. In general, the payload weight capacity can be enhanced
- Flying with lesser weight will offset the power profile of the aircraft, resulting in lesser energy for the same range travelled. In essence, energy savings can be enhanced
- An Additional number of cells equivalent to the available weight can be added in a strategic way which can increase the range of the aircraft

4. *"What is the significance of system-level voltage in weight minimisation?"*

   Based on the preliminary calculations outlined in Section 3.3, it is evident that the weight of power cables employed in electric aircraft is profoundly influenced by the system-level voltage. The preferred condition of lowest energy losses and minimum weight of the cables yields an optimum system level voltage point of 3610 V. Lower voltages either cause higher current flow in the cables leading to I^2R losses or larger conductor diameters add extra weight to the system to reduce the resistance in power cables. Conversely, higher voltages reduce the circulating current. However, at higher altitudes, the breakdown voltage of air drops significantly, posing a risk to safety if any defects are present in the power cable layers. To mitigate this, thicker layers of insulator around the power cables are required again, leading to increased weight of the cables.

5. *"What is the effect on cell ageing due to reconfigurability? Is the benefit of weight saving compromised for higher ageing of cells?"*

   Capacity loss due to LLI is considered the cell ageing factor as it depends on the C-rate of discharge of the cells. Reconfigurability qualitatively showed a negative effect on cell ageing due to higher C-rates of discharge compared to fixed configuration. However, quantitatively, the capacity loss of the reconfigurable battery pack after 500 cycles is only 0.4% more than the fixed configuration battery pack. Taking into consideration the number of cycles, the difference in capacity loss of two configurations and respective weights, the reconfigurable battery pack emerges as the preferred battery configuration

6.2. Future scope and recommendation

Electric aviation is a modern industry that is rapidly developing. Research in various aspects of the aircraft is taking place, out of which battery pack is essential. This study provided a preliminary comparative analysis of fixed configuration and reconfigurable battery packs, which can serve as a basis for future research work. The following are the prospective recommendations by the author:

- Futuristic battery chemistries can potentially extend the range of electric aircraft significantly. In the selection process, Li-S chemistry emerged as a promising candidate, attributed to its high specific energy. Further in-depth exploration of this battery technology for integration into electric aircraft battery packs is warranted.

- Regarding high specific power requirements, supercapacitors are emerging as viable solutions. While their specific energy currently presents a significant challenge, coupling them with Li-S or lithium-air batteries allows for the synergistic advantages of both technologies.

- Several aircraft companies actively pursue silent taxiing using an electric motor in the nose landing gear, recognising taxiing as one of the least efficient phases in conventional aircraft operations. This presents an opportunity for regenerative braking during landing, capturing energy typically lost as friction and heat. However, the rapid release of a large amount of power poses a challenge in converting mechanical energy to electrical energy and storage. Supercapacitors may be able to handle such power surges and capture some of this energy. It is crucial to consider the additional weight of the added machinery.

- A more comprehensive ageing analysis, including State of Health (SOH) estimation and the development of a thermal model, can be conducted for reconfigurable battery packs.

- A tailored BMS can be designed for monitoring the battery pack parameters such as temperature, SOC and SOH along with the communication network for reconfiguration signals

Bibliography

[1] Bright Appiah Adu-Gyamfi and Clara Good. "Electric aviation: A review of concepts and enabling technologies". In: *Transportation Engineering* 9 (Sept. 2022), p. 100134. ISSN: 2666-691X. DOI: 10.1016/J.TRENG.2022.100134.

[2] Airbus. "Airbus Global Market Forecast 2023-2042". In: (). URL: https://www.airbus.com/sites/g/files/jlcbta136/files/2023-06/GMF%202023-2042%20Take%20away%20Messages_2.pdf.

[3] *Aircraft – Eviation*. URL: https://www.eviation.com/aircraft/.

[4] *Ampaire Tailwind Aircraft*. URL: https://www.ampaire.com/vehicles/Tailwind%E2%84%A2-Aircraft.

[5] Eliot Aretskin-Hariton et al. "Power Cable Mass Estimation for Electric Aircraft Propulsion". In: ().

[6] *Aviation - IEA*. URL: https://www.iea.org/energy-system/transport/aviation#tracking.

[7] *Aviation – Analysis - IEA*. URL: https://www.iea.org/reports/aviation.

[8] Boeing. "Boeing Commercial Market Outlook 2023-2042". In: (). URL: https://www.boeing.com/resources/boeingdotcom/market/assets/downloads/2023-Commercial-Market-Outlook-Executive-Summary.pdf.

[9] Cheryl Bowman et al. "Key Performance Parameter Driven Technology Goals for Electric Machines and Power Systems". In: (). URL: www.nasa.gov.

[10] Peter G. Bruce et al. "Li–O2 and Li–S batteries with high energy storage". In: *Nature Materials 2011 11:1* 11.1 (Dec. 2011), pp. 19–29. ISSN: 1476-4660. DOI: 10.1038/nmat3191. URL: https://www.nature.com/articles/nmat3191.

[11] Wenzhuo Cao, Jienan Zhang, and Hong Li. "Batteries with high theoretical energy densities". In: *Energy Storage Materials* 26 (Apr. 2020), pp. 46–55. ISSN: 24058297. DOI: 10.1016/j.ensm.2019.12.024.

[12] Chang-Hui Chen et al. "Development of Experimental Techniques for Parameterization of Multi-scale Lithium-ion Battery Models". In: *Journal of The Electrochemical Society* 167.8 (Jan. 2020), p. 080534. ISSN: 0013-4651. DOI: 10.1149/1945-7111/ab9050.

[13] F. C. Cheng. "Insulation Thickness Determination Of Polymeric Power Cables". In: *IEEE Transactions on Dielectrics and Electrical Insulation* 1.4 (1994), pp. 624–629. ISSN: 10709878. DOI: 10.1109/94.311705.

[14] Song Ci, Ni Lin, and Dalei Wu. "Reconfigurable Battery Techniques and Systems: A Survey". In: *IEEE Access* 4 (2016), pp. 1175–1189. ISSN: 21693536. DOI: 10.1109/ACCESS.2016.2545338.

[15] Matthew Clarke and Juan J. Alonso. "Lithium–ion battery modeling for aerospace applications". In: *Journal of Aircraft* 58.6 (July 2021), pp. 1323–1335. ISSN: 15333868. DOI: 10.2514/1.C036209/ASSET/IMAGES/LARGE/FIGURE17.JPEG. URL: https://arc.aiaa.org/doi/10.2514/1.C036209.

[16] *Commission Implementing Regulation (EU) No 923/2012*. URL: https://eur-lex.europa.eu/legal-content/EN/TXT/HTML/?uri=CELEX:32012R0923&from=EN.

[17] Timothy P Dever et al. "Assessment of Technologies for Noncryogenic Hybrid Electric Propulsion". In: (2015). URL: http://www.sti.nasa.gov.

[18] *Eviation CEO Talks Electrifying The Skies With Its Upcoming Plane*. URL: https://insideevs.com/news/676120/eviation-electric-airplane-ceo-talk/.

[19] *Find and Compare Batteries - Get started with the Batemo Cell Explorer!* URL: https://www.batemo.de/products/batemo-cell-explorer/.

[20] Nicolas Fontenai and Ruben De Graaff. *Design of Propulsion Sys-tem for 9 PAX Electric Air-craft Motors and Power Distribution for AEA BSc Thesis*. Tech. rep. URL: http://repository.tudelft.nl/..

[21] Abbas Fotouhi et al. "A review on electric vehicle battery modelling: From Lithium-ion toward Lithium–Sulphur". In: *Renewable and Sustainable Energy Reviews* 56 (Apr. 2016), pp. 1008–1021. ISSN: 1364-0321. DOI: 10.1016/J.RSER.2015.12.009.

[22] N g- and By J W Wetmore. "CAS C THE ROLLING FRICTION OF SEVERAL AIRPLANE WHEELS AND TIRES AND THE EFFECT OF ROLLING FRICTION ON TAKE-OFF NASA FILE COpy". In: ().

[23] Albert R. Gnadt et al. *Technical and environmental assessment of all-electric 180-passenger commercial aircraft*. Feb. 2019. DOI: 10.1016/j.paerosci.2018.11.002.

[24] Goksel Gunlu. "Dynamically Reconfigurable Independent Cellular Switching Circuits for Managing Battery Modules". In: *IEEE Transactions on Energy Conversion* 32.1 (Mar. 2017), pp. 194–201. ISSN: 08858969. DOI: 10.1109/TEC.2016.2616190.

[25] Mahammad A. Hannan et al. *State-of-the-Art and Energy Management System of Lithium-Ion Batteries in Electric Vehicle Applications: Issues and Recommendations*. Mar. 2018. DOI: 10.1109/ACCESS.2018.2817655.

[26] Mohamed S.E. Houache et al. *On the Current and Future Outlook of Battery Chemistries for Electric Vehicles—Mini Review*. July 2022. DOI: 10.3390/batteries8070070.

[27] Ralph H Jansen, Cheryl Bowman, and Amy Jankovsky. "Sizing Power Components of an Electrically Driven Tail Cone Thruster and a Range Extender". In: ().

[28] Fangjian Jin and Kang G. Shin. "Pack sizing and reconfiguration for management of large-scale batteries". In: *Proceedings - 2012 IEEE/ACM 3rd International Conference on Cyber-Physical Systems, ICCPS 2012*. 2012, pp. 138–147. ISBN: 9780769546957. DOI: 10.1109/ICCPS.2012.22.

[29] Hagen Kellermann et al. "Design of a Battery Cooling System for Hybrid Electric Aircraft". In: *Journal of Propulsion and Power* 38.5 (Sept. 2022), pp. 736–751. ISSN: 15333876. DOI: 10.2514/1.B38695/ASSET/IMAGES/LARGE/FIGURE12.JPEG. URL: https://arc.aiaa.org/doi/10.2514/1.B38695.

[30] Hahnsang Kim and Kang G. Shin. "DESA: Dependable, efficient, scalable architecture for management of large-scale batteries". In: *IEEE Transactions on Industrial Informatics* 8.2 (May 2012), pp. 406–417. ISSN: 15513203. DOI: 10.1109/TII.2011.2166771.

[31] Hahnsang Kim and Kang G. Shin. "On dynamic reconfiguration of a large-scale battery system". In: *Proceedings of the IEEE Real-Time and Embedded Technology and Applications Symposium, RTAS*. 2009, pp. 87–96. ISBN: 9780769536361. DOI: 10.1109/RTAS.2009.13.

[32] T Kim, W Qiao, and L Qu. "Series Connected Self Reconfigurable Multicell Battery". In: ().

[33] Taesic Kim, Wei Qiao, and Liyan Qu. "Power electronics-enabled self-X multicell batteries: A design toward smart batteries". In: *IEEE Transactions on Power Electronics* 27.11 (2012), pp. 4723–4733. ISSN: 08858993. DOI: 10.1109/TPEL.2012.2183618.

[34] LG Chem. *PRODUCT SPECIFICATION Rechargeable Lithium Ion Battery Model : INR21700 M5018.20Wh*. Tech. rep. URL: https://www.dnkpower.com/wp-content/uploads/2019/02/LG-INR21700-M50-Datasheet.pdf.

[35] Ya Li et al. "Ultrafine and polar ZrO2-inlaid porous nitrogen-doped carbon nanofiber as efficient polysulfide absorbent for high-performance lithium-sulfur batteries with long lifespan". In: *Chemical Engineering Journal* 349 (Oct. 2018), pp. 376–387. ISSN: 1385-8947. DOI: 10.1016/J.CEJ.2018.05.074.

[36] Hendrik Löbberding et al. "From Cell to Battery System in BEVs: Analysis of System Packing Efficiency and Cell Types". In: *World Electric Vehicle Journal 2020, Vol. 11, Page 77* 11.4 (Dec. 2020), p. 77. ISSN: 2032-6653. DOI: 10.3390/WEVJ11040077. URL: https://www.mdpi.com/2032-6653/11/4/77/htm%20https://www.mdpi.com/2032-6653/11/4/77.

[37] lygte-info. *Test of LG 21700 M50 5000mAh (Grey)*. URL: https://lygte-info.dk/review/batteries2012/LG%2021700%20M50%205000mAh%20(Grey)%20UK.html.

[38] lygte-info. *Test of Samsung INR21700-40T 4000mAh (Cyan)*. URL: https://lygte-info.dk/review/batteries2012/Samsung%20INR21700-40T%204000mAh%20(Cyan)%20UK.html.

[39] Adam Mcloughlin and Royce Plc. "More electric — Ready for take off?; More electric — Ready for take off?" In: *2009 13th European Conference on Power Electronics and Applications* (2009).

[40] *MIL-Spec Aerospace*. URL: https://www.awcwire.com/mil-spec-aerospace.

[41] Chen Mingtai. *Static Thrust Measurement for Propeller-driven Light Aircraft*. Tech. rep.

[42] Rodrigo Paludo, Guilherme Cunha Da Silva, and Vitoldo Swinka Filho. "The study of semiconductor layer effect on underground cables with Time Domain Reflectometry (TDR)". In: 7.6 (), pp. 1–07. URL: www.iosrjournals.orgwww.iosrjournals.org.

[43] Tobias Placke et al. "Lithium ion, lithium metal, and alternative rechargeable battery technologies: the odyssey for high energy density". In: *Journal of Solid State Electrochemistry* 21.7 (July 2017), pp. 1939–1964. ISSN: 14328488. DOI: 10.1007/s10008-017-3610-7.

[44] Gregory L. Plett. *Battery Management Systems Equivalent-Circuit Methods*. 2016. ISBN: 978-1-63081-027-6. URL: https://app.knovel.com/hotlink/toc/id:kpBMSVECM3/battery-management-systems/battery-management-systems.

[45] Gregory L. Plett. *Battery Management Systems Volume I Battery Modeling*. 2015. ISBN: 978-1-63081-023-8. URL: https://app.knovel.com/hotlink/toc/id:kpBMSVBM02/battery-management-systems/battery-management-systems.

[46] Harry J Ploehn, Premanand Ramadass, and Ralph E White. "Solvent Diffusion Model for Aging of Lithium-Ion Battery Cells". In: *Journal of the Electrochemical Society* (2004), pp. 456–462. DOI: 10.1149/1.1644601. URL: http://www.electrochem.org/Publisher'slink:http://dx.doi.org/10.1149/1.1644601.

[47] Karsten Propp et al. "Multi-temperature state-dependent equivalent circuit discharge model for lithium-sulfur batteries". In: *Journal of Power Sources* 328 (Oct. 2016), pp. 289–299. ISSN: 0378-7753. DOI: 10.1016/J.JPOWSOUR.2016.07.090.

[48] *PyBaMM - About PyBaMM*. URL: https://pybamm.org/about/.

[49] P. Ramadass et al. "Development of First Principles Capacity Fade Model for Li-Ion Cells". In: *Journal of The Electrochemical Society* 151.2 (Jan. 2004), A196. ISSN: 00134651. DOI: 10.1149/1.1634273/XML. URL: https://iopscience.iop.org/article/10.1149/1.1634273%20https://iopscience.iop.org/article/10.1149/1.1634273/meta.

[50] Manuel A. Rendón et al. "Aircraft Hybrid-Electric Propulsion: Development Trends, Challenges and Opportunities". In: *Journal of Control, Automation and Electrical Systems* 32.5 (Oct. 2021), pp. 1244–1268. ISSN: 21953899. DOI: 10.1007/S40313-021-00740-X/FIGURES/19. URL: https://link.springer.com/article/10.1007/s40313-021-00740-x.

[51] F Russo. *EVIATION ALICE ANALYSIS OF AIRCRAFT PERFORMANCES AND COMPARISON WITH OFFICIAL CLAIMS*. Tech. rep. URL: https://www.linkedin.com/posts/fabio-russo-51375a33_eviation-alice-performances-analysis-ugcPost-6939894153900134401-_Ayo/?utm_source=linkedin_share&utm_medium=ios_app.

[52] M. Safari et al. "Multimodal Physics-Based Aging Model for Life Prediction of Li-Ion Batteries". In: *Journal of The Electrochemical Society* 156.3 (2009), A145. ISSN: 00134651. DOI: 10.1149/1.3043429.

[53] Smruti Sahoo, Xin Zhao, and Konstantinos Kyprianidis. "A review of concepts, benefits, and challenges for future electrical propulsion-based aircraft". In: *Aerospace* 7.4 (Apr. 2020). ISSN: 22264310. DOI: 10.3390/AEROSPACE7040044.

[54] SAMSUNG SDI. *Lithium-ion rechargeable cell for power tools Model name: INR21700-40T*. Tech. rep. 2017. URL: https://dnkpower.com/wp-content/uploads/2019/02/SAMSUNG-INR21700-40T-Datasheet.pdf.

[55] Amy Schwab et al. *Electrification of Aircraft: Challenges, Barriers, and Potential Impacts*. Tech. rep. 2018. URL: https://www.nrel.gov/docs/fy22osti/80220.pdf..

[56] Arne Seitz et al. *Conceptual Studies of Universally-Electric Systems Architectures Suitable for Transport Aircraft*. Tech. rep. 2012. URL: https://www.researchgate.net/publication/274705769.

[57] L. Shadbolt. *HDI Global Specialty SE HDI Global Specialty Study Electric Aviation April 2022 Technical Study Electric Aviation in 2022 HDI Global Specialty SE 02 HDI Global Specialty SE HDI Global Specialty Study Electric Aviation April 2022*. Tech. rep. URL: https://www.hdi.global/globalassets/_local/international/downloads/specialty/aviation/e-flight_whitepaper.pdf.

[58] Neda Shateri et al. "An Experimental Study on Prototype Lithium-Sulfur Cells for Aging Analysis and State-of-Health Estimation". In: *IEEE Transactions on Transportation Electrification* 7.3 (Sept. 2021), pp. 1324–1338. ISSN: 23327782. DOI: 10.1109/TTE.2021.3059738.

[59] Aditya Shekhar et al. "Impact of DC Voltage Enhancement on Partial Discharges in Medium Voltage Cables-An Empirical Study with Defects at Semicon-Dielectric Interface". In: (). DOI: 10.3390/en10121968. URL: www.mdpi.com/journal/energies.

[60] *Simscape Battery - MATLAB*. URL: https://nl.mathworks.com/products/simscape-battery.html.

[61] Fabian Single, Arnulf Latz, and Birger Horstmann. "Identifying the Mechanism of Continued Growth of the Solid-Electrolyte Interphase". In: ().

[62] *Taxi times - Summer 2021 | EUROCONTROL*. URL: https://www.eurocontrol.int/publication/taxi-times-summer-2021.

[63] Bsc Thesis, Calvin Wijnveen, and Raf Van De Luijtgaarden. *Design of Propulsion Sys-tem for 9 PAX Electric Air-craft Energy Storage and Transfer*. Tech. rep.

[64] Venkatasubramanian Viswanathan et al. *The challenges and opportunities of battery-powered flight*. Jan. 2022. DOI: 10.1038/s41586-021-04139-1.

[65] Vijayaragavan Viswanathan, Lakshimi Narayanan Palaniswamy, and Padma Balaji Leelavinodhan. *Optimization techniques of battery packs using re-configurability: A review*. June 2019. DOI: 10.1016/j.est.2019.03.002.

[66] Volta foundation. "Volta Foundation". In: (). URL: https://report.volta.foundation/annual-battery-report/public/Battery_Report_2022.pdf?utm_medium=email&_hsmi=253710816&_hsenc=p2ANqtz-80MFok8Rds0cuw_NPx3PM4yQXq6GanycF1BEBBFWn4Tlh0ziyMPp9BQW0aMS5aFmjR12c1lxviXi-VH37o6R5rpLPYhg&utm_content=253710816&utm_source=hs_automation.

[67] Chun Wang et al. "Efficiency analysis of a bidirectional DC/DC converter in a hybrid energy storage system for plug-in hybrid electric vehicles". In: *Applied Energy* 183 (Dec. 2016), pp. 612–622. ISSN: 03062619. DOI: 10.1016/j.apenergy.2016.08.178.

[68] Whittaker R. *Staff from Abingdon battery manufacturer take legal action after business collapse | Oxford Mail*. 2021. URL: https://www.oxfordmail.co.uk/news/19458937.staff-abingdon-battery-manufacturer-take-legal-action-business-collapse/.

[69] *Wright Electric*. URL: https://www.weflywright.com/.

[70] *Wright Electric White-paper*. URL: https://docsend.com/view/faijiijzkvqdccjg.

[71] Oliver Wyman and Source Link. "Projected number of narrowbody jets in the global aircraft fleet from 2022 to 2032". In: (2023). ISSN: 2022-2032. URL: https://www.statista.com/statistics/410857/projected-number-of-narrowbody-aircraft-in-global-fleet/.

[72] Oliver Wyman and Source Link. "Projected number of widebody jets in the global aircraft fleet from 2022 to 2032". In: (2022). ISSN: 2022-2032. URL: https://www.statista.com/statistics/410799/projected-number-of-widebody-aircraft-in-global-fleet/.

[73] Xiao-Guang Yang et al. “Modeling of lithium plating induced aging of lithium-ion batteries: Transition from linear to nonlinear aging”. In: (2017). DOI: 10.1016/j.jpowsour.2017.05.110. URL: http://dx.doi.org/10.1016/j.jpowsour.2017.05.110.

[74] Yu Zhang and Qing Wang. “Methods for determining unimpeded aircraft taxiing time and evaluating airport taxiing performance”. In: *Chinese Journal of Aeronautics* 30.2 (Apr. 2017), pp. 523–537. ISSN: 1000-9361. DOI: 10.1016/J.CJA.2017.01.002.

[75] Yu Zhu et al. “A novel design of reconfigurable multicell for large-scale battery packs”. In: *2018 International Conference on Power System Technology, POWERCON 2018 - Proceedings* (Jan. 2019), pp. 1445–1452. DOI: 10.1109/POWERCON.2018.8602284.

A

Appendix

A.1. Paschen curve

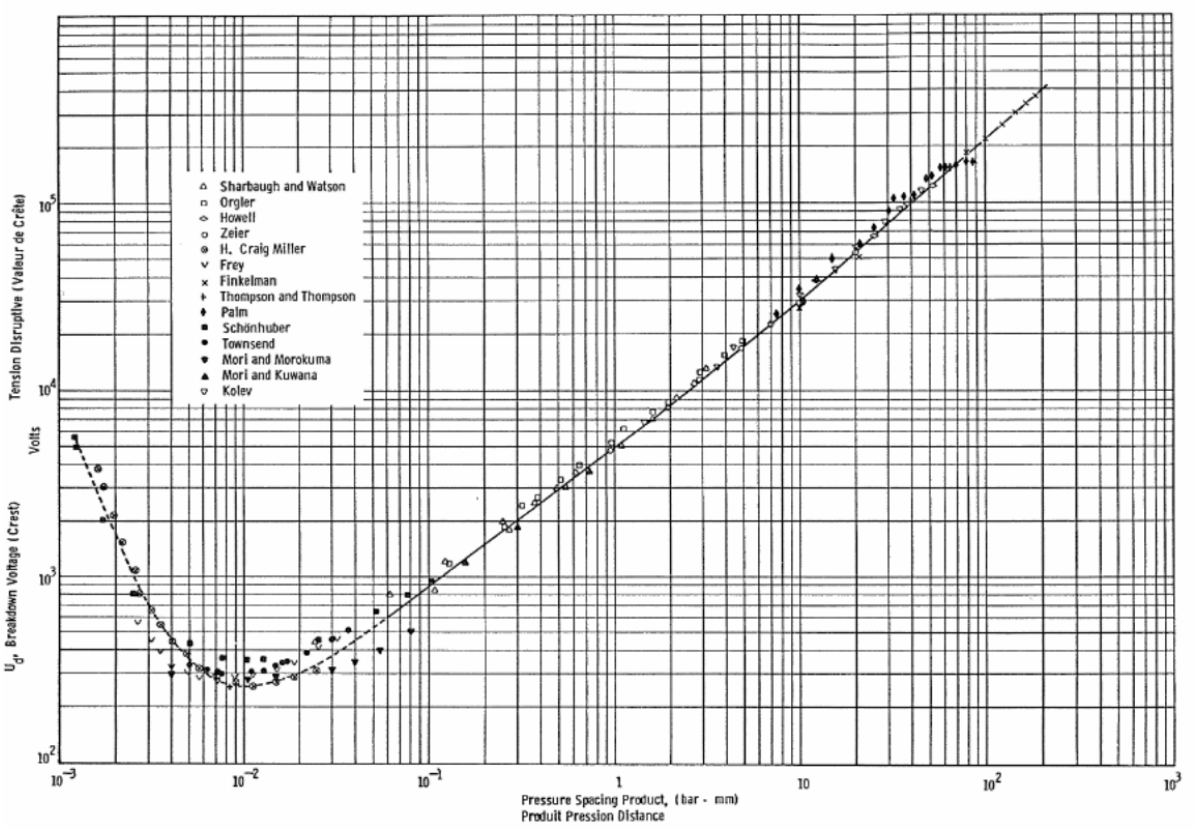

Figure A.1: Paschen Curve [63]

A.2. Resistacne and time constant values of ECM

Temperature (deg C)	R0	R1	R2	R3	τ_1	τ_2	τ_3
15	0.0165	0.001	0.001	0.0412	0.9740	5.0047	31.5961
25	0.0150	0.001	0.001	0.036	0.9842	5.1196	32.7584
35	0.0135	0.001	0.001	0.0322	1.009	5.4076	35.7573

Table A.1: Values of resistances and time constants at test temperatures for reconfigurable battery pack

Temperature (deg C)	R0	R1	R2	R3	τ_1	τ_2	τ_3
15	0.0204	0.001	0.001	0.0336	0.3877	8.5473	38.5879
25	0.018	0.001	0.001	0.0291	0.3808	8.4605	36.1698
35	0.0153	0.001	0.001	0.0265	0.3804	8.2759	32.52

Table A.2: Values of resistances and time constants at test temperatures for fixed configuration battery pack

A.3. LG and SAMSUNG cell data

Test	current	(A)	0.2	0.5	1	2	3	5	7.275
Measured	capacity	(Ah)	4.921	4.908	4.904	4.861	4.838	4.810	4.750
Measured	energy	(Wh)	18.074	17.972	17.863	17.522	17.265	16.851	16.15

Table A.3: Test data of LG-INR21700-M50 [37]

Test	current	(A)	1	2	3	5	10	15	20
Measured	capacity	(Ah)	3.849	3.836	3.801	3.779	3.725	3.685	3.650
Measured	energy	(Wh)	14.073	13.948	13.773	13.586	13.038	12.713	12.410

Table A.4: Test data of SAMSUNG-INR21700-40T [38]

A.4. Fixed configuration Simulink model

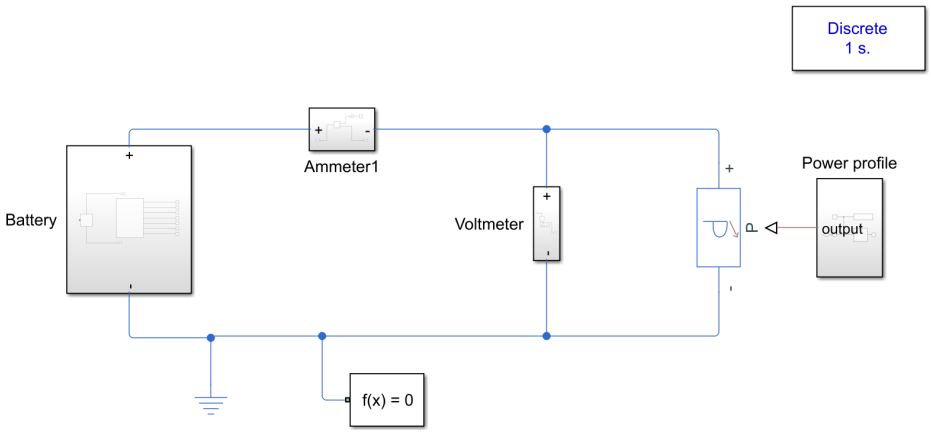

Figure A.2: Fixed configuration battery pack Simulink model

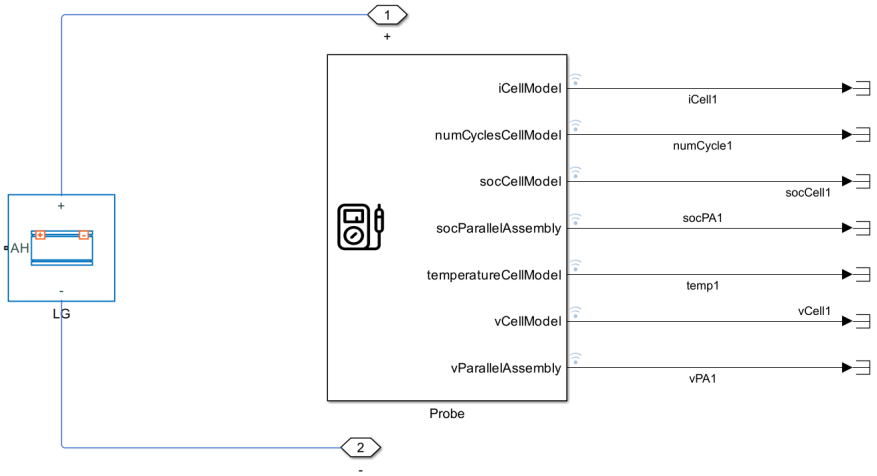

Figure A.3: Fixed configuration Simulink battery